Feasibility study of once through cooling for 50 MW_e Solar Thermal Power Plant on/near the lower Orange River.

By
Abiola Gboyega Kehinde

Thesis presented in fulfilment for a
Master's degree in Mechanical Engineering in the Faculty of Engineering at Stellenbosch University

Supervisor: Dr Jaap Hoffmann
December 2019

Declaration

By submitting this thesis electronically, I declare that the entirety of the work contained therein is my own, original work, that I am the sole author thereof (save to the extent explicitly otherwise stated), that reproduction and publication thereof by Stellenbosch University will not infringe any third party rights and that I have not previously in its entirety or in part submitted it for obtaining any qualification.

Signature: ……
A.G Kehinde

Date: …December 2019…...

Abstract

The rapid increase in demand for solar energy and its contribution to the national grid has placed new emphasis on the performance of Concentrating Solar Power (CSP) Plant. Plant performance can be enhanced by using once-through water-cooling instead of the conventional direct air-cooled systems. Water withdrawn from the Orange River for agricultural irrigation purposes near Upington, in the Northern Cape can accommodate once-through cooling. To achieve this, a detailed study of CSP plant and different types of the cooling systems that are available was undertaken. The different types of CSP plant were evaluated and the best CSP plant based on the technology advancement was identified. The use and management of the irrigation system, government policies and environmental legislation along the lower Orange River was studied to look for synergy between CSP and agricultural water use.

Once-through cooling for CSP plant that is also known as open-cycle cooling was modelled and fully analysed. The components of the CSP plant were also modelled, with emphasis on condenser fouling. This includes heliostat field, receiver tower, thermal storage, steam generator and power block. The heliostat field model determined the heliostat field optical efficiency over the year. The power block model determined the thermal efficiency of CSP plant and the function of growth with the cooling water temperature in the cooling system. The model was also used to determine the impact of changing different CSP plant operating parameters on the cooling system and evaluate the plant output.

All existing CSP plants, except Bokpoort, make use of direct air-cooled condensers. Hence, direct air-cooling was adopted as benchmark for this study. Compared to a direct air-cooled CSP plant, once-through cooling shows that there is an improvement in the thermal efficiency of 2.9 percentage points. The model is based on hourly fluctuations in cooling water temperature from the river that ranges from 20°C to 25 ℃.

Uittreksel

Die snel toename in die vraag na son-termiese energie, en die bydrae daarvan tot die nasionale kragleweringsnetwerk, het die effektiwiteit van son-termiese kragstasies (STK) onder die vergrootglas geplaas. Direkte deurvloei water verkoeling is ‘n aantreklike opsie in die Noord Kaap, siende dat water vir vloedbesproeing uit die rivier onttrek word, vir verkoeling gebruik kan word. Die sinergie tussen verkoeling en landbou behoeftes van die hipotetiese STK is krities ondersoek. Om die mees geskikte aanleg konfigurasie te kies, is ‘n oorsig oor bestaande STK en verkoelingsisteme gedoen. ‘n Volledige model van ‘n deurvloei verkoelde STK, wat die heliostate, onvanger, termiese energie stoor, stoom-opwekker en Rankine kringloop insluit, is ontwikkel.

Die model voorspel die aanleg se uitset oor ‘n volle kalender jaar, om veranderinge in son straling, water temperature en aanpakking van die kondenser buise op die aanleg se kraglewering insluit. Bestaande wetgewing rondom die ontrekking van water vanuit, en terugvoer na ekosisteme soos van toepassing op die landbou, eerder as industrie, is gevolg. Dit bied groot voordele om die voorgestelde stelsel te bedryf.

Alle bestaande CSP-aanlegte, behalwe Bokpoort, maak gebruik van direkte lugverkoelde kondenseerders. Daarom is direkte lugverkoeling as maatstaf vir hierdie studie aangeneem. Vergeleke met 'n direkte lugverkoelde CSP-aanleg, wys eenmalige verkoeling dat die termiese doeltreffendheid van 2,9 persentasiepunte verbeter word. Die model is gebaseer op uurlikse skommelinge in koelwatertemperatuur vanaf die rivier wat wissel van 20 ° C tot 25 ℃.

Dedication

To my father, Musiliu Alabi Kehinde,

and

my mother, Amoke Iyabo Kehinde

Acknowledgements

I wish to express my profound gratitude to almighty God for giving me the wisdom, strength and inspiration to put this report together. All Glory belongs to him.

My profound appreciation goes to my supervisor, Dr Jaap Hoffmann, for believing in me and extending an offer to further my studies at Stellenbosch University and provided a bursary for me. I also thank him for his patience, motivation, enthusiasm and expertise. His support helped me in all the times of the research and writing of this thesis. My sincere gratitude goes to Prof. Wikus van Niekerk, for his support and his advice on my thesis as well as Prof. Thomas Harms.

A special thanks to Dr Toyosi Craig for his encouragement, practical advice and support. I also thank him for reading my report, commenting on my views and helping me to enrich my views. Further appreciation goes to the Centre for Renewable and Sustainable Energy (CRSES) and Solar Thermal Energy Research Group (STERG) for their counterpart financial support for this study, and my office friend, for providing a favourable research atmosphere – Andani Siavhe and most especially, Brian Ssebabi for his moral support.

I also want to thank my friends, Babatunde Elemide, Idowu Sodiq, Emmanuel Okene, Rapheal Popoola, John Kolawole, Adegoke Adetoro and Ajila Gbenga for their moral support as well as the pastors and workers of the Redeemed Christian Church of God, Desire of Nations, Stellenbosch and Revelation of Christ Gospel Church, Abeokuta, Nigeria. Many thanks to my dear friend Pharmacist Ogooluwa Omotoso for her timely encouragement. God bless you.

I want to say a big thank you to my sibling especially Rhoda Kehinde, thank you so much for your support. God's grace shall continue to be with you, in Jesus' name, Amen.

Table of Contents

Declaration ..... **ii**
Abstract ..... **iii**
Uittreksel ..... **iv**
Dedication ..... **v**
Acknowledgements ..... **vi**
List of figures ..... **xi**
List of tables ..... **xiii**
Nomenclature ..... **xiv**
Chapter 1: Introduction **1**
1.1 Background 1
1.2 Research problem statement 4
1.3 Research aim and objectives 5
1.4 Research limitations 5
1.5 Thesis framework 6
Chapter 2: Literature review **7**
2.1 Concentrating solar power plant 7
2.2 CSP and its costing in South Africa 9
2.3 CSP plant cooling system 11
2.3.1 Once-through cooling 11
2.3.2 Closed Cooling 12
2.4 Condenser in a CSP plant system 12
2.4.1 Condenser 13
2.4.2 Types of condenser 13
2.5 Quality of Water for Cooling System 14
2.6 Lower Orange River and Agricultural use 14
Chapter 3: Once-through cooling condenser **15**
3.1 Description of a vacuum steam surface condenser 15
3.2 Factors affecting a surface condenser tube 17
3.2.1 Fouling 17
3.2.2 Erosion and corrosion 18
3.3 Modification of fractured condenser tube 19

Chapter 4: Description of CSP plant 21
4.1 Heliostat Field 21
4.2 Central receiver 23
4.3 Thermal energy storage 25
4.4 Steam generator 27
4.5 Power block 28
Chapter 5: CSP plant modelling 31
5.1 Weather data and site location 31
5.2 Heliostat field 31
5.2.1 Parametric simulation 32
5.2.2 Sun's position 32
5.3 Receiver 35
5.4 Thermal energy storage 38
5.5 Steam generation 39
5.6 Power block 40
5.6.1 Steam generator 41
5.6.2 Turbine 42
5.6.3 Feed-water heater 42
5.6.4 Feed pump 43
5.6.5 Condenser 43
5.6.6 Thermal efficiency 48
Chapter 6: Model validation 49
6.1 Heliostat Field Comparison 49
6.2 Receiver tower comparison 50
6.3 Power block comparison 50
6.3.1 Air-cooled comparison 50
6.3.2 SAM comparison 52
Chapter 7: Model result 53
7.1. Heliostat field 53
7.2. Receiver tower 54
7.3 Power block 55
7.4 Agricultural and Environmental constraint 61

Chapter 8: Conclusion and recommendations 62

8.1 Conclusions 62

8.2 Recommendations 63

References 64

Appendix A: Thermo-physical properties 71

A.1 Thermo-physical properties of molten salt (Sandia National Laboratories, 2001) 71

A.2 Thermo-physical properties of saturated water from 273.15 K to 380 K (Kröger, 1998) 72

Appendix B: Different types of CSP plant in South Africa 73_Toc22885064

Appendix C 74

Heliostat field simulated result 74

C.1 Heliostat field boundary 74

C.2 Heliostat field layout 75

C.3 Heliostat field efficiency 76

Appendix D: Analysis of modelled once-through cooling condenser 77

Appendix E: Sample calculations 79

E.1 Analysis of heliostat field efficiency 79

E.1.1 Weather data 79

E.1.2 Sun's position 80

E.2 Analysis of Centre Receiver 82

E.3 Analysis of power block 85

E.3.1 Steam generator 86

E.3.2 Turbine 87

E.3.3 Feed-water heater 87

E.3.4 Feed-pump 88

E.3.5 Condenser 88

E.3.6 Thermal efficiency 89

E.4 Analysis of fouling factor 90

E.4.1 Calculating thermo-physical properties of water 90

E.4.2 Flow cross-sectional area 92

E.4.3 Rate of heat transfer 92

E.4.4 Reynolds number 93

E.4.5 Frictional factor.....93
E.4.6 Nusselt number 93
E.4.7 Fouling factor.....94

List of figures

Figure 1-1: Different types of CSP plant 2
Figure 1-2: CSP central receiver plant (Cabeza *et al.*, 2012). 3
Figure 2-1: South Africa average daily direct normal irradiation (SolarGIS, 2011) 10
Figure 2-2: Average bid windows price for CSP (Department of Energy, 2015). 10
Figure 2-3: Once through cooling (EPRI, 2013) 12
Figure 2-4: Examples of direct and indirect contact type 13
Figure 3-1: Schematic of a two pass, single compartment steam surface condenser (Goodenough, 2013) 16
Figure 3-2: Example of pitting corrosion in condenser tubes 19
Figure 4-1: Heliostat (Wikipedia, 2018) 21
Figure 4-2: Heliostat field of Gema-solar STPP (García and Calvo, 2012) 22
Figure 4-3: Cosine, blocking and shadowing losses from heliostat (Scheffler, 2015) 22
Figure 4-4: External receiver (Solar Reserve, 2017) 23
Figure 4-5: Cavity receiver (CMI, 2016) 24
Figure 4-6: Receiver losses (Stine and Geyer, 2001) 24
Figure 4-7: Different types of thermal energy storage 25
Figure 4-8: Power tower plant with two-tank molten salt system (Meybodi and Beath, 2016) 26
Figure 4-9: Schematic diagram of steam generator 27
Figure 4-10: Schematic diagram of a simple ideal Rankine cycle 28
Figure 4-11: Pump and turbine effect on Rankine cycle 29
Figure 4-12: Schematic diagram of re-heat Rankine cycle 29
Figure 4-13: Schematic diagram of regenerative Rankine cycle 30
Figure 5-1: Parametric simulation table 32
Figure 5-2: Angles of the sun 33
Figure 5-3: Schematic diagram of thermal energy storage 39
Figure 5-4: Schematic diagram of pinch point steam generator 40
Figure 5-5: Schematic diagram of STPP power block 41
Figure 5-6: Measured fouling factor for admiralty brass tube (Reuter et al., 2017) 46

Figure 6-1: Heliostat field efficiency comparison 49
Figure 6-2: Receiver comparison.....50
Figure 6-3: STPP with air-cooled condenser.....51
Figure 6-4: Model vs SAM comparison 52
Figure 7-1: Zenith angle effects on heliostat optical field efficiency over the year 53
Figure 7-2: Effect of wind speed onto receiver 54
Figure 7-3: Effects of ambient temperature onto receiver.....55
Figure 7-4: Energy received and discharged energy on December 22, 2017 55
Figure 7-5: Effects of thermal energy supplied to steam generator on turbine output 56
Figure 7-6: Performance curve of the power block based on turbine output 56
Figure 7-7: Performance of the power block based on thermal energy supplied ..57
Figure 7-8: Effects of cooling water on power block 57
Figure 7-9: Annual hourly occurrence of inlet cooling water (Orange River) temperature 58
Figure 7-10: Function of growth with temperature 59
Figure 7-11: The performance of the drop in thermal efficiency against condenser fouling factor.....60
Figure 7-12: The performance of the turbine output against condenser fouling factor 60
Figure C-1: Field boundary in Solar-PILOT 74
Figure C-2: Field layout in Solar-PILOT 75
Figure C-3: Heliostat optical field efficiency 76
Figure D-4: Power block layout with three feed-water heaters 85

List of tables

Table 5-1: Site Location 31
Table 5-2: Conversion of date to day number 34
Table 6-1: Comparison between once-through cooling and air-cooled.....51
Table 6-2: Performance of OTC and AC on STPP.....51
Table 7-1: Simulation result from Solar-PILOT.....54
Table 7-2: STPP result at design point 58
Table B-1: Various CSP in South Africa.....73
Table D-2: Modelling parameter for once-through cooling condenser 77
Table D-3: Upington weather data.....79
Table D-4: Upington site data.....79
Table D-5: Modelling parameter used Solar-PILOT for heliostat field efficiency79
Table D-6: Modelling parameter for receiver tower.....82
Table D-7: Modelling parameter for power block obtained from X-Steam 86

Nomenclature

Symbols

A	Area (m^2)
F	Radiation shape factor
f_D	Frictional factor
h	Heat transfer coefficient (W/m^2K)
H_s	Height of the salt (m)
H_t	Total number of heliostat
ITD	Initial temperature difference (K)
k	Thermal conductivity $(W/m\ K\ )$
TTD	Terminal temperature difference (K)
$\dot{m}$	Mass flow rate (kg/s)
R''	Fouling factor (W/K)
SM	Solar multiple
T	Temperature (K)
$\bar{T}$	Mean Temperature (K)
U	Overall heat transfer coefficient (W/m^2K)
V	Volume (m^3)
y	Height of the receiver (m)

Greek letters

α	Absorptivity
ε	Emissivity
η	Efficiency (%)
μ	Kinematic viscosity $(kg/m.s)$
ρ	Density (kg/m^3)
σ	Stefan-Boltzmann constant (W/m^2K^4)

Subscripts

a	Air
C	Condenser
CS	Condensed steam
cw	Cold water
cwi	Cold-water input
cwo	Cold-water output
eff	Effective
EG	Electric generator
F	Feed-water
fa	Field aperture
fc	Forced coefficient
fwh	Feed-water heater
he	Heliostat
$HPFH$	High-pressure feed-water heater

HPT	High-pressure turbine
IPT	Intermediate pressure turbine
ir	Inner receiver
is	Inlet salt
$LPFH$	Low-pressure feed-water heater
LPT	Low-pressure turbine
max	Maximum
min	Minimum
mr	Mean radiation
ms	Molten salt
nc	Natural coefficient
of	Optical field
os	Outlet salt
or	Outer receiver
ra	Receiver absorber
RH	Re-heat
RS	Reheat steam
s	Steam
si	Steam input
so	Steam output
S	Salt
SD	Steam entering deaerator
SG	Steam generator
SH	Steam leaving high-pressure turbine
SHH	Steam entering high-pressure feed-water heater
SI	Steam leaving low-pressure turbine
SL	Steam leaving low-pressure turbine
SLH	Steam leaving low-pressure feed-water heater
SSG	Steam leaving the steam generator
tm	Tube material
w	Water

Dimensionless groups

Nu	Nusselt number
Pr	Prandtl number
Ra	Rayleigh number
Re	Reynolds number

Acronyms

CSP	Concentrating Solar Power
DEA	Department of Environmental Affairs
DNI	Direct Normal Irradiance
DoE	Department of Energy
DWA	Department of Water Affairs
HTF	Heat Transfer Fluid

ICMA	Integrated Coastal Management Act (Act No. 24 of 2008)
IRENA	International Renewable Energy Agency
IRP	Integrated Resource Plan
LCOE	Levelised cost of electricity
NREL	National Renewable Energy Laboratory
NWA	National Water Act (Act No. 36 of 1998)
OTC	Once Through Cooling
OCC	Once-through Cooling Condenser
PV	Solar Photovoltaic
REI4P	Renewable Energy Independent Power Producer Procurement Programme
RET	Renewable Energy Technology
SA	South Africa
SAM	System Advisor Model
SAWS	South African Weather Service
SEGS	Solar Electric Generating System
STPP	Solar Thermal Power Plant
TES	Thermal Energy Storage
USA	United State of America
WWF	World Wide Fund for Nature

Chapter 1

Introduction

Overview

An introduction to the basic principle and different ways of generating electric power from solar energy is presented, with a brief description of the once-through cooling system. Also, factors affecting the once-through cooling system are discussed with their solution. And lastly, the research problem, aim and objective, limitations and scope of this work are given.

1.1 Background

The issue of energy crises, in addition to increasing in demand for electricity, has given solar energy further consideration in the last decades. Solar energy is a form of renewable energy[1] of which its source comes from the sun. It has two major ways of generating electricity, which is photovoltaic cell (PV), and solar thermal power. Photovoltaics cell contains a thin layer of silicon, which directly converts sunlight into electricity. According to Wu et al. (2010), photovoltaic technology involves the direct conversion of solar radiation into electricity by means of photovoltaic materials.

For solar thermal power, (also known as concentrating solar power) contains solar collectors that concentrate sunlight, typically to raise steam and then use it to generate electricity. Concentrating solar power (CSP) technology began full operation in the 1980s when oil crises (1973) arises which prompted many countries to begin to invest in renewable energy as a substitute to fossil fuel (Worthington, 2015). Meanwhile, PV technology has been increasingly challenged by CSP because of the good thermal energy storage that can produce electricity after sundown. Due to this, solar thermal power plant (STPP) also known as CSP plant has been considered and installed in different countries like USA, Spain, Europe, China, and South Africa.

In figure 1-1, different types of concentrating solar power plant system (CSPPS) that are being employed for power generation are shown. CSP plant can also be used as a hybrid system[2] and still produce electricity.

---

[1] Renewable Energy represents an indispensable power supply for the sustainable development of infrastructure

[2] Hybrid system is a system that uses fuel like natural gas to complement solar energy all through the periods of low solar irradiation.

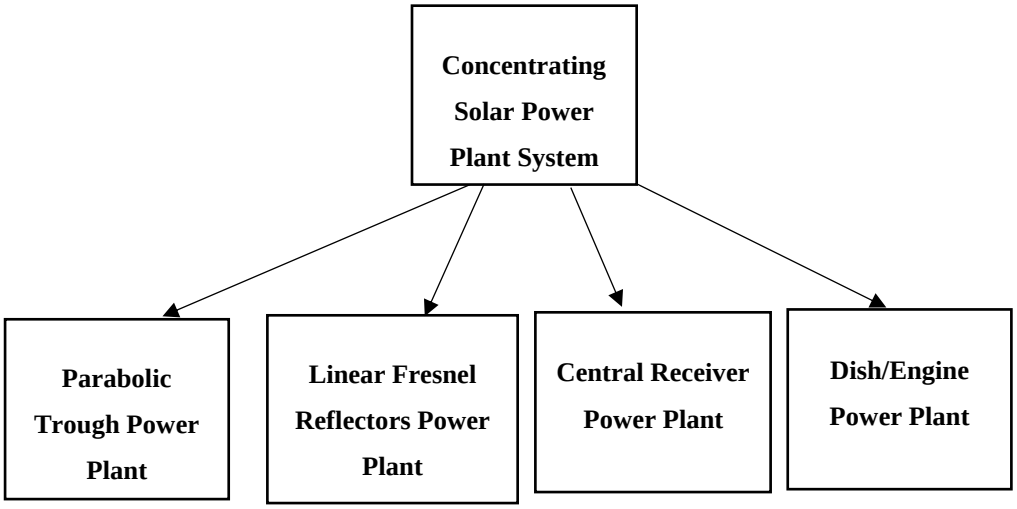

Figure 1-1: Different types of CSP plant

Currently, in South Africa, six CSP plants have been constructed and are fully operational. Five of these plants (Xina, KaXu, Ilanga, Kathu Solar Park and Bokpoort) are parabolic trough power plants and the remaining one (Khi power plant) is a central receiver plant.

The central receiver or power tower technology is the most promising CSP technology for the future as it has the capacity to reach a higher temperature, and hence thermal efficiency, than the other existing CSP technologies. Figure 1-2 displays an example of a central receiver power plant. The central receiver power plant system comprises of mirrors called heliostats that track the sun about two axes. The heliostats reflect solar energy onto a receiver to heat a heat transfer fluid (HTF) which in turn is used to heat the working fluid (steam) inside the power block to generate electricity.

CSP plants are typically build in arid regions with good solar irradiation. Water is invariably scarce, and once-through cooling is usually not considered due to the large amount of water passing through the condenser. Furthermore, environmental legislation restricts the pre-treatment of water, and limits the maximum water outlet temperature to protect aquatic organisms, should the water return to its source. Once-through cooling holds a great advantage over direct-air cooling in terms of increasing the efficiency of the thermal power plant.

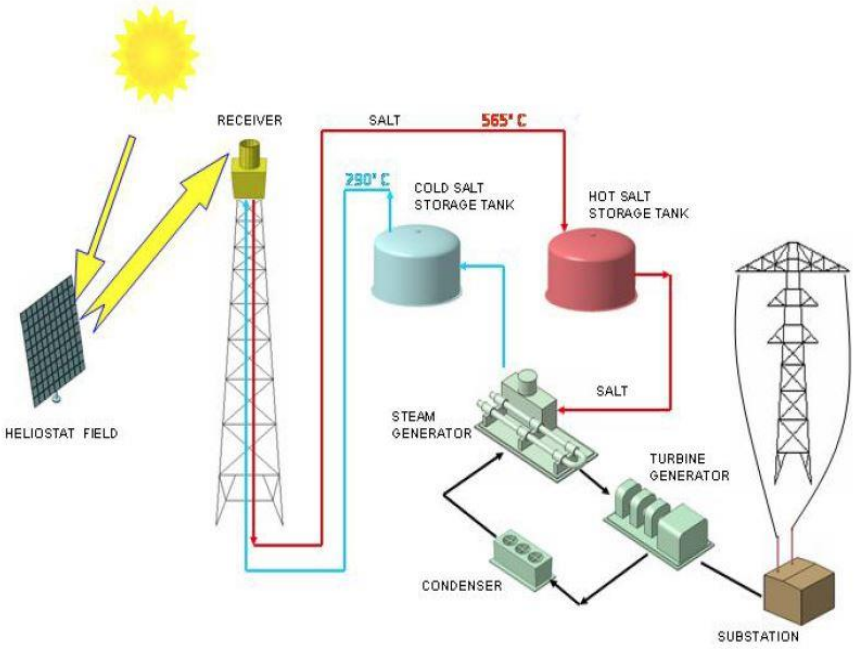

Figure 1-2: CSP central receiver plant (Cabeza *et al.*, 2012).

In South Africa, none of its CSP plants has been built on using the once-through cooling system for power production. This is due to a moratorium in SA to only use dry cooling in order to save water for human consumption. High rainfall regions typically have low solar irradiation that precludes the construction of the CSP plant in these regions. CSP plants are typically build in arid regions with limited water resources where there is high solar irradiation.

In 2005, the Geological survey in the United States of America (USA) estimated that thermal power plants were accountable for closely 52 % of surface freshwater removed from the ground or diverted from a water source. Most of the water is used by the closed evaporative cooling system (Kenny *et al.*, 2005). According to Feeley et al. (2008), once-through cooling only account for 7 % of the water used in power plants due to leakages while closed evaporative cooling account for 70 % which shows that once-through cooling has less water consumption than closed evaporative cooling technology. This is because once-through cooling will return almost all the cooling water back to its source.

In South Africa, 8 % of water is used in large industries and power generations, 18 % of water for rural and urban use, and 62 % of water resources are used for agriculture and irrigation (Roux *et al.*, 2012). The same patterns were observed in the sectoral water usage breakdown presented in the second National Water Resources Strategy (Water Affairs, 2013). This shows that agriculture and irrigation consume more water than power generations.

Flood irrigation is widely used by the farmers next to the Orange River in the Northern Cape. The water is withdrawn from the Orange River at the Buchuberg

Dam and used when needed by the farmers. The Department of Water Affairs (DWA) established the Kakamas Water User Association (Irrigation scheme) in 1994, one of three such schemes on the lower Orange River.The scheme consists of a canal on both sides of the Orange River which more or less track to the river course.

The scheme has a total area of 10 609 hectares, at a scheduled quota of 15 000 m^3/ha/a (Water Affairs, 2013), or an average flow rate of 5 m^3/s. The farmers are mostly pumped water from the canal while some pump directly from the river to their farmland. Designed as a flood irrigation scheme, only 10 % is irrigated with micro and drip irrigation system while 90 % are majorly still irrigated by flood irrigation system (Water Affairs, 2013). As water is used to irrigate crops, and not returned to the river, the restrictions imposed by environmental legislation can be relaxed.

All engineering circuits cooled with natural freshwater or seawater is affected by the occurrence of biological fouling consisting of biofilm growth and settlements of several kinds of living organisms. Most of these power generation plants efficiently operate by using the basic tool of physical screening, physical cleaning and chemical treating. The traditional way of chemical control of microbial growth and biofouling in power plants is the use of chlorine, in spite of the fact that chlorination was subjected to the environmental authority's attention for more than 25 years, because of its halo-methane and other by-products items.

1.2 Research problem statement

Over decades, the once-through cooling system is known for using water withdrawn from the river to cool the steam entering the condenser and returned the water back to the river. Although this process can increase the thermal performance of the power plant (Fleischli and Hayat, 2014) but it has many factors that affect aquatic life, which includes the fouling and outlet water temperature.

Due to water scarcity in arid regions, once-through cooling has not been used in CSP plant but they rather use direct air-cooling, closed cooling or a hybrid cooling system. The ambient air temperature affects the performance of direct air cooling systems and often reduces thermal efficiency of the CSP plant.

In South Africa, the availability of water is a challenge since the majority of CSP plants are built in arid regions (for good solar resource) where water is scarce. They mostly rely on dry cooling, except for the Bokpoort Power Plant that uses an evaporative cooling system.

Due to the recirculation of the cooling water in a closed system, fouling agents build up, and some of the cooling water has to be replaced with fresh (make-up) water. The cold-water temperature is limited by the wet-bulb temperature of the air and the approach temperature that is a function of fill design. This limits the thermal efficiency of an evaporative cooled CSP plant, although it is usually better than that

of a direct air-cooled plant. This reduction in the thermal power efficiency may impact on the income from the plant over a typical calendar year.

Since there is an existing irrigation system that is bypassing the river in Upington, there is an opportunity to look at the synergy between this system and CSP plant. Here, we look into the possibility of using once-through cooling on 50 MW_e solar thermal power plant, on/near the Orange River. We will determine if the irrigation system can provide sufficient water for once-through cooling of the CSP plant, and if it can indeed increase the performance of the CSP plant. Furthermore, it will be determined if discharge water from the condenser would be suitable to return to the irrigation system. We will identify any legislation constraint or government policy that limits the use of irrigated water for cooling CSP plant. Finally, we'll determine how many power stations can be served by the irrigation system.

1.3 Research aim and objectives

The primary aim of this thesis is to present a feasibility study of having a 50 MW_e STPP on/near the lower Orange River using the once-through cooling system, which is also known as open cycle cooling system. To fulfil this aim, the research was carried out with the following objectives:

- To investigate the impact of condenser fouling on the improved thermal efficiency
- To analyse the suitability of the discharge cooling water for irrigation agricultural purposes.
- To identify the agricultural and environmental constraints.

1.4 Research limitations

CSP plant is a large-scale project that is expensive to build at the time of this study. Its mechanisms and services need to be on a large scale before they can be highly effective. Although Goodenough (2013) developed a portable fouling test facility, budget constraints ruled out fouling tests on the Orange River. Extrapolation of test data from the Vaal River will be used instead. The study assumes that land suitable for the development of a solar thermal power station is available close to the irrigation canal, and that access to a nearby power distribution line is available. These challenges might prevent the construction and performance prediction of a real CSP plant.

1.5 Thesis framework

This thesis contains the following sections, which are:

Chapter 1: Introduction - entails background information, problem statement, aim and objectives, limitations and thesis framework

Chapter 2: Literature review – entails history of CSP plant, the state of CSP in South Africa, CSP plant cooling system, condenser in a CSP plant system, quality of water used in the cooling system and lower Orange River and Agricultural use

Chapter 3: Once-through cooling condenser - includes a description of a surface condenser, factors affecting surface condenser, modification of fractured condenser tube

Chapter 4: Description of CSP plant – entails the heliostat field, central receiver, thermal energy storage, steam generator, and power block.

Chapter 5: Plant modelling – includes weather and site location, heliostat field, central receiver, thermal energy storage, steam generator, and power block.

Chapter 6: Model validation – includes the heliostat field validation, receiver tower validation, power block validation.

Chapter 7: Model result – entails heliostat field, receiver tower, and power block.

Chapter 8: Conclusions and recommendations

Appendices: This includes thermos-physical equations, different cooling systems in CSP plant in South Africa, heliostat field simulation result and sample calculations.

Chapter 2

Literature review

Overview

In this chapter, the history of CSP plant with thermal energy storage is explained in detail. Then the state of the CSP plant in South Africa is discussed. Different cooling systems are presented and the importance of water quality for CSP plant is discussed. Finally, agronomy in lower the Orange River Irrigation Scheme is addressed.

2.1 Concentrating solar power plant

The first concentrating solar power (CSP) plant, called Solar Electric Generating System (SEGS 1), was constructed in 1984 (Pavlović *et al.*, 2012) and began operation in 1985. This plant was extended to include an additional eight SEGS plants, which are located in California. SEGS is still in operation today.

Solar One, completed in 1981, was the first pilot scale central receiver plant; build by the US Department of Energy at Barstow, California. In 1995, Solar One was retrofitted with an increased number of heliostats and a molten salt HTF system. The retrofitted plant was named Solar Two (Plaza, 2008). After the success of Solar One and Solar Two, the 20 MW_e Gemasolar Power Plant, near Seville in Spain became the first commercial central receiver solar thermal plant. Gemasolar has 15 hours of thermal energy storage, which results in 24 hours of power production by means of Solar energy only (García and Calvo, 2012). In 2007, the 110 MW_e Crescent Dunes CSP plant was constructed in Nevada (Moore *et al.*, 2010).

According to Dinter and Möller (2016), Andasol 1 was the first profit-making CSP plant to be built in Europe, in 2008. This plant set an example for the next generation of CSP plant, after which Andasol 2 and 3 were also constructed. These 50 MW_e Spanish parabolic trough plants have about 7 hour molten salt thermal storage each (ESTEA, 2013). The scale of CSP plant was enlarged in the United States by Solana. Solana is a parabolic trough CSP plant with an expected electrical yield of 944 GWh_e per year and a solar field with an area of 2.2 million m^2 (Solar, 2013)

Between 2008 and 2013, government support through attractive feed-in tariffs and renewable energy quotas made the growth of many more CSP plant in Spain possible. The Italian electrical utility, ENEL, built a 5 MW_e demonstration CSP plant in Sicily in 2010 (Falchetta and Rossi, 2013). In Chile, a 110 MW_e power tower CSP plant is currently under construction with about 18 hours of direct thermal storage using molten salt (Nacional and Brasile, 2012). The use of molten salt as HTF and storage medium makes these CSP plants more attractive than direct

steam central receiver CSP plant. This is because of their storage abilities and low working pressures compared to steam.

In recent years, CSP technology has been implemented on the African continent where six CSP plants in South Africa and Noor I - III in Morocco are all in operation. Also in South Africa, the 100 MW_e Redstone Central Receiver Plant with molten salt as HTF and with 12 hours thermal energy storage is currently under construction (SolarReserve, 2018).

Ivanpah solar electric generating system in the Mojave Desert is the biggest CSP complex in the world according to peak generating capacity of 377 MW_e (Boyd and Byron, 2010). The recent state of the art of CSP power tower technology that will come into operation in the Crescent Dunes in the USA is the 110 MW_e plant with 10 hours of direct molten salt storage installed (SolarReserve, 2017). This shows that power tower technology is considered the best technology for the future because of its ability to reach high temperature and that it enables storage capacity.

In the central receiver CSP plant system, Li et al. (2016) modelled solar concentrators of increase in area. The steering constraints on mirror orientations and shadow effects by blocking the incident or reflected solar radiation are two factors considered. Talebizadeh et al. (2013) established six categories of heliostat field layouts for determining maximum efficiencies in central receiver CSP plant and likely potential enhancement because of multiple apertures in the central receiver systems with secondary concentrators. Wu et al (2010) studied different gap sizes between the facets of the mirrors experimentally and numerically for the purpose of reduction of wind load on mirrors.

Sánchez and Romero (2006) described an optimization technique to determine the yearly-normalized energy available for a known tower height. Zoschak et al. (2009) concentrated on the design and operating features of a natural circulation steam-generating receiver (cavity-type) for a 10 MW_e central receiver CSP plant. Eck et al (2006) presented the dual receiver model for the improvement of the central receiver performance to the steam cycle in a CSP plant. The water is vaporized directly into the cylindrical steam generator, while preheating and superheating is done in heat exchangers by means of hot air from the volumetric receiver. The results confirm the benefits of the new concept for the annual mean efficiency, which increased from 13 % to 16 %.

Frang et al. (2011) suggested a joined Monte-Carlo calculation technique for assessing the thermal performance of the solar cavity receiver. With this technique, under different wind environments, the thermal performance of a solar cavity receiver and a saturated steam receiver is simulated. (Ávila-Marín, 2011) studied volumetric receivers and development of new designs to reduce heat losses and also discussed other significant issues, such as the basic plant configuration, flow stability phenomenon and the main problems of window design for pressurized receivers. Montes et al. (2009) examined a new optimized heat transfer model in the absorber surface of a thermos-fluid dynamic design of a solar central receiver. This theoretical scheme has been applied to the precise instance of a molten salt single cavity receiver, although the configuration proposed is appropriate for other

receiver designs and working fluids. (Collado and Guallar, 2013) presented a quick way of evaluating the annual overall energy collected by a surrounding heliostat field to improve on CSP power tower technology.

Yang et al. (2010) investigated the interaction between the heat transfer performance and the thermal efficiency of a molten salt receiver used in the central receiver CSP plant. The results of the test show that the heat transfer performance of the molten salt receiver is improved and the radiation and convection losses are significantly reduced, using the spiral tube as the heat transfer tube. Xu et al. (2011) analyse a theoretical framework for the energy and exergy of the central receiver CSP plant system using molten salt as the heat transfer fluid. Both the energy losses and exergy losses in each component and in the overall system are assessed to detect the causes and locations of the thermodynamic deficiency. The results show that the maximum exergy loss occurs in the receiver system, followed by the heliostat field system, and the main energy loss occurs in the condenser of the power cycle system. They also presented a model of 1 MW_e Dahan central receiver CSP plant using a mathematical modular modelling method. The dynamic and static characteristics of the power plant are studied based on these models (Xu *et al.*, 2011). With the improvement in the central receiver (power tower) CSP plant technology, it shows that CSP power tower has the potential to reach a higher temperature than any other CSP plant and its technology will be used for modelling in this thesis. It also shows that none of these CSP technologies uses once-through cooling system.

2.2 CSP and its costing in South Africa

CSP is one of the renewable energy technologies that depend on the direct normal irradiance (DNI). South Africa (SA) is one of the highest DNI's in the world based on the yearly solar irradiation, making solar energy a serious contender in the generation of renewable energy, adding to the existing grid and reducing carbon emission (Gauché, Backström and Brent, 2012). South Africa's best DNI is in the Northern Cape region where the annual DNI received varies between 2800 to 3000 kWh/m^2 as shown in figure 2-1. This is greater than the DNI available in either Spain (2100 kWh/m^2) or the USA (2700 $kWh/m^{2)}$, both countries with STPP in operation at full capacity (Fluri, 2009).

South Africa intends to generate 42 percent of its electricity from renewable energy by the year 2030 of which CSP is one of the key renewable energies that has been prioritised (DoE, 2017). In order to achieve this, the SA Department of Energy (DoE) through its Renewable Energy Independent Power Producer Procurement Programme (REIPPPP) rolled out sets of bid windows to regularise the Renewable Energy Technology (RET) price. The sets of windows 1, 2, 3, 3.5, and 4 have confirmed the economic viability of CSP, as they attracted investment capital of up to ZAR 53 billion (DoE, 2018).

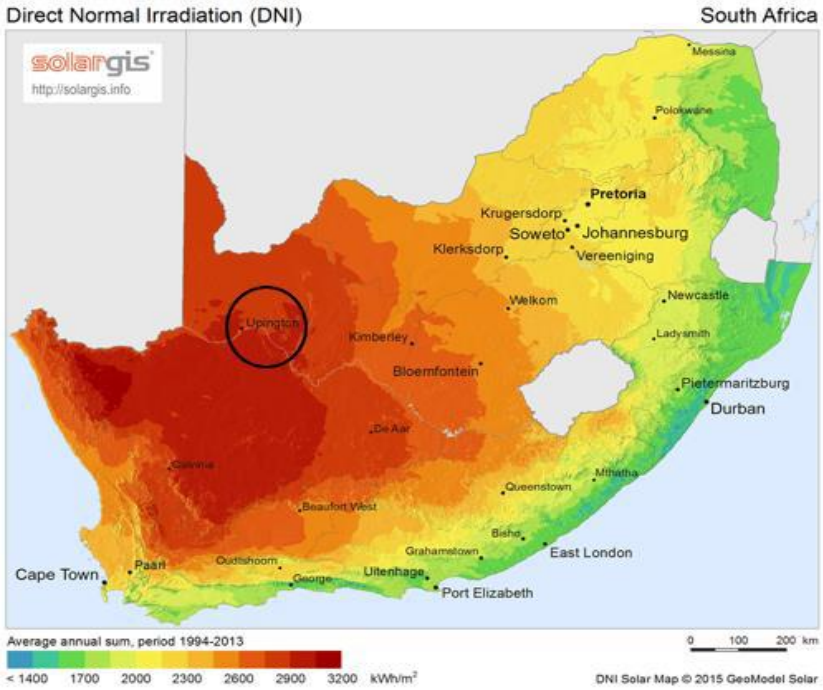

Figure 2-1: South Africa average daily direct normal irradiation (SolarGIS, 2011)

During the bid windows 3 and 3.5, a two-tier tariff plan was introduced which divided the initial single tariff plan into a peak hour rate and a base rate. The electricity price increases by 270 percent of the base rate during the peak hours (Department of Energy, 2015). Figure 2-2 shows the base hour price of 1.82 ZAR/kWh and peak hour price 1.70 ZAR/kWh at bid window 3 while 1.70 ZAR/kWh base hour price and 4.58 ZAR/kWh as peak hour price at bid window 4. The bid window 3.5 was not inclusive to CSP in order to inspire the two-tier tariff established.

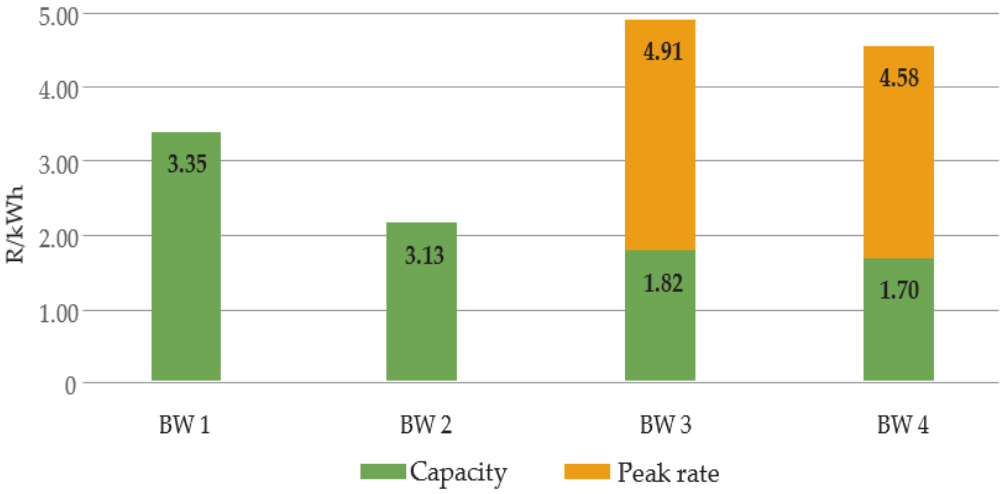

Figure 2-2: Average bid windows price for CSP (Department of Energy, 2015).

Meanwhile, 600 MW_e of CSP was bought during the fourth bid windows, and 500 MW_e is now connected to the grid, while the remaining 100 MW_e plant is under construction (NREL, 2018a).

The technology type, capacity, cooling system and locations of various CSP plants in SA are presented in Table B-1. The DNI resource at a CSP location has a great impact on the price of CSP electricity (Barlev, Vidu and Stroeve, 2011). The price of CSP electricity at the first bid window was lower than that of PV, but as the bid windows progressed, PV and other RETs experienced drastic reductions in their prices whilst electricity cost from CSP remained fairly expensive (Viebahn, Lechon and Trieb, 2011).

According to International Renewable Energy Agency (2018) (IRENA, 2018), the levelised cost of electricity (LCOE) of CSP is difficult to analyse because of the factors affecting the determination of the LCOE which include high initial investment capital, a relatively low operational and maintenance cost, and small or no fuel price. Therefore, due to the availability of solar resources in SA, CSP has the potential to achieve the lowest electricity price under good policies and support.

2.3 CSP plant cooling system

To improve the net output of the CSP plant, it is important to develop a cooling system that has the capacity to cool the steam leaving the condenser to the lowest possible temperature. This cooling system is divided into two types namely, once-through cooling system and closed cooling system.

2.3.1 Once-through cooling

Once through cooling is also called open cycle cooling system. It is used for power plants sited beside large water bodies such as the sea, lakes or large rivers that have the ability to dissipate the waste heat from the steam cycle. Figure 2-3 shows an open cycle system; water is pumped from the intakes on one side of the power plant, passes through the condensers and is discharge at a point remote from the intake, to prevent recycling of the warm water discharge.

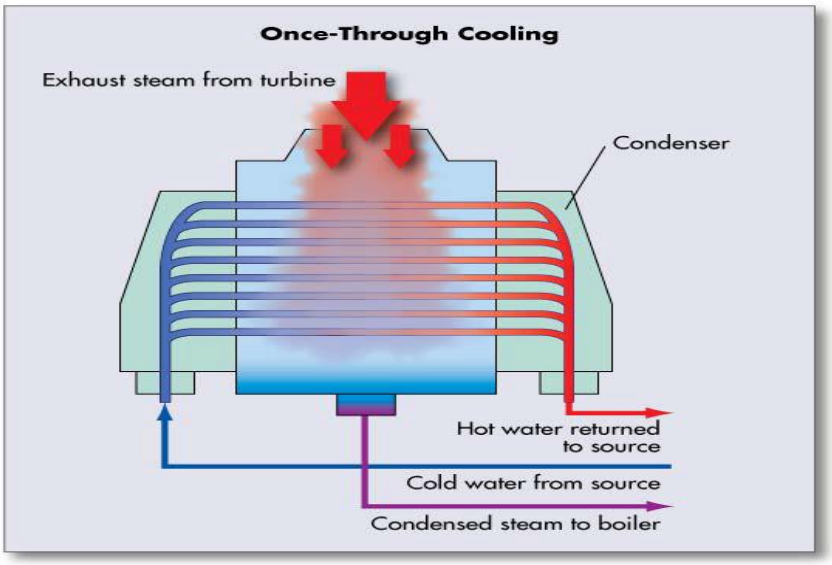

Figure 2-3: Once through cooling (EPRI, 2013)

Environmental requirements have become more stringent on the allowable rise in temperature of the receiving waters, so that in many countries worldwide, often open cycle cooling systems are used only when sea water is available and for inland power plant installations, closed cooling systems are more commonly used (EPRI, 2013).

2.3.2 Closed Cooling

Micheletti et al. (2002) describes closed cooling as a radical decrease in water requirements, which is accomplished by avoiding the release of cooling water once it has absorbed heat from the condenser. Then, the water itself is cooled by rejecting heat to the atmosphere and recycled. The water is merely a carrier or heat exchange fluid between air and steam.

Close cooling systems partially remove the constraint of water availability in power plant and contribute to a great reduction in water needs. Water is saved because of recirculation in a higher cycle system. The number of cycles depends on the technology of the system with respect to tolerable temperatures, water quality, and discharge requirement. Good water quality allows a longer retention time; hence a higher number of cycles before new water must be introduced into the system (EPRI, 2013). The different types of closed-cooling systems include evaporative towers, dry towers, hybrid towers, ponds and spray-ponds. These technologies are more expensive than once-through cooling because of the higher condenser temperature and extra capital equipment.

2.4 Condenser in a CSP plant system

In CSP plant system, the condenser determines the temperature at which the steam condenses and its performance has a key effect on the net output of the plant (Moon and Zarrouk, 2012).

2.4.1 Condenser

The function of a condenser in a CSP plant is to condense exhaust steam leaving the steam turbine by rejecting the heat of vaporisation to the cooling water passing through the condenser. Once the steam has left the turbine, it enters the condenser where heat is removed until it condenses back to water. This is done by passing the wet steam around thousands of small-bore cold-water tubes and the cold water is usually supplied from a lake, the sea, a river or from a cooling tower. The condensed steam is collected at the bottom of the condenser and returned to the boiler by means of feed water pumps, to start the water-to-steam, steam-to-water cycle again.

As the steam experience a phase change in the condenser, its temperature and pressure are linked. The corresponding pressure is called the turbine backpressure. At the exhaust of the low-pressure turbine, the higher the exhaust steam pressure entering the condenser the lower the condenser vacuum will be and the turbine efficiency will be lower (Çengel, Cimbala and Turner, 2017). Haldkar et al. (2013) explain further that decreasing the condensate temperature will result in a lowering of the turbine backpressure and increasing turbine power output and efficiency.

2.4.2 Types of condenser

According to Cengel et al. (2017), condensers are divided into two types, namely, direct-contact type and indirect- surface type. In direct contact types, the cooling water is sprayed directly into the steam. This type of condenser is used in applications where the cooling water is of the same quality as the steam condensate. Systems that have dry-cooling sometime use direct contact condensers whilst steam and water is separated by a physical wall in indirect-surface type condensers. Steam is converted from its gaseous to liquid state at pressures below atmospheric pressure. This type of condenser (vacuum surface condenser) will be use in this study hereafter on STPP. Examples of direct and indirect condenser are shown in figure 2-4 below

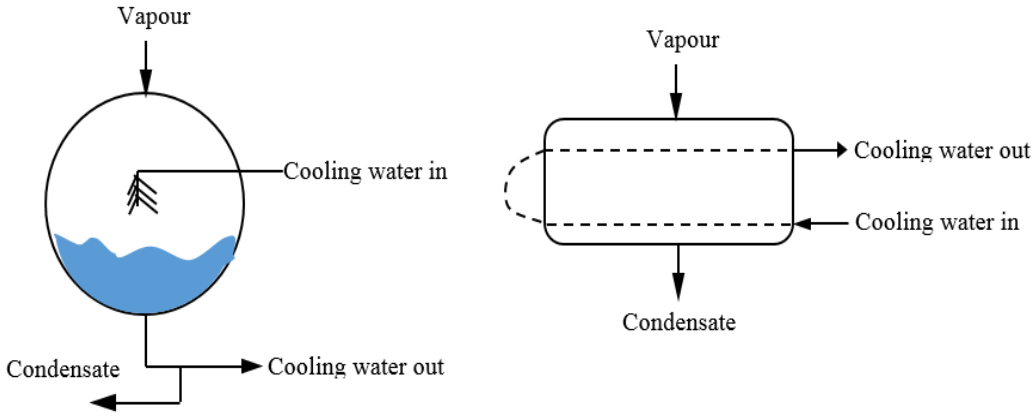

(a) Direct type: direct contact spray condenser (b) Indirect type: shell and tube condenser

Figure 2-4: Examples of direct and indirect contact type

2.5 Quality of Water for Cooling System

When considering the quality of water for a cooling system in STPP, the main concern is that it should not form a scale, fouling, coating, or film on the condenser tubes. A scale thickness of 1 mm can reduce the heat transfer by one-half (Moon and Zarrouk, 2012). Another concern is that no corroding constituents are present in the water especially with semi noble metal systems. Unfortunately, plenty of the control processes that reduce scale also act to enhance corrosion. Therefore, control of water quality must be done carefully and on an individual basis with respect to the specific water being used.

2.6 Lower Orange River and Agricultural use

The Orange River, which is SA's major river, originates in the Drakensberg Mountains in Lesotho. The river flows 2200 km westward, ending up in the Atlantic Ocean at Alexander Bay. At the Orange River's source, the rainfall is approximately 2000 mm per annum and the levels of the rainfall decreases as the river flow westward. The Buchuberg and Kakamas Irrigation Schemes along the Orange River in the Northern Cape were established by the Department of Water Affairs (DWA), ranges from roughly 120 km southeast and to 95 km southwest of Upington (Water Affairs, 2013).

Agriculture is the major economic activity along the lower reaches of the Orange River. Farms usually stretch from the riverbanks to land beyond the canal, which divides them into "inner land" and "outer land". The inner land is arable land situated between the river and the canal and is coupled to a canal water right. Flood irrigation is usually used for this land unless the land is unusually steep. The outer land is land situated on the inland side of the canal and requires an alternative form of irrigation if the land is to be developed. Livestock farming with high-value crops such as grapes, pistachios, citrus, pecans and vegetables grown in a narrow riparian strip along the Orange River, supported by intensive irrigation supplied directly from the river (Water Affairs, 2013).

Chapter 3

Once-through cooling condenser

Overview

The vacuum steam surface condenser with the factors affecting the condenser tube is described in this chapter. The ways of modifying fractured condenser tube is discussed.

3.1 Description of a vacuum steam surface condenser

Cooling water goes into the water-box before transiting through the half of the set of tubes at the right side as shown in Figure 3-1. The return water-box channels the cooling water to the other half of the set of tubes to complete the second pass and lastly, the cooling water leaves the water-box on the left side. This water-box is usually provided with man holes on hinged covers to allow inspection and cleaning. The exhaust steam coming out of the turbine goes into the top of the condenser and flows down through the ducts between the tubes. These ducts, or steam paths, are designed to avoid extreme condensate flooding, lessen excessively high vapor velocities, and reduce steam pressure drop. As latent heat is removed from the steam, it condenses and drops into the sump region (often referred to as hot-well region) under gravity. Non-condensable gases are liable to build up in the region of lowest pressure. Air and other non-condensable gases are removed in the air removal zone. Basically the air removal is accomplished by venting the steam space of the shell by means of either steam jet-air ejectors or liquid ring vacuum pumps. A drip roof (also called vent duct) is created to form a channel to remove the non-condensable gases and also helps to reduce the quantity of entrained water being removed along with the non-condensable gases as shown in Figure 3-1. The condenser is one of the essential components in the power block cycle; any tube leak in the condenser will result in forced downtime of the power plant.

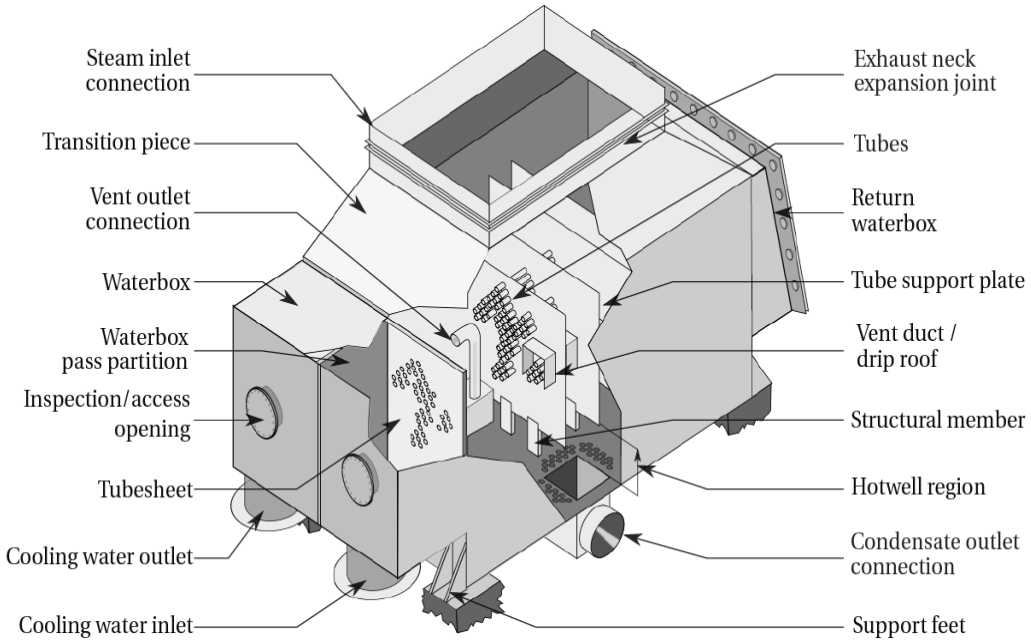

Figure 3-1: Schematic of a two pass, single compartment steam surface condenser (Goodenough, 2013)

Leaks may occur from tube erosion or punctures through tube-to-tube sheet joint, and cause cooling water of the low-grade to infiltrate and pollute the high-grade condensate in the steam space. The situation is driven by the condenser operating under vacuum, so any small pin-hole results in abundant quantities of cooling water leaking into the steam space. When this happens, it decreases the thermal efficiency of the steam power plant, increases the requirement of cooling water, reduces the heat transfer due to the poor thermal conductivity, increases the boiler feed water corrosion and also it can have an effect on the turbine blades.

Corrective action begins by decreasing power output and if a condenser has a multi compartment shell, the turbine is ran under partial load. This permits for draining off the affected compartment of the condenser to permit access into the water-box. Then the leak needs to be recognized, which in itself is a formidable task as the tube bundle can consist of about 10 000 tubes. The damaged tube is then isolated from service by fitting sealing plugs at both of its ends. Thereafter, a high-level water test is performed to ensure that the fitted plugs successfully seal the injured tube (Goodenough, 2013).

Janikowski (2003) classifies materials used for tubes in steam surface condensers into three categories which are stainless steels, copper alloys, and titanium. The type of materials to be used, is based on the operating conditions of the condenser and whether the cooling fluid is fresh water or sea water.

Stainless steels are often used in air removal areas and in peripheral zones of the tube bundles because of its higher corrosion resistance and lower thermal conductivity.

Copper alloys have a high thermal conductivity, high corrosion resistance and it is widely used throughout condenser history, especially in sea water applications. The increase in copper alloy's resistance to corrosion is due to the additional alloy elements such as tin and arsenic added to copper alloy. Copper is also inhibits bacterial growth.

Titanium has the highest corrosion resistance, but it suffers from stress cracking. Due to this, handling and installation of such tubes needs great care. Harmonics also need to be considered when changing current copper alloy tubes with titanium. The relatively low thermal conductivity of titanium is countered by the reduced wall thickness, made possible by its good mechanical strength.

3.2 Factors affecting a surface condenser tube

There are three essential factors affecting the performance of the surface condenser tube, which are fouling, corrosion and erosion.

3.2.1 Fouling

Fouling referred to as the accumulation of the unwanted deposits on the heat transfer surfaces of a heat exchanger. It has an impact on the heat rejected by the condenser by creating extra resistance to heat transfer and flow, which results in an increase in turbine backpressure and reduction in power plant efficiency. The fouling factor represents the theoretical resistance to heat flow due to a build-up of a layer of dirt or other fouling substance on the tube surfaces of the heat exchanger (or condenser), but they are often overstated by the end user in an attempt to minimize the frequency of cleaning.

In reality, if the wrong fouling factor is used, cleaning may actually be required more frequently. Goodenough (2013) built a double-pipe counter flow heat exchanger and calculated the fouling factor to determine the fouling rate over time for the heat exchanger. The condenser was built and tested at the Kriel coal fired power station. Cleaning of the condenser tubes was based on the fouling factor that was calculated.

Fouling is divided into micro and macro fouling. Macro fouling refers to organic or inorganic material, which causes a restriction of flow in the tube while micro fouling is a result of scaling, particulate and biological fouling and corrosion. Scaling and particulate fouling increase over time due to insoluble ions such as calcium and magnesium, which are present in the cooling water.

Calcium salts, which are less soluble in hot than cold water, are usually matted together with finely divided particles of other materials so that the scale looks dense, uniform and is sometimes porous in nature. This condenser fouling (or scaling) can be controlled by chemical treatment or mechanical descaling processes. These mechanical descaling processes entails the use of wire brushes or application of high –pressure water jets.

Dobersek and Goricanec (2007) analysed the influence of water scale on thermal flow losses on the surface of plate and pipe heat exchangers in domestic appliances and discovered that the water scale causes a lot of problems of heat transfer due to its very low thermal conductivity. Also, deposition of this scale restricts the cross-sectional flow area of the condenser tubes. Malayeri (2007) investigated the formation of fouling deposits on heat transfer surfaces by highlighting governing fouling mechanisms and introduced a revolutionary prediction method using radial basis functions.

Most times, the cooling water used in the condenser is not clean, contributing to the formation of scale and fouling in the condenser. For instance, the upper Orange River has a relatively large suspended sediment load and ranks as the most turbid river in Africa and the fourth most turbid in the World (Compton et al., 2007). In contrast, the lower Orange River considered for here for cooling the STPP have a low suspension load (60 mg/l, most of which was living green algae and not sediment) due to two large dams upstream of the confluence of the Orange and Vaal (its major contributory) Rivers. The water quality in the lower Orange River is comparable to that of the Vaal River (Compton et al., 2007).

3.2.2 Erosion and corrosion

Erosion occurs due to high levels of suspended solids and high velocities. Increase in turbulence at the inlet and outlets of the tubes trigger erosion and this is referred to as inlet-outlet erosion. Failure of the condenser tubes may be due to either pitting, surface-, galvanic-, or crevice corrosion, inlet erosion, or erosion-corrosion due to localized flow eddies.

Pitting corrosion is the localized corrosion of a metal surface confined to a point or small area that takes the form of cavities. Pitting corrosion is one of the most damaging forms of corrosion.

Pitting corrosion is usually found on passive metals and alloys such as brass alloys, stainless steels and stainless alloys when the ultra-thin passive film (oxide film) is chemically or mechanically damaged and does not immediately re-passivate. The resulting pits can become wide and shallow or narrow and deep which can rapidly penetrate the wall thickness of a metal. The shape of pitting corrosion can only be identified through metallography where a pitted sample is cross-sectioned and the pit shape, pit size, and depth of penetration can be determined.

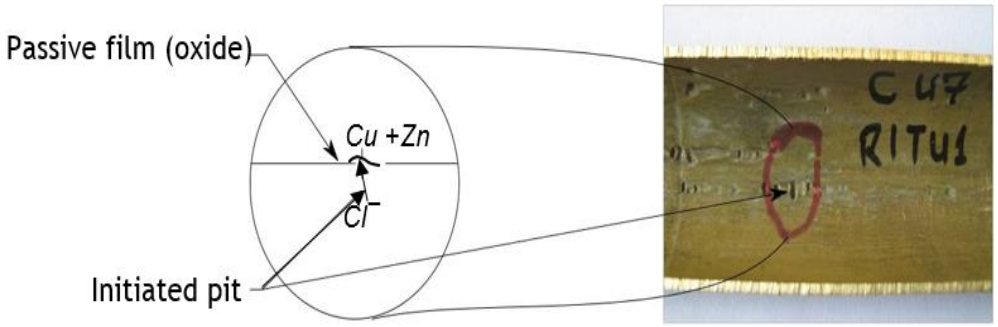

(a) Cross-section diagram of pit (b) pitting corrosion Picture (Goodenough, 2013)

Figure 3-2: Example of pitting corrosion in condenser tubes

Pitting corrosion is caused by the chloride ion present in the cooling water. Chloride ions damage the passive film (oxide) so that pitting can initiate at oxide breaks. Once this happen, the localized corrosion areas deteriorate until the material fails. If the tube is made of brass alloy as shown in Figure 3-2, the chloride ions will react with zinc strongly. This occurs because zinc reacts more readily with chloride containing water than copper. Then zinc chloride is produced, leaving a porous copper behind which is open to mechanical failures. This has been a key factor affecting the condenser tube failure especially in South Africa, which led to steam contamination as well as downtime of the equipment.

3.3 Modification of fractured condenser tube

To modify damaged condenser tube, there are major methods that can be used, which include refurbishment of the current tubes or replacement of the tubes. Refurbishment methods for the damaged condenser tubes include linings and artificial protective coatings. Putman's (2001) experiments on linings, which have been used before, shows that the lining can affect the performance of the tubes if not installed properly.

For the artificial protective coatings, application must begin with proper preparation of the surface of the tube before coating. Before this preparation takes place, the situation of the tubes must be observed and decision must be taken based on case specific standards. Meanwhile with the scale deposits and other contaminants, abrasive grit blasting, high pressure water lancing and or chemical cleaning can be used to remove them.

Curran (2009) examined condenser tube coatings as a substitute to re-tubing, and concluded that condenser tube coating can successfully extend the lifespan of a seawater condenser overhaul interval up to five years. He also showed that some condenser tube coatings had no adverse effect on the heat transfer rate. This is because the coated tube thermal conductivity after removal of the fouling layer was comparable to the fouled tube conductivity and it was further revealed that the

coated tubes had better heat transfer performance after three years of service than cleaned tubes in the unit. He concluded that coated tubes did not foul as quickly as the uncoated tubes. Field tests done by Malaga and Bengtsson (2008) on artificial protective coatings, suggested that APCs inhibit corrosion and fouling.

Goodenough (2013) evaluated the thermal performance of artificial coatings applied to individual tubes of a surface condenser in South Africa. He also found that artificial protective coatings has the ability to reduce fouling, corrosion and extend the lifespan of the tubes up to 10 years.

Tube replacement leads to production losses, a significant material, and labour costs. To replace damaged tubes may take up to three months, which means that during that period, the power plant will not be able to produce electricity. In cases where the current tubes have become irreparable and damaged, tube replacement remains the only way out.

Chapter 4

Description of CSP plant

Overview

This chapter describe in details the components of central receiver CSP plant (also known as central receiver STPP) which are heliostat, receiver tower, thermal energy storage, steam generator and power block.

4.1 Heliostat Field

From Figure 4-1, a heliostat contains a reflecting element that is typically a thin, low-iron glass mirror. The combination of several mirror module panels forms a heliostat, which is used instead of a single large mirror. When designing a heliostat, the following factors have to be considered: tracking and positioning errors, heliostat errors, and environmental conditions.

Heliostat error has to do with the mirror surface waviness, the gross curvature error of each mirror segment and the error linked to accurate canting of each mirror segment on the heliostat frame, which influences the flux profile produced at the receiver. Environmental conditions has to do with the wind speed and direction where the heliostat will be installed, while the tracking and positioning involve the movement of the heliostat about its azimuth and elevation axes so that it can produce slow, accurate and powerful tracking motion.

Figure 4-1: Heliostat (Wikipedia, 2018)

A heliostat is a sun-tracking mirror and a group of heliostat is called heliostat field, which gives us the ability to extract energy from the sun as shown in Figure 4-2. Due to the losses that occur in the heliostat field, the receiver will not be able to absorb all the energy collected from the sun by the heliostat field. These losses emanate because of heliostat field layout in the form of cosine losses, reflection losses, atmospheric attenuation, shadowing and blocking.

Figure 4-2: Heliostat field of Gema-solar STPP (García and Calvo, 2012)

Cosine losses, which is the main losses that decide the heliostat field layout, results from an individual heliostat's location relatively to the receiver and the position of the sun. To have a good heliostat field layout, the heliostats are positioned by tracking device so that its surface typically bisects the angle between the rays of the sun and a line from the heliostat to the receiver.

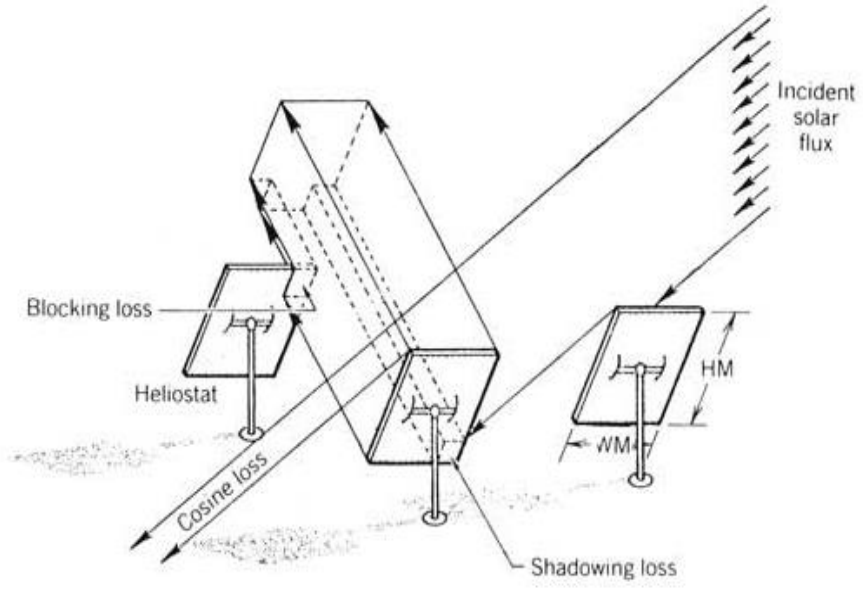

Figure 4-3: Cosine, blocking and shadowing losses from heliostat (Scheffler, 2015)

Then the heliostat effective reflection area is reduced by the cosine of one-half of this angle. Shadowing occurs at small angles of the sun when a heliostat casts a shadow on another heliostat at its back while blocking is caused when a heliostat is in front of another, intercepting the reflected flux going to the receiver as shown in Figure 4-3.

Blocking can be detected practically in a heliostat field by observing the reflected light at the backs of the heliostats. Atmospheric attenuation is due to scattering and absorption of sunlight by particles and water vapour, and mainly affects very large heliostat fields, where the outer heliostats are far from the receiver. Sengupta and Wagner (2012) analysed atmospheric attenuation in central receiver systems from DNI measurement.

4.2 Central receiver

The central receiver absorbs energy coming from the heliostat field and transfers it to the HTF running inside the tower as shown in Figure 4-4. This type of receiver is positioned at the top of a tower where reflected energy from the heliostats could be intercepted efficiently. During the construction of a central receiver, heat flux has to be considered. This heat flux must be able to pass through the surface of the receiver, and into the HTF, without overheating the walls of the receiver tubes or the HTF within them. The design of the tower and the types of HTF also has to be considered. Central receivers are divided into external receivers and cavity receivers.

External receivers consists of panels of several small-bore vertical tubes joined to form a cylinder. The top and base of the vertical tubes are connected to headers that allow the HTF to flow through the receiver.

Figure 4-4: External receiver (Solar Reserve, 2017)

In cavity receivers, the flux-absorbing surface is positioned inside an insulated cavity so that heat loss by convection from the receiver is reduced. It has a limited acceptance angle of 60° to 120°, which result in placing multiple cavities adjacent to each other, or restricting the heliostat field view to the cavity aperture's view. Not all energy absorbed by receiver can be transferred to the HTF due to receiver losses, which are convection losses, conduction losses, reflective losses, spillage losses, and radiative losses as shown in Figure 4-6.

Figure 4-5: Cavity receiver (CMI, 2016)

The major losses in the receiver are the radiation and convection losses which depend on the design of the receiver whether cavity or external receiver, its aperture area and its operating temperature. Conduction losses means heat conducted away from the receiver, which occurs because of heat lost through the receiver supporting brackets that connect the receiver to the tower structure.

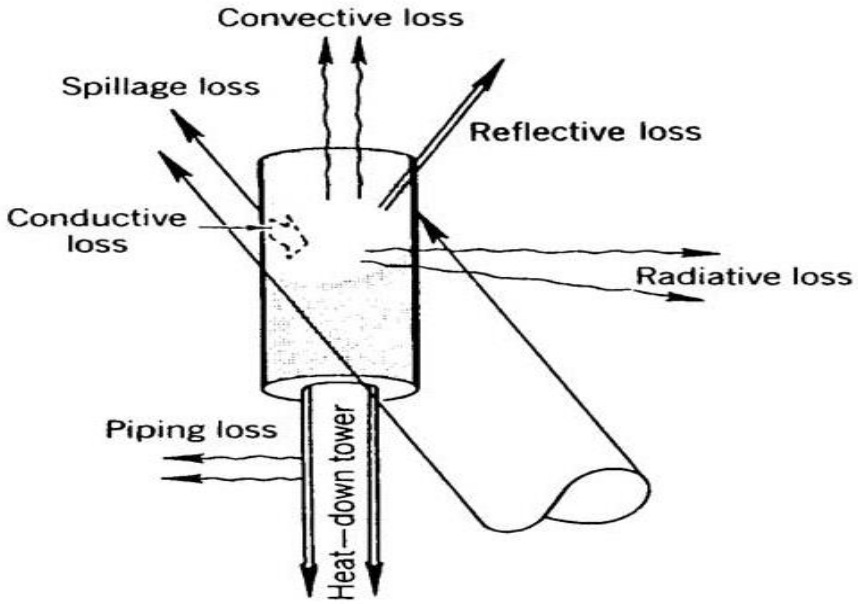

Figure 4-6: Receiver losses (Stine and Geyer, 2001)

Spillage losses occurs when not all the energy coming from the heliostat field falls on the absorbing surface of the receiver and are caused by both heliostat field and the receiver design. To minimise reflection losses, most receivers use high temperature, high absorptivity paint with an absorptivity of approximately 0.95 in the visible spectrum (Lambert, 2010) on its absorbing surfaces.

4.3 Thermal energy storage

Thermal energy storage (TES) is used during diurnal operation of a CSP plant. It stores energy during high DNI (day) and releases it to generate electricity when there is low or no DNI (night). Three major storage methods that can be used to store solar thermal energy which are latent energy, sensible energy and thermochemical energy, as shown in Figure 4-7.

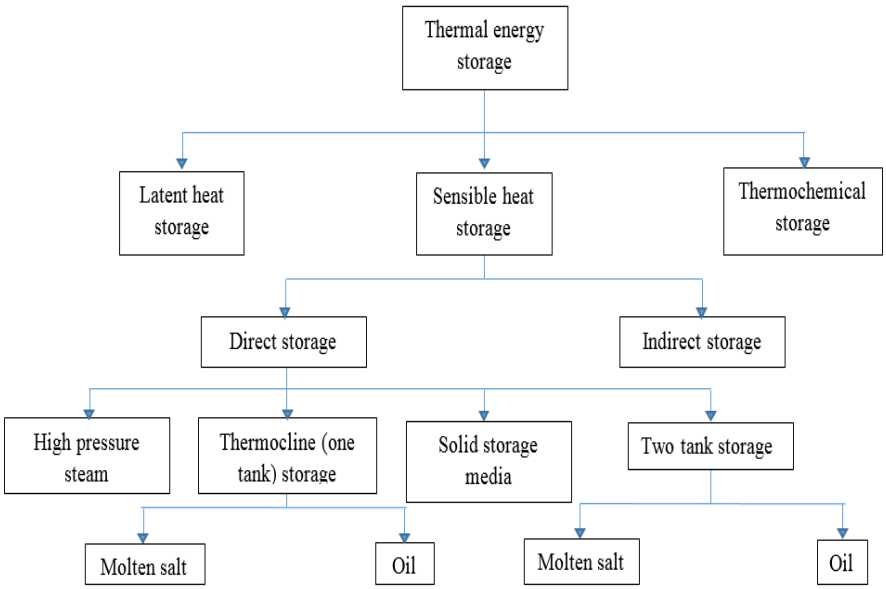

Figure 4-7: Different types of thermal energy storage

Gil et al. (2010) describes thermochemical energy as the use of chemical reaction for storage. This chemical reaction must be completely reversible so that the thermal energy can be recovered by the reverse reaction. Siddiq and Khushnood (2013) examined the use of sulphates, hydrides, ammonia, hydroxides and carbonates for thermochemical energy storage. They discovered that the gases required high-pressure storage to enable exothermic reactions that discharges heat for operation.

For latent energy storage, energy is can be stored isothermally due to the latent heat of phase change. This phase change can either be solid-liquid phase changes or liquid-vapour phase change but solid-liquid phase change is mostly used (Fernandes *et al.*, 2012).

Sensible heat storage requires a change in internal energy because of change in temperature of the material used. This material must have a high thermal capacity (product of density and specific heat), a good thermal conductivity, must not experience a phase change and must be inexpensive. When selecting a suitable material for sensible heat storage, density, vapour pressure, specific heat, operational temperatures, diffusivity and thermal conductivity must be considered. Sensible heat storage is further divided into indirect and direct storage.

Indirect storage entails the use of different mediums as HTF and for storage. According to Dunn (2010), indirect thermal energy storage is used in Andasol 1 CSP plant. Thermal oil is used as HTF. Part of the heated oil is used to generate steam inside the heat exchanger for instant power production whilst the remaining heated oil is used to heat the molten salt stored in the tank.

Direct storage uses the same medium (oil or salt) as storage and HTF. Solid storage media made of high temperature concrete, high-pressure steam, thermocline system (uses one tank for hot and cold fluid), and two tank molten salt systems are good examples of direct storage.

According to Gil et al. (2010), only sensible heat storage have been commercially used for STPP. Latent heat and thermochemical storage are still at the research stage. Two-tank molten salt storage has been widely used in CSP plant as both HTF and storage medium. The most commonly used molten salt, Solar Salt™, consists of a mixture of 60 % sodium nitrate and 40 % potassium nitrate by mass. It is inexpensive and has a high maximum operational temperature of 565 °C that increases the Ranking cycle's efficiency. Due to the relatively high solidification temperature (230 °C) of the salt, trace heating is employed to ensure that the salt will remain in a molten state in the pipes when there is insufficient solar radiation (Cavallaro, 2009).

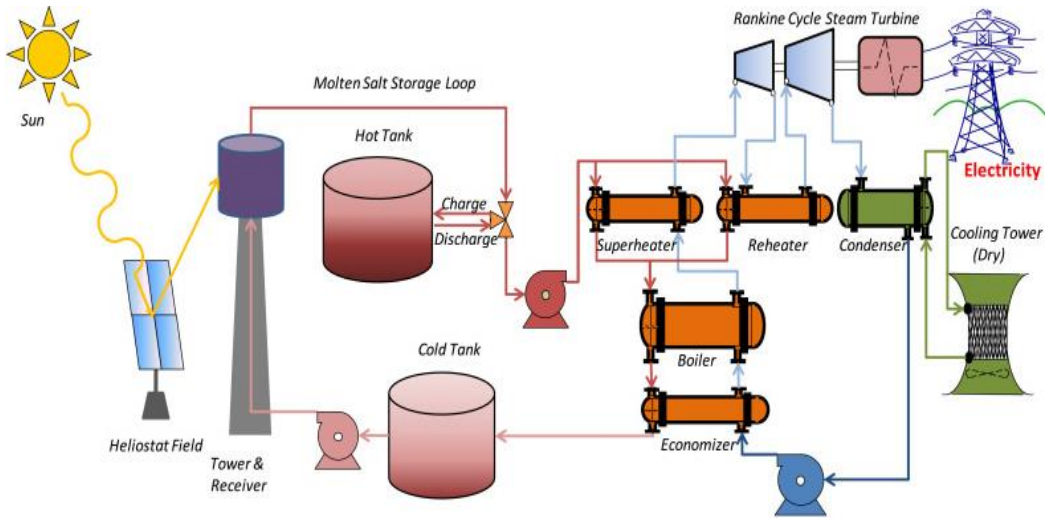

Figure 4-8: Power tower plant with two-tank molten salt system (Meybodi and Beath, 2016)

Figure 4-8 describes the process of a two-tank molten salt CSP plant. The molten salt collects heat from the receiver and is stored in the hot storage tank until needed. When there is need for power generation, the hot molten salt is pumped through the steam generator to generate steam that is used in the power cycle (Rankine cycle) for electricity production. The molten salt leaving the steam generator returns to the cold tank in order to begin the operation again.

4.4 Steam generator

Steam generator produces steam used in power cycle for power generation in CSP plant. The power block and molten salt system are the two main systems linked to the SG as shown in Figure 4-8. The SG consists of preheater, evaporator, super-heater and re-heater as shown in Figure 4-9.

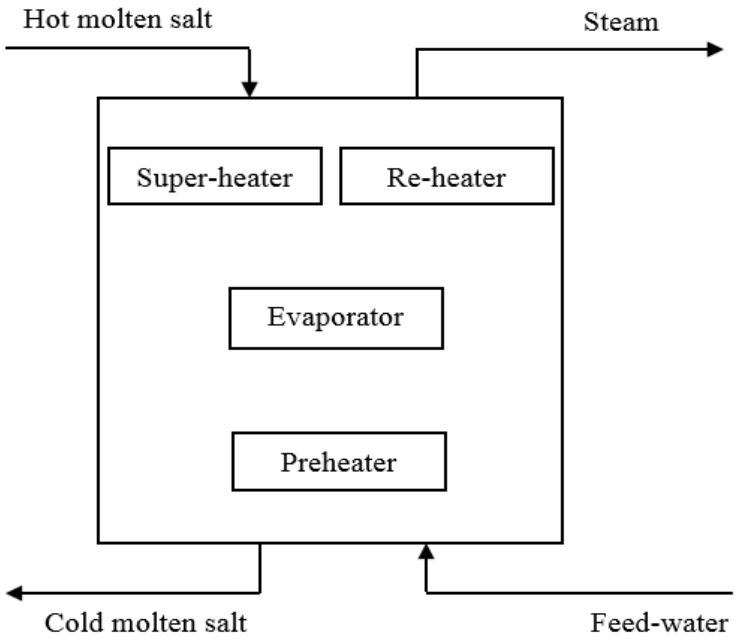

Figure 4-9: Schematic diagram of steam generator

The hot salt coming from the hot tank enters the steam generator (SG) at the super-heater where the saturated steam coming out from the evaporator is changed to superheated steam used in the power block for electricity production. The temperature of the hot salt drops as it passes through the heaters inside the SG and the pressurized feed-water is evaporated and superheated. In the evaporator, the hot molten salt leaving the super-heater changes the feed-water to saturated steam. The difference in temperature at the evaporator inlet between the molten salt and feed-water is called pinch point temperature.

4.5 Power block

An ideal Rankine cycle, as used inside power block of CSP plant consists of four processes which are isentropic compression in a pump (1-2), isobaric heat supply in a SG (2-3), isentropic expansion in a turbine (3-4), and isobaric heat rejection in a condenser (4-1) as shown in Figure 4-10.

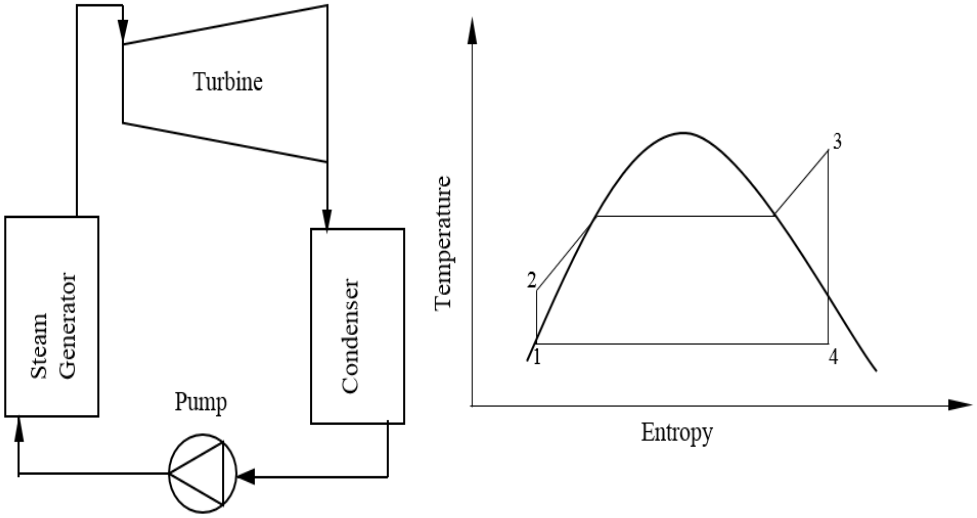

Figure 4-10: Schematic diagram of a simple ideal Rankine cycle

In a real Rankine cycle, steam generated from saturated feed-water is used as the working fluid. This steam flows through the turbine, where most of its enthalpy energy is changed into mechanical work to run a power generator that produces electricity. Not all the energy from the steam can be used for running the generating system because of losses due to viscosity and friction. The low-pressure steam from the turbine at state 3 is firstly condensed to liquid at state 4 and then pressurized in a pump to state 1. This high-pressure liquid water then flows through the SG, where it is heated to state 2 and reused in the Rankine cycle as shown in Figure 4-10.

In reality, heat loss to the surroundings and fluid friction across each component is irreversible which makes the actual steam power cycle differ from the ideal Rankine cycle. These factors affect the efficiency of the cycle. Because of the irreversibility of these processes, the pump inefficiency increases the enthalpy of the liquid leaving the pump and then, reduces the amount of energy required to evaporate the liquid. The efficiency of a real turbine directly is less than the work produced in an ideal turbine, as shown in Figure 4-11.

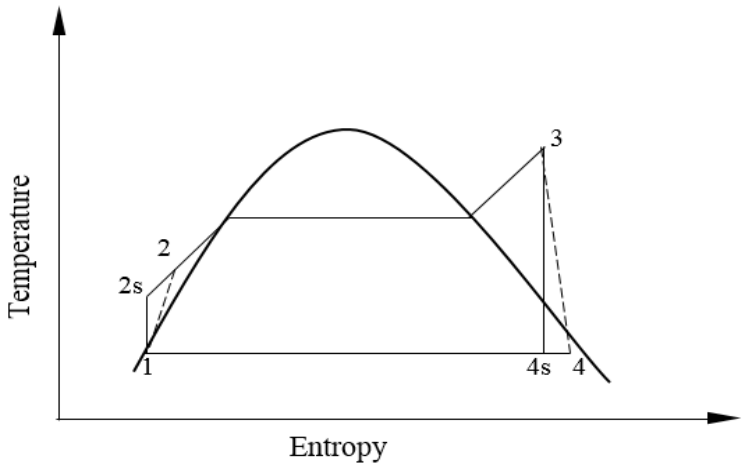

Figure 4-11: Pump and turbine effect on Rankine cycle

Increasing the SG pressure at a fixed turbine inlet temperature will increase the steam moisture content at the turbine output, which is undesirable in the system. This can be rectified by reheating the steam in between two stages of the steam turbine, as shown in Figure 4-12. The steam is partially expanded at the high-pressure turbine and returned back to the SG where it is re-heated at constant pressure, enters the low-pressure turbine where it is expanded to the condenser pressure. Optimum re-heat pressure is about one-quarter of the maximum cycle pressure (Çengel and Boles, 2011).

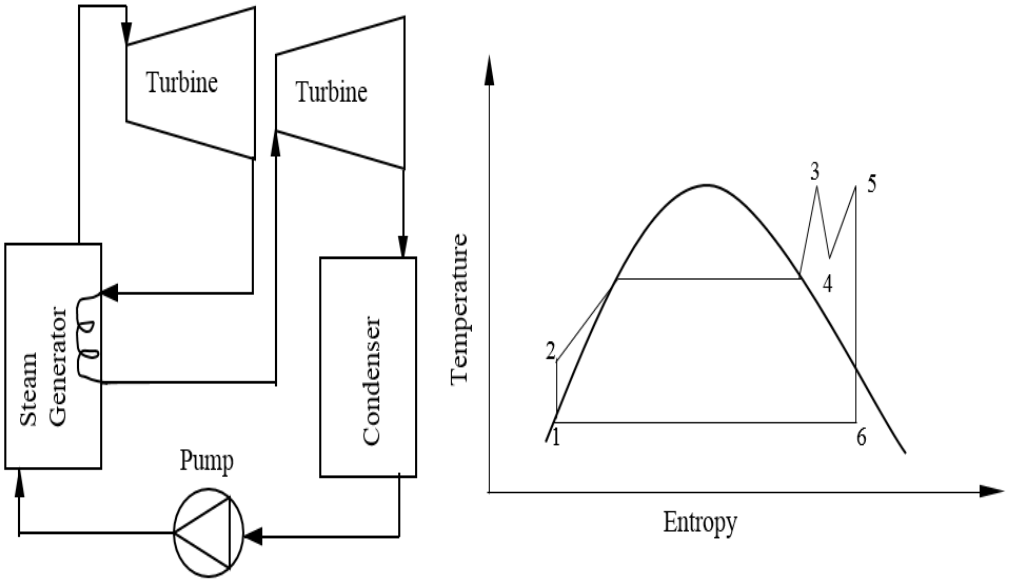

Figure 4-12: Schematic diagram of re-heat Rankine cycle

Increasing the SG inlet temperature will increase the average temperature at which heat is supplied. This is done by preheating the feed-water with steam bled from the turbine through a process called regenerative heating, as shown in Figure 4-13.

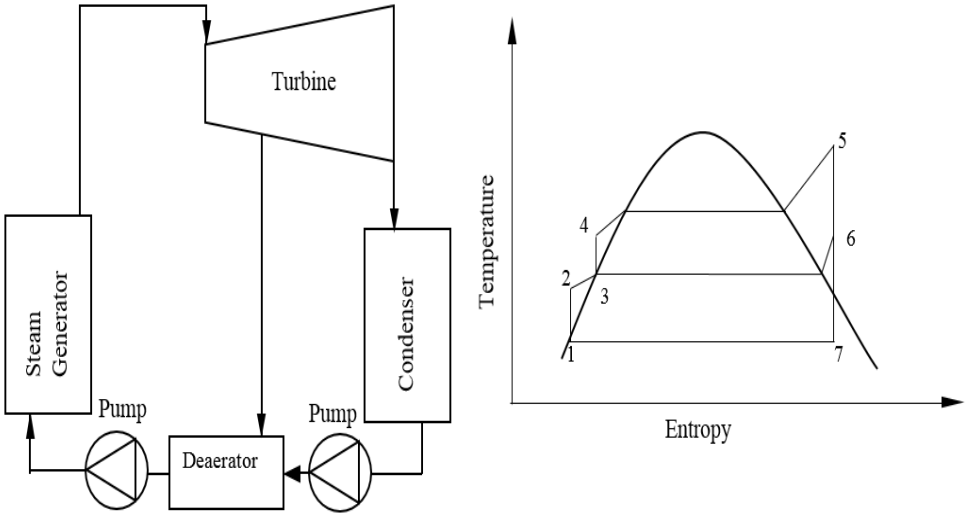

Figure 4-13: Schematic diagram of regenerative Rankine cycle

Small quantities of steam may be extracted from the turbine at different extraction points to heat the input SG feed-water. Regeneration helps to eliminate the air that escapes from the condenser in the deaerator, which prevents corrosion in the SG and it is used to increase the thermal efficiency of the Rankine cycle.

.

Chapter 5

CSP plant modelling

Overview

This chapter covers selection of site location for CSP plant and how the weather data for the site selected is collected. The code Solar-PILOT was used to calculate heliostat field efficiency is described. Modelling of the heliostat field efficiency, receiver, thermal energy storage, steam generation, power block and once-through condenser is discussed in detail.

5.1 Weather data and site location

The site selected for the case study for modelling CSP plant is Upington, in the Northern Cape Province of South Africa, with the coordinates listed in table 5-1 below. Upington is situated on the banks of the Orange River.

Table 5-1: Site Location

Latitude	Longitude	Elevation
-28.395	21.2368	879

The weather data was collected from the Solar Radiation Data database, called SoDa (SoDa, 2018). SoDa is a web service, comprising of several services for generating weather data for a particular location such as Solar Radiation and Metrological data. The resulting typical meteorological year (TMY) data is centred on statistical analysis of SoDa multiyear time series of solar resources and metrological data. Hourly time step data was used to model STPP over the period of one year, as cloud transients were excluded from the model.

5.2 Heliostat field

Solar-PILOT is used to determine the heliostat field efficiency of CSP plant. Solar-PILOT is a National Renewable Energy Laboratory (NREL) software tool used for design, characterization and optimization of concentrating solar power plant configuration (NREL, 2018b). Solar-PILOT requires the design point DNI, weather data, and heliostat field layout as input, and outputs the efficiency of the heliostat field and receiver.

The weather data is inputted into the Solar-PILOT software by location name, atmospheric conditions, weather file state name, time zone, plant elevation, plant latitude, plant longitude and the sun’s flux distribution. The heliostat field layout is

set up at design-point DNI where the field boundaries, field configuration, solar azimuth angle and solar elevation are specified. The heliostat geometry, focus parameters, mirror performance parameters and optical error parameters are assumed known, to determine how efficient each heliostat will be. After this, simulation is carried out to know the land boundary, field layout, the performance of the each heliostat on the field and the total efficiency of the heliostat field at design-point DNI as shown in Appendix C. To calculate the efficiency of the heliostat field in hourly increments of DNI over the year, a parametric simulation variable table is used as shown in Figure 5-1.

5.2.1 Parametric simulation

The parametric simulation variable table allows any specified number of parameters, any number of runs, and manually assigns values for each variable to run.

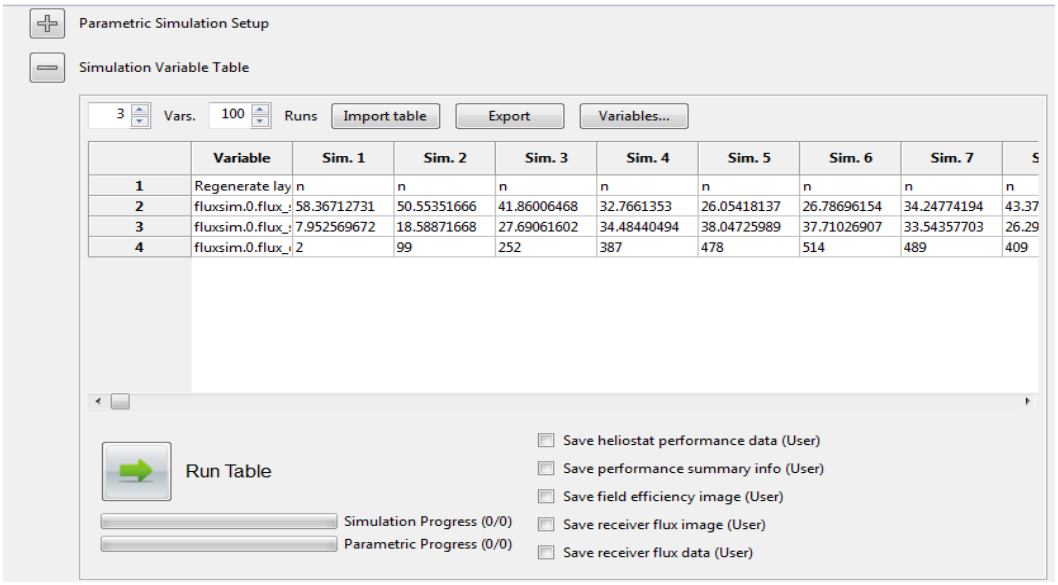

	Variable	Sim. 1	Sim. 2	Sim. 3	Sim. 4	Sim. 5	Sim. 6	Sim. 7	S
1	Regenerate lay	n	n	n	n	n	n	n	n
2	fluxsim.0.flux_	58.36712731	50.55351666	41.86006468	32.7661353	26.05418137	26.78696154	34.24774194	43.37
3	fluxsim.0.flux_	7.952569672	18.58871668	27.69061602	34.48440494	38.04725989	37.71026907	33.54357703	26.29
4	fluxsim.0.flux_	2	99	252	387	478	514	489	409

Figure 5-1: Parametric simulation table

Before running a parametric simulation variable table in Solar-PILOT, DNI and the position of sun (azimuth and altitude angle) for the heliostat field over the year is required.

5.2.2 Sun's position

To get instantaneous values for the azimuth and altitude angles of the sun to be used in Solar-PILOT, the equations below are used:

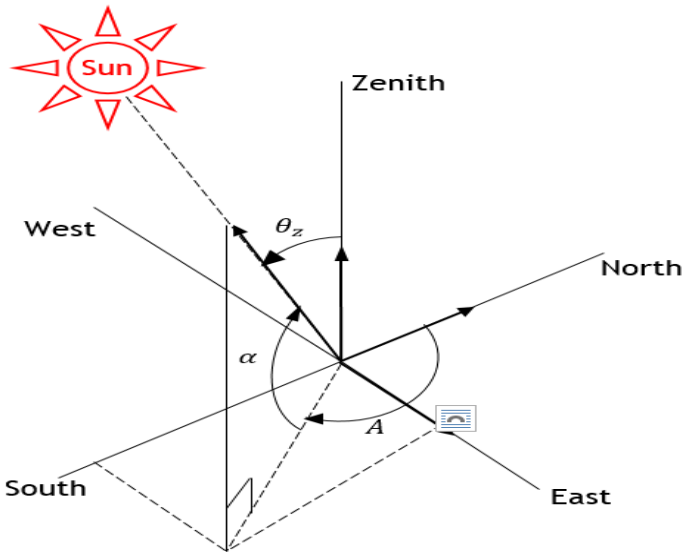

Figure 5-2: Angles of the sun

The equation of time (*EOT*) in minutes presented by Stine and Geyer (2001) is represented by

$$EOT = 0.25\cos x - 7.4168\sin x - 3.648\cos 2x - 9.2288\sin 2x \tag{5.1}$$

where angle x is in degrees and it's determined by

$$\chi = \frac{(N-1)360}{365} \tag{5.2}$$

N is the number of days calculated from January to December, as shown in Table 5.2 and solar time t_s is then calculated using

$$t_s = LCT + \frac{EOT}{60} - LC - D \tag{5.3}$$

Table 5-2: Conversion of date to day number

Month	Day number, N
January	d
February	31 + d
March	59 + d
April	90 + d
May	120 + d
June	151 + d
July	181 + d
August	212 + d
September	243 + d
October	273 + d
November	304 + d
December	334 + d

The solar time t_s, local time (LCT) and longitude correction (LC) are in hours. D is the daylight saving (not used in South Africa) and the longitude correction is defined as:

$$LC = \frac{(local\ longitude) - (longitude\ of\ standard\ time\ zone\ meridian)}{15} \quad (5.4)$$

The hour angle (ω) is calculated as a function of solar time.

$$\omega = 15(\mathrm{T}_s - 12) \quad (5.5)$$

The declination angle is the angle between a ray from the sun relative to the earth's equatorial plane, and is determined by

$$\delta = sin^{-1}\, 0.39795\, cos[0.98563(N - 173)] \quad (5.6)$$

Both the hour and declination angles are in degrees. Then solar altitude angle, which is the angle between the horizontal and the rays of the sun, is calculated by

$$\alpha = sin^{-1}(sin\,\delta\,sin\,\phi + cos\,\delta\,cos\,\omega\,cos\,\phi) \tag{5.7}$$

where ϕ is the latitude angle. The zenith angle, which is the angle between the vertical and the rays of the sun, is determined by

$$\theta_z = 90 - \alpha \tag{5.8}$$

The azimuth angle is calculated as a function of the declination angle, hour angle and the latitude angle, as

$$A' = cos^{-1}\left(\frac{sin\,\delta\,cos\,\phi - cos\,\delta\,cos\,\omega\,sin\,\phi}{cos\,\alpha}\right) \tag{5.9}$$

When $sin\,\omega \leq 0, A = A'$and when $sin\,\omega > 0, A = 360° - A'$. This is because the solar azimuth angle is measured from due north in a clockwise direction as shown in Figure 5-2. Both zenith angle and azimuth angle are in degrees.

5.3 Receiver

To determine the total energy received from the optical heliostat field, it is assumed that an external receiver is used with 40 % of KNO_3 by weight / 60 % of $NaNO_3$ by weight molten salt, which flows perpendicularly through the spherical tubes (Hoffmann and Madaly, 2015). The crystallization of the salt mixture start at 240 ºC whilst thermal decomposition of the salt starts at temperature above 600 ºC. The total heat received ($\mathbb{Q}_{of}$) is calculated as:

$$\mathbb{Q}_{of} = (DNI)(\eta_{of})(A_{fa})(SM) \tag{5.10}$$

where the field aperture area A_{fa} is

$$A_{fa} = (H_t)(A_{he}) \tag{5.11}$$

The model does not allow circumferential differences in the average heat flux on the receiver throughout the day. The heat transfer to the salt is determined by an energy balance for the receiver.

$$(\alpha)\mathbb{Q}_{of} = \sigma\varepsilon FA(\bar{T}_{mr}^4 - T_a^4) + UA_{ra}(T_{mrs} - T_a) + \mathbb{Q}_{salt} \tag{5.12}$$

It is assumed that the receiver heat flux q'_{max} is limited to 700 kW_t/m^2 as presented by Sargent and Lundy LLC Consulting Group (2003) and that the receiver has an aspect ratio (L/D) of 1.6. This allows one to calculate its height L and diameter D respectively. The overall heat transfer coefficient *U* is assumed approximately equal to the airside convective heat transfer coefficient. The receiver absorber area is determined by

$$A_{ra} = \pi LD \tag{5.13}$$

It is also assumed that the heat lost to the ground, air and surrounding structures of the receiver are due to radiation at ambient air temperature. Since the mean radiation temperature is much greater than the air temperature, the impact of this assumption will be insignificant. Since the receiver is completely enclosed by its environment, the radiation shape factor will be 1, and the radiation loss is establish from the integration over the receiver surface presented by Hoffmann and Madaly (2015).

$$\mathbb{Q}_{rad} = \sigma\varepsilon \int_0^L [T^4(\xi) - T_a^4]\pi D \, d\xi \tag{5.14}$$

$$\mathbb{Q}_{rad} = \sigma\varepsilon\pi D \int_0^L T^4(\xi) d\xi - \sigma\varepsilon\pi DLT_a^4 \tag{5.15}$$

$$= \sigma\varepsilon \, \pi DL(\bar{T}_{mr}^4 - T_a^4) \tag{5.16}$$

For a linear salt temperature distribution in the receiver, which is approximately true for once through salt flow, the mean radiation temperature at the receiver surface is calculated by

$$\bar{T}_{mr}^4 = \int_0^L T^4(\xi) d\xi \tag{5.17}$$

$$\bar{T}_{mr}^4 = \frac{T_{max}^4 + T_{max}^3 T_{min} + T_{max}^2 T_{min}^2 + T_{max} T_{min}^3 + T_{min}^4}{5} \tag{5.18}$$

where

$$T_{max} = T_{os} + \frac{2q'_{max}D_{or}\, log(D_{or}/D_{ir})}{k_c} \tag{5.19}$$

$$T_{min} = T_{is} + \frac{2q'_{max}D_{or}\, \log(D_{or}/D_{ir})}{k_c} \tag{5.20}$$

The receiver also experiences heat losses due to convection. To determine the convective loss which comprises of natural and forced (wind driven) convection, the convective heat transfer coefficient is determined from

$$h = \sqrt{h_{nc}^2 + h_{fc}^2} \tag{5.21}$$

The convective heat transfer coefficient is reliant on the extent of the mixed velocity through the receiver which will recover both the limiting cases for forced convection when $h_{nc}^2 = 0$ and natural convection for which $h_{fc}^2 = 0$.

The Nusselt number presented in Cengel and Ghajar (2015) for natural convection Nu_{nc} is determined by Rayleigh number Ra as

$$Nu_{nc} = \frac{h_{nc}D}{k_a} = 0.1Ra^{1/3} \tag{5.22}$$

where k_a is the thermal conductivity of air, and the air properties are calculated at the mean film temperature. The mean receiver surface temperature is calculated from the salt temperature, and is expressed by

$$T_{mrs} \approx \frac{T_{os} + T_{is}}{2} + \frac{2q'_{max}D_{or}\, log(D_{or}/D_{ir})}{k_{tm}} \tag{5.23}$$

The receiver is approximated as a cylinder. The forced convection heat transfer coefficient for flow across a circular cylinder is given by Zukauskas (Çengel and Ghajar, 2015) as

$$Nu_{fc} = \frac{h_{fc}D}{k_a} = 0.027Re^{0.805}Pr^{0.333} \tag{5.24}$$

The air properties for use in the calculation of the Reynolds Re and Prandtl numbers Pr are evaluated again at the mean film temperature. The Reynolds number is defined as

$$Re = \frac{\rho V(y)D}{\mu} \tag{5.25}$$

The exact shape of the wind profile depends on the atmospheric stability, but for modelling purposes, the wind speed at the receiver height is calculated from the 1/7th law for a neutral (adiabatic) atmosphere, which is given by

$$V(y) = V_{10}\left(\frac{y}{10}\right)^{1/7} \tag{5.26}$$

V(y) is typically measured at 10 m above the ground level, and is encompassed in the metrological data for the site used. Hence, the convection loss is determined by

$$\mathbb{Q}_{conv} = \pi\ D\ L\ h_{fc}(T_{mrs} - T_a) \tag{5.27}$$

5.4 Thermal energy storage

From the Figure 5-3, it is assumed that thermal energy storage loss is limited to the tank sidewalls only, and only up to the salt level inside the tank. Since there is a direct connection between the salt inventories stored inside the tank and heat loss from the tank, assuming that the overall heat transfer coefficient (U) is constant. According to (Sioshansi and Denholm, 2010), U≈ 6 W/ºC which translates to 1.5 % loss of the energy stored per day from a fully changed tank. The thermal energy loss is given as

$$\mathbb{Q}_{tel} = \pi D H_s U(\bar{T}_{ms} - T_a) \tag{5.28}$$

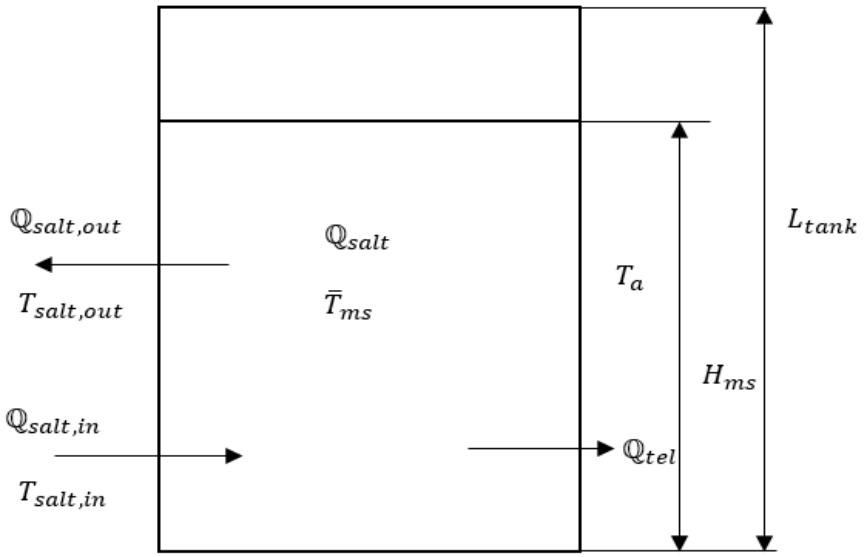

Figure 5-3: Schematic diagram of thermal energy storage

Rodriguez et al (2013) gives a comprehensive calculation of the heat losses in a storage tank. If the receiver heat flux is adequate for full load operation when the storage runs out, the turbine will start again and this will partially offset the thermal lag of the solar thermal power plant.

The amount of thermal energy stored per hour is determined by

$$\mathbb{Q}_{tes} = \mathbb{Q}_{salt,in} - \mathbb{Q}_{tel} \tag{5.29}$$

5.5 Steam generation

From the Figure 5-4, it is assumed that the preheater and evaporator are in series, and that the super-heater and re-heater are in parallel. It is assumed that the salt exit temperatures from the latter components are equal. With this assumption, the salt flow rate between the super-heater and re-heater can be determined by using the thermodynamically optimized pinch point for heat recovery boiler, which is set at about 5 °C (Behbahani-Nia et al., 2010). Though the pinch point model is not directly appropriate to a molten salt steam generator, it can be used as a first approximation and it is set to 5 °C at 130 bar. The hot salt temperature is fixed to 565 °C and the cold salt temperature is not allowed to drop below 270 °C. The temperature of the cold salt differs in an insignificant band around 273 °C. To calculate the salt flow rate, a heat balance is established from the inlet of the pre-heater to the super-heater and re-heater outlets on the steam generator.

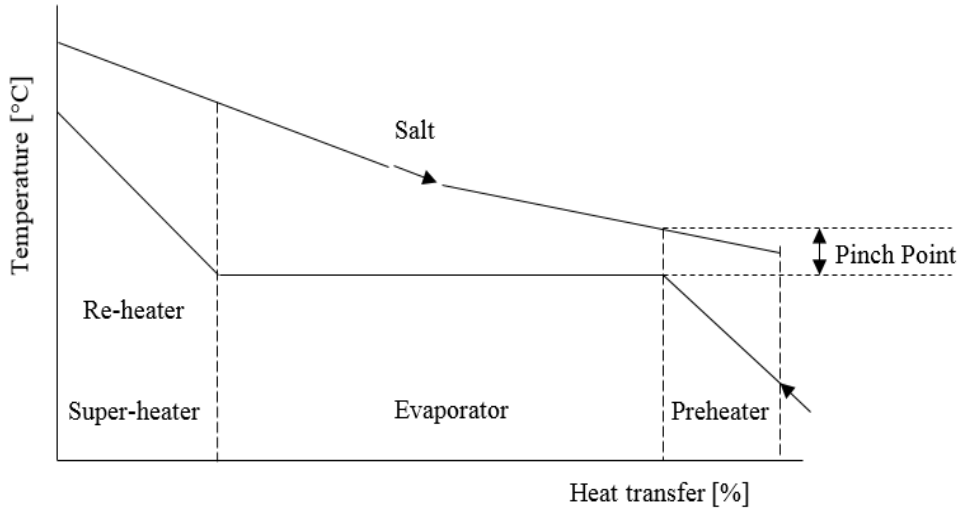

Figure 5-4: Schematic diagram of pinch point steam generator

$$\dot{m}_S \bar{C}_{pmst}[T_{is} - (T_{sat} + \Delta T_P) - T_{os}] = \dot{m}_{hpt}(h_{sh} - h_{fw} + h_{ph}) + \dot{m}_{rh}\Delta h_{rh} \quad (5.30)$$

Where: Δh_{rh} is the increase in enthalpy in the re-heater, h_{fw} is the saturated feed-water enthalpy entering the evaporator, $\dot{m}_{rh}$ is the mass flow rate of the steam through the re-heater, h_{sh} the enthalpy of the steam exiting the super-heater, h_{ph} is the steam enthalpy entering the pre-heater, $\dot{m}_{hpt}$, the mass flow rate of the steam through the high pressure turbine, T_{sat}, the water/steam saturation temperature at the existence steam pressure, ΔT_P the temperature difference at the pinch point, T_{is}, the inlet salt temperature, T_{os}, the outlet salt temperature, $\bar{C}_{pmst}$, the salt specific heat at the mean salt temperature, and $\dot{m}_S$, the mass flow rate of the salt.

5.6 Power block

The power block model assumes a steady-state single reheat Rankine cycle as shown in Figure 5-5. The power block contains the following components: steam generator, high, intermediate and low-pressure steam turbines, electrical generator, condenser, feed-pump, two closed and one open feed-water heaters. It was modelled in the Microsoft Excel software. In order to calculate the thermodynamic properties of water and steam at the inlet and outlet of all components, the Excel add-in X Steam, developed by the International Association for Properties of Water and Steam Industrial Formulation 1997 (IAPWS IF-97) was added to Microsoft Excel. X Steam allows one to calculate any steam property from two independent properties. The power block model is assumed to operate in successive hourly steady states, since its characteristic time is relatively small compared it to the hourly changes in DNI.

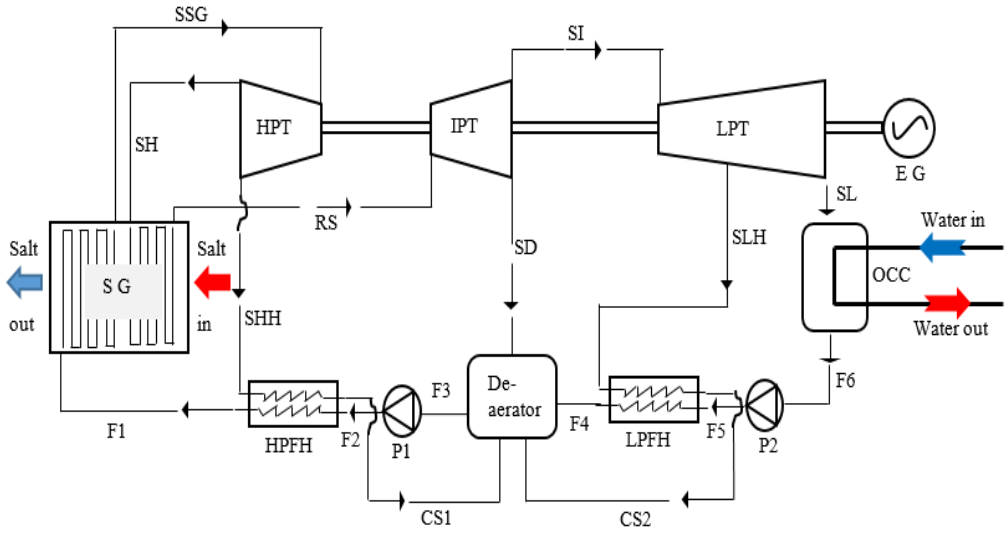

Figure 5-5: Schematic diagram of STPP power block

The turbine used is loosely based on the Siemens SST-800 series with a life steam pressure of 130 bar and temperature of 540 °C (Siemens, 2011). The life steam states remains fixed at the maximum capacity rating of the turbine. The reheat pressure is assumed one quarter of the life steam pressure, and the reheat temperature is assumed the same as the inlet temperature of the HPT. The isentropic efficiencies of the low, intermediate and high-pressure turbines are assumed to be 90 %, 85 % and 82 % respectively.

5.6.1 Steam generator

The heat added for steam generation (SG) is determined by

$$\mathbb{Q}_{SG} = \dot{m}_{F1}(h_{SSG} - h_{F1}) \tag{5.31}$$

The heat required from the re-heater (RH) is given by

$$\mathbb{Q}_{RH} = \dot{m}_{SSG}(h_{RS} - h_{SH}) \tag{5.32}$$

The total heat input is determined by adding equation 5.30 and equation 5.49.

$$\mathbb{Q}_{T} = \mathbb{Q}_{SG} + \mathbb{Q}_{RH} \tag{5.33}$$

The heat balance at the steam generator including re-heat is known as

$$\dot{m}_s \bar{C}_{ps}(T_{is} - T_{os}) = \dot{m}_{F1}(h_{SSG} - h_{F1}) + \dot{m}_{SH}(h_{RS} - h_{SH}) \quad (5.34)$$

5.6.2 Turbine

The work done by the HPT is given by

$$w_{HPT} = \dot{m}_{SH}(h_{SSG} - h_{SH}) + \dot{m}_{SHH}\,(h_{SSG} - h_{SHH}) \quad (5.35)$$

For the IPT and LPT, the work done is determined by

$$w_{IPT} = \dot{m}_{SI}(h_{RS} - h_{SI}) + \dot{m}_{SD}\,(h_{RS} - h_{SD}) \quad (5.36)$$

$$w_{LPT} = \dot{m}_{SL}(h_{SI} - h_{SL}) + \dot{m}_{SLH}\,(h_{SI} - h_{SLH}) \quad (5.37)$$

The total turbine work is calculated by

$$w_T = w_{HPT} + w_{IPT} + w_{LPT} \quad (5.38)$$

5.6.3 Feed-water heater

The plant is equipped with three feed-water heaters as shown in figure 5.5. The steam extracted from the high-pressure turbine leaves the feed-water heater as saturated liquid, and dumped directly into the deaerator. It is assumed that the increase in temperature across each feed-water heater is equal (Nag, 2007). Hence, the temperature rise for each feed-water heater can be determined by

$$T_r = \frac{T_{F1} - T_{F5}}{N_{fwh}} \quad (5.39)$$

The heat balance at high-pressure feed-water heater (HPFH) is given by

$$\dot{m}_{SHH}\,(h_{SHH} - h_{CS1}) = \dot{m}_{F2}(h_{F1} - h_{F2}) \quad (5.40)$$

And at the deaerator, the heat balance is known as

$$\dot{m}_{F3}(h_{F3}) = \dot{m}_{F4}(h_{F5}) + \dot{m}_{CS1}(h_{CS1}) + \dot{m}_{CS2}(h_{CS2}) + \dot{m}_{SD}(h_{SD}) \tag{5.41}$$

Finally, the heat balance at the low-pressure feed-water heater (LPFH) is determined as

$$\dot{m}_{SLH}\,(h_{SLH} - h_{CS2}) = \dot{m}_{F5}(h_{F4} - h_{F5}) \tag{5.42}$$

5.6.4 Feed pump

The isentropic efficiency of both condensate pump (P1) and feed-water pump (P2) is assumed 75 %. The work required at the condensate pump P1 is given by

$$w_{P1} = \dot{m}_{F3}(h_{F2} - h_{F3}) \tag{5.43}$$

And at the feed-water pump P2, the required is given by

$$w_{P2} = \dot{m}_{F6}(h_{F5} - h_{F6}) \tag{5.44}$$

The total feed-water pump is calculated as

$$w_{TP} = w_{P1} + w_{P2} \tag{5.45}$$

5.6.5 Condenser

The once-through condenser is assumed a shell and tube heat exchanger with admiralty brass tubes, similar to the one at Kriel Power Station. Its specifications were given by Goodenough (2013) and available in appendix D. The size and the number of tubes were design parameters in order to have a once-through cooling condenser fit for the STPP to be modelled. The size of the tube is given by the inner and outer diameter of the tube. The inner diameter and outer diameter is designed to be 0.02291 m and 0.0277 m respectively. The number of tubes per pass is designed to be 8 400. The surface areas based on the outer diameter of the tubes is calculated by

$$A_h = \pi(d_1)(\mathrm{L})(N_p) \tag{5.46}$$

The designed output cooling water temperature is determined by

$$T_{cwo} = \frac{\mathbb{Q}_{max}}{\dot{m}_{cw} c_{p,cw}} + T_{cwi} \tag{5.47}$$

Having known the designed output temperature of the cooling water, the increase in temperature of the water is define as

$$\Delta T_{C,w} = T_{cwo} - T_{cwi} \tag{5.48}$$

Also, the terminal temperature difference and initial temperature difference as

$$TTD = T_s - T_{cwo} \tag{5.49}$$

and

$$ITD = T_s - T_{cwi} \tag{5.50}$$

The designed overall heat transfer coefficient is determined by

$$U = \frac{\mathbb{Q}_{max}}{A_h(\Delta T_{LMTD})} \tag{5.51}$$

Where the log mean temperature difference is define as

$$\Delta T_{LMTD} = \left[\frac{T_{cwo} - T_{cwi}}{\ln\left(\frac{T_s - T_{cwi}}{T_s - T_{cwo}}\right)}\right] \tag{5.52}$$

The analysis of the modelled condenser is available in appendix D. The designed TTD, ITD and $\Delta T_{C,w}$ is assumed to remain constant during the operation of the once-through cooling condenser in the STPP. The properties of cooling water (river

water) entering the condenser is assumed to be the same as the clean water, since the total dissolved solids in the water is low (60 mg/l, according to Compton et al, 2007). The condenser backpressure depends on the condensate temperature that is determined by the cooling water inlet temperature. It is also assumed that there is no pressure drop across the plant. The condenser heat transfer area is constant. The potential and kinetic energies of the flow and heat losses from all the equipment and pipes are assumed negligible. Since the temperature of the cooling water varies seasonally and very slowly, it is assumed that the inlet cooling water temperature is constant for each time step. At constant TTD, ITD, and $\Delta T_{C,w}$, the amount of heat rejected from the condenser $\mathbb{Q}_{rej}$ is calculated as

$$\mathbb{Q}_{rej} = \dot{m}_{SL}(h_{SL}) - \dot{m}_{F6}(h_{F6}) \tag{5.53}$$

Which is equal to equation (5.54)

$$\mathbb{Q}_{rej} = \dot{m}_{cwi} c_{cwi} (T_{cwo} - T_{cwi}) \tag{5.54}$$

Both equation (5.53) and (5.54) are also related to equation (5.55)

$$\mathbb{Q}_{rej} = UA_h(\Delta T_{LMTD}) \tag{5.55}$$

with

$$UA_h = \left[\frac{1}{h_w \pi d_2 L_{eff}} + R_f'' + \frac{\ln(d_3/d_2)}{2\pi k_t L_{eff}} + \frac{\ln(d_2/d_1)}{2\pi k_t L_{eff}} + \frac{1}{h_s \pi d_3 L_{eff}}\right]^{-1} \tag{5.56}$$

During the operation, fouling is expected to occur on the cooling waterside. Goodenough (2013) determined a theoretical fouling factor to calculate the fouling resistance of the condenser. The type of condenser and mass fluxes through it are the same as those used by Goodenough, but the heat transfer surface is smaller.

Due to the size of the condenser, which is quite big (500 MW_e power station) compared to the modelled condenser (50 MW_e power station), the fouling factors will not match exactly. In order to determine the fouling factor in the modelled condenser, a conservative approach was followed in adopting the asymptotic fouling factor given by Goodenough.

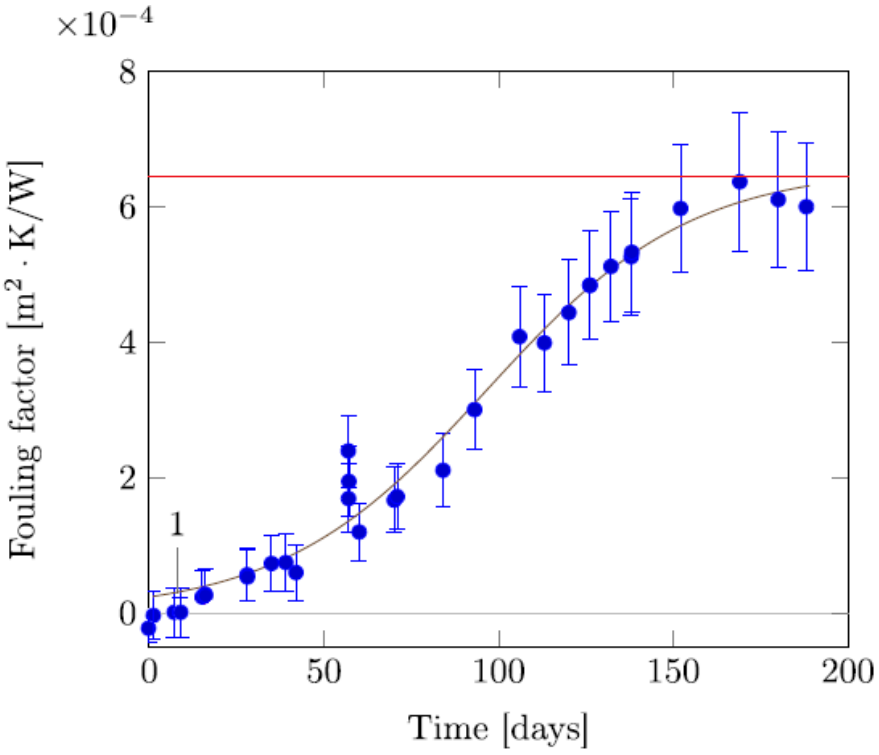

Figure 5-6: Measured fouling factor for admiralty brass tube (Reuter et al., 2017)

Fouling factor can also be calculated from the combination of the equation (5.54), (5.55), and (5.56), which is developed by Goodenough (2013) as

$$R_f'' = \pi d_1 L_{eff}\left[\frac{(T_{C,si}-T_{C,wo})-(T_{C,so}-T_{C,wi})}{\mathbb{Q}_{C,m}\ln\left(\frac{T_{C,si}-T_{C,wo}}{T_{C,so}-T_{C,wi}}\right)} - \left(\frac{\pi d_2 L_{eff} k_{fs}}{d_3-d_2}Nu_s\right)^{-1} - \frac{\ln\left(\frac{d_2}{d_1}\right)}{2\pi k_t L_{eff}} - \left(\pi L_{eff} k_{fw}\frac{\left(\frac{f_D}{8}Re_w Pr_w\right)}{1+12.7\left(\frac{f_D}{8}\right)^{0.5}(Pr^{2/3}-1)}\right)^{-1}\right] \quad (5.57)$$

Where $\mathbb{Q}_{C,m}$, is the averaged heat transfer rate, and it is determined by

$$\mathbb{Q}_{C,m} = \frac{(m_{C,si}\Delta h_{C,sm} + m_{C,w}C_{C,pw}\Delta T_{C,wm})}{2} \quad (5.58)$$

The enthalpy difference $\Delta h_{C,sm}$ is define as

$$\Delta h_{C,s} = h_{si} - h_{so} \tag{5.59}$$

And $\Delta T_{C,wm}$, is the water temperature difference.

From equation (5.52), the steam Nusselt number of the condenser tube Nu_s is given by Goodenough (2013)

$$Nu_s = \frac{d_3 - d_2}{\pi d_2 L_{eff} k_s}\left[\frac{(T_{C,si} - T_{C,wo}) - (T_{C,so} - T_{C,wi})}{\mathbb{Q}_{C,m} \ln\left(\frac{T_{C,si} - T_{C,wo}}{T_{C,so} - T_{C,wi}}\right)} - \frac{1}{\pi L_{eff} k_w Nu_i} - \frac{\ln\left(\frac{d_2}{d_1}\right)}{2\pi k_t L_{eff}}\right]^{-1} \tag{5.60}$$

where Nu_i, the inner Nusselt is number is determined by

$$Nu_i = \frac{\left(\frac{f_D}{8} Re_w Pr_w\right)}{1 + 12.7\left(\frac{f_D}{8}\right)^{0.5}(Pr^{2/3} - 1)} \tag{5.61}$$

And the Darcy-Weisbach friction factor $f_D$which depend on the Reynolds number of the tube is determined by

$$f_D = (1.8 \log_{10} Re - 1.5)^{-2} \tag{5.62}$$

The Reynold number of the tube Re which is the determining factor of the flow regime whether the flow is laminar, transitional or turbulent for both steam and water is calculated by

$$Re = \frac{\rho v d}{\mu} \tag{5.63}$$

And the velocity is given by

$$v = \frac{V}{A} \tag{5.64}$$

The cross sectional area is known as

$$A = \frac{\pi d^2}{4} \tag{5.65}$$

Thermo-physical properties of the saturated water from 273.15 K to 380 K in Appendix A.2 was used to determine the density, specific heat, kinematic viscosity, thermal conductivity, Prandtl number of the steam and water inside the condenser.

5.6.6 Thermal efficiency

The thermal efficiency of the STPP is calculated as

$$\eta_t = \frac{W_{net}}{\mathbb{Q}_T} \tag{5.66}$$

and the net work done of the STPP is determined by

$$W_{net} = w_T - w_{TP} \tag{5.67}$$

Chapter 6

Model validation

Overview

Comparison of the model results with system advisor model (SAM) is discussed. SAM is a computer program that calculates an hourly energy output over a single year for solar thermal energy system and calculates the energy cost for a solar thermal energy project over the project's life. The comparison entails the heliostat field efficiency, receiver tower and power block. A comparison of the once-through cooled power block results with air-cooled power block results is discussed.

6.1 Heliostat Field Comparison

At design point[3], heliostat field was modelled in SAM as imitation model to know the heliostat field efficiency. The relationship between the SAM and heliostat field model is represented in Figure 6-1. Based on the annual heliostat field efficiency of both SAM and heliostat field model, the results shows that there a good comparison between both of them except that there is some outliers occur from SAM model. These outliers are as a result of receiver curtailment when the hot thermal energy storage reached full capacity.

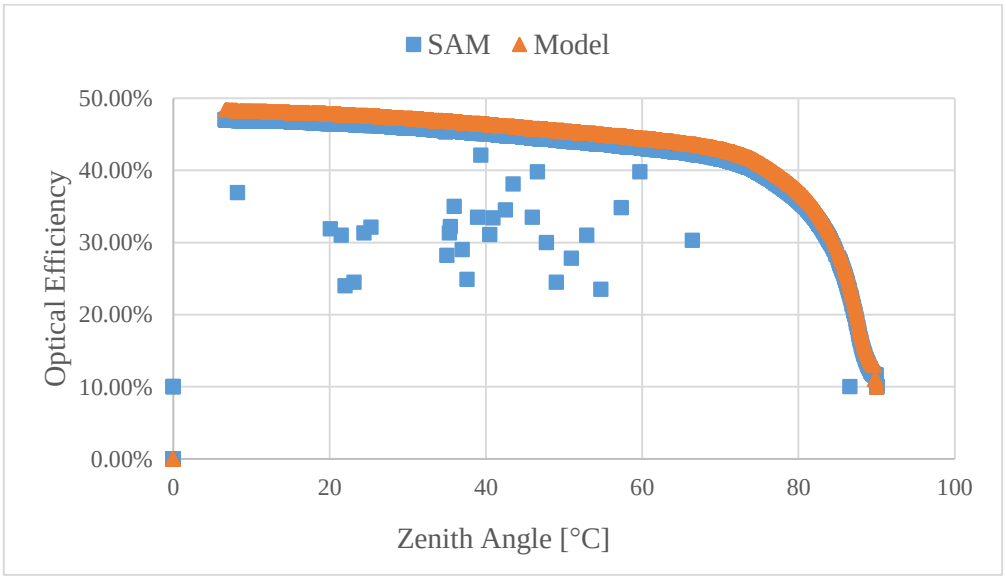

Figure 6-1: Heliostat field efficiency comparison

[3] Design point is a point in time and conditions for which the CSP plant is designed to produce its nominal power.

However, the result of the heliostat field shown in Figure 6-1 do not account for the effect of the receiver flux limitation.

6.2 Receiver tower comparison

The comparison between the receiver model and SAM model based on the energy loss to the surroundings over the day is presented in Figure 6-2. These loses occur due to radiation and convection from the receiver to the atmosphere. The results are in good agreement except that the receiver model predicts marginally higher losses than the SAM model in a day.

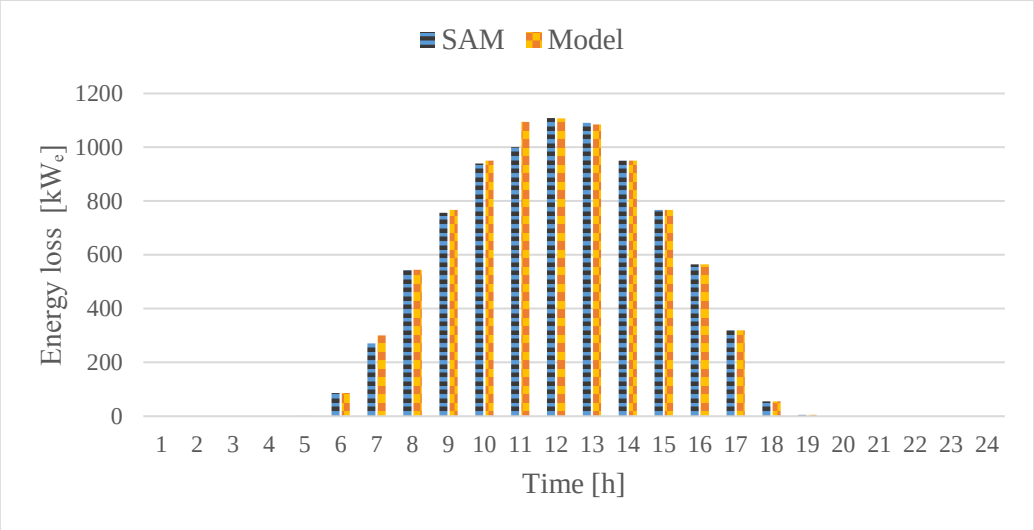

Figure 6-2: Receiver comparison

6.3 Power block comparison

6.3.1 Air-cooled comparison

The power block using an air-cooled condenser with three feed-water heater was modelled in order to compare its performance with a once-through cooling model. The air-cooled condenser is assumed a forced draft condenser, and the condenser temperature is simply the sum of the ambient temperature and a constant initial temperature difference of 25 ºC (Madaly, 2015). At the design point, the condenser backpressure is 20.04 kPa and the steam temperature 60.11 ºC. The air inlet temperature is assumed 35.11 ºC (air temperature at solar noon on autumn equinox).

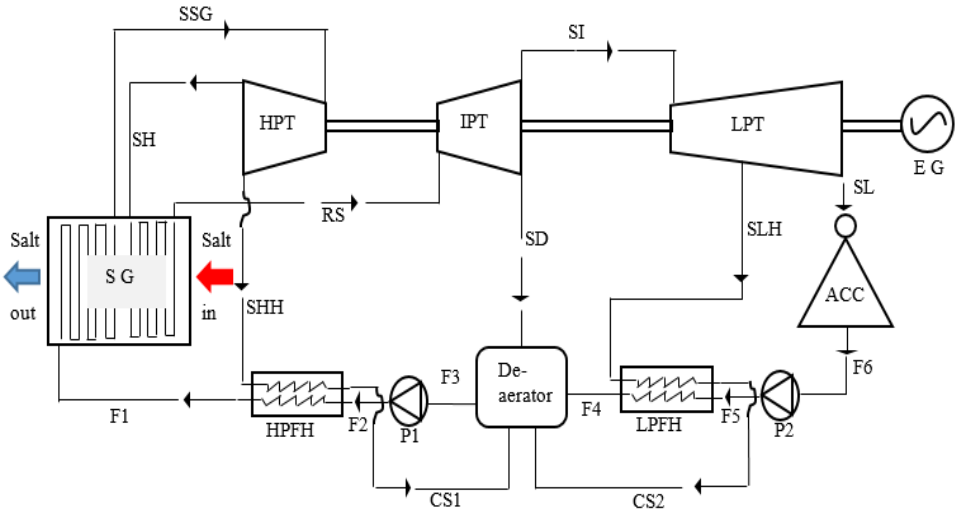

Figure 6-3: STPP with air-cooled condenser

The wind speed at design point is 6.2 m/s. The steam mass flow rate that resulted into 50 MW_e power output of air-cooled CSP plant is 37.86 kg/s. The result is presented in Table 6-1, and it shows that there is an improvement in the thermal efficiency of once-through cooling CSP plant with a difference of 2.9 % after integrating over full year.

Table 6-1: Comparison between once-through cooling and air-cooled

	Units	**Once-through cooling**	**Air-cooled**
Energy supplied to steam generator	kJ/kg	104719.3	111555.2
Efficiency	%	47.7	44.8
Mass flow rate	kg/s	35.54	37.86
Power output	MW_e	50	50

At design power output, the steam mass flow rate of air-cooled CSP plant is higher than that for the once-through cooled CSP plant. Due to this difference in mass flow rate, the energy supplied to the steam generator increases by 3 %. If we assume that the life steam flow stays the same for both the air-cooled CSP plant and the once-through cooled CSP plant, the energy supplied to the steam generator will remain the same, but the power output and the thermal efficiency are different for the two plants, as shown in Table 6-2. Under both scenarios, the OTC plant is more efficient than the ACC plant.

Table 6-2: Performance of OTC and AC on STPP

	Units	**Once-through cooling**	**Air-cooled**
Energy supplied to steam generator	kJ/kg	104719.3	104719.3
Efficiency	%	47.7	44.8
Mass flow rate	kg/s	35.54	35.54
Power output	MW_e	50	47

6.3.2 SAM comparison

The modelled thermal efficiency was compared with the SAM results, as shown in Figure 6-4. The results show that there is a good agreement between the model and SAM during summer and winter solstices.

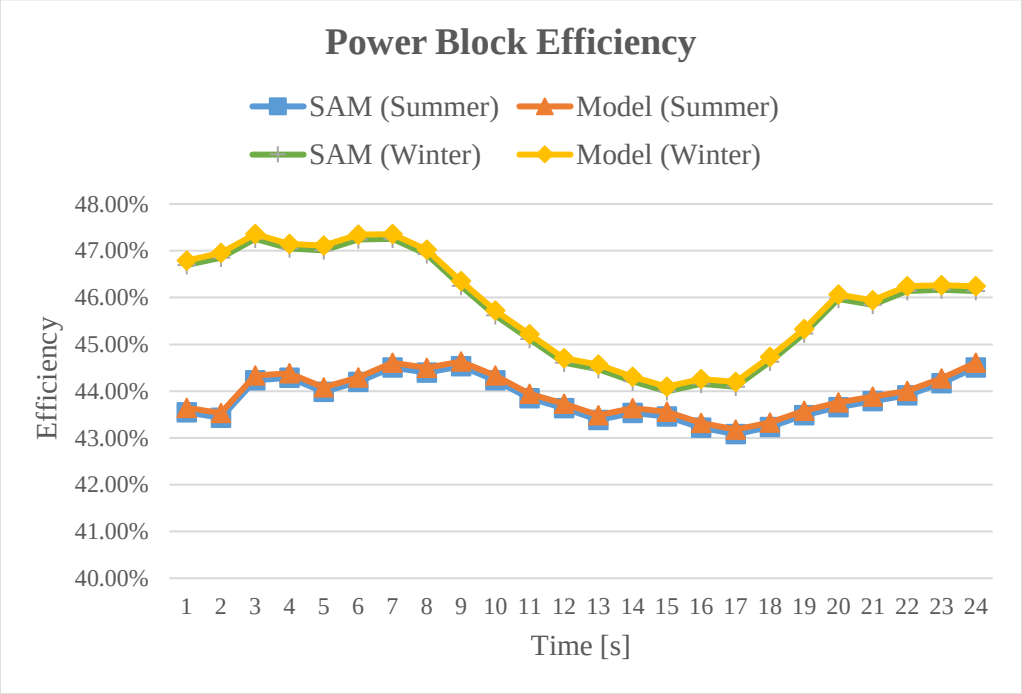

Figure 6-4: Model vs SAM comparison

The model is accurate to within 3 % of the SAM results, with the model consistently predicting higher values, irrespective of the use of a once through or air-cooled condenser. It is deemed validated for the purpose of comparative studies.

Chapter 7

Model result

Overview

The result of the CSP plant model is discussed in detail. The analysis starts with the effect of zenith angle on the heliostat field efficiency, and subsequently looks into the effect of ambient temperature and wind speed on the receiver and the performance of the power block. Lastly, the cooling water leaving the condenser is evaluated and a decision is made whether it can be used for irrigation and agriculture purpose or not. Factors constraining the use of OTC were identified and fully discussed.

7.1. Heliostat field

The heliostat field efficiency depends on the sun's position, given by the solar altitude (or zenith) and azimuth angles. Figure 7-1 shows the effect of zenith angle on the heliostat optical field efficiency, which is expressed as a performance curve for the heliostat field.

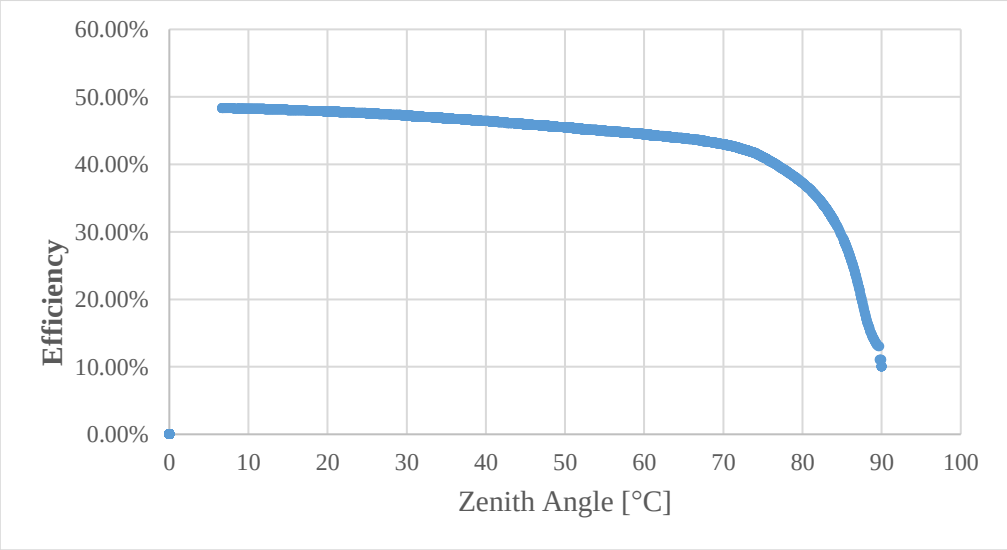

Figure 7-1: Zenith angle effects on heliostat optical field efficiency over the year

At the design point, the heliostat field efficiency generated from the Solar-PILOT is 46.90 %, as shown in Table 7-1. This is mainly due to the cosine effect. A summary of cosine, reflection, blocking, shading, image intercept and atmospheric attenuation is given in Table 7-1.

Table 7-1: Simulation result from Solar-PILOT

	Units	Value
Simulated heliostat area	m^2	3333104.20
Simulated heliostats	-	24844
Cloudiness efficiency	%	100.00
Shading efficiency	%	100.00
Cosine efficiency	%	75.88
Reflection efficiency	%	95.25
Blocking efficiency	%	96.69
Attenuation efficiency	%	97.12
Image intercept efficiency	%	69.10
Solar field optical efficiency	%	46.89

7.2. Receiver tower

The central receiver did not absorb all the energy coming from the heliostat field. This is due to the effect of wind speed and ambient temperature. At design point, the wind speed is varied at constant ambient temperature of the field to test the sensitivity of the receiver to convection losses. The ambient temperature at design point is 35.11 ℃. Figure 7-2 shows the effect of wind speed on receiver. As the wind speed increases, the heat loss to the surroundings increase which reduces the efficiency of the receiver.

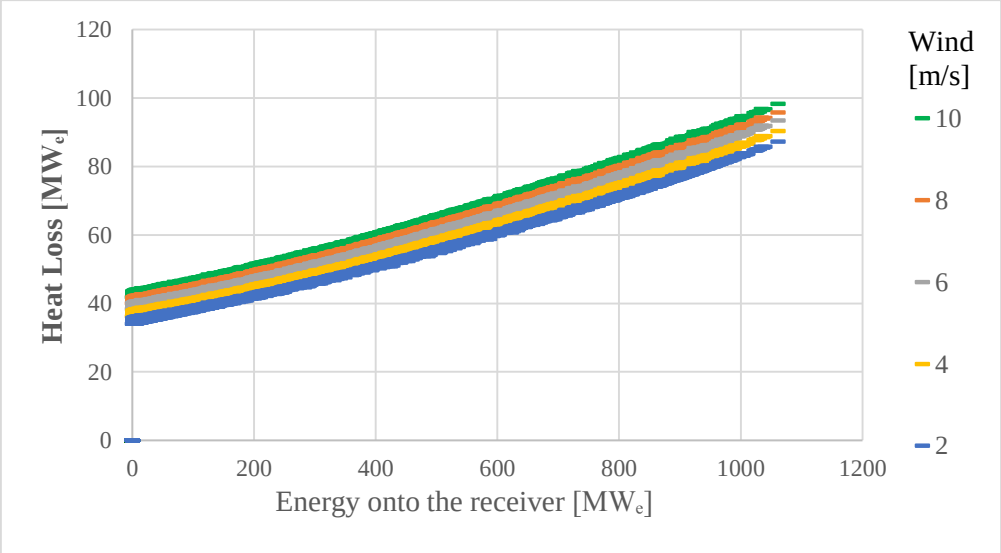

Figure 7-2: Effect of wind speed onto receiver

The ambient temperature is varied at constant receiver temperature and a wind speed of 6.2 m/s and its effects on the convection and radiation losses encountered at the receiver is shown in Figure 7-3. As the ambient temperature increases the heat loss to the surroundings decreases, which means the impact of ambient temperature on the receiver, helps to increase the energy absorbed on the receiver.

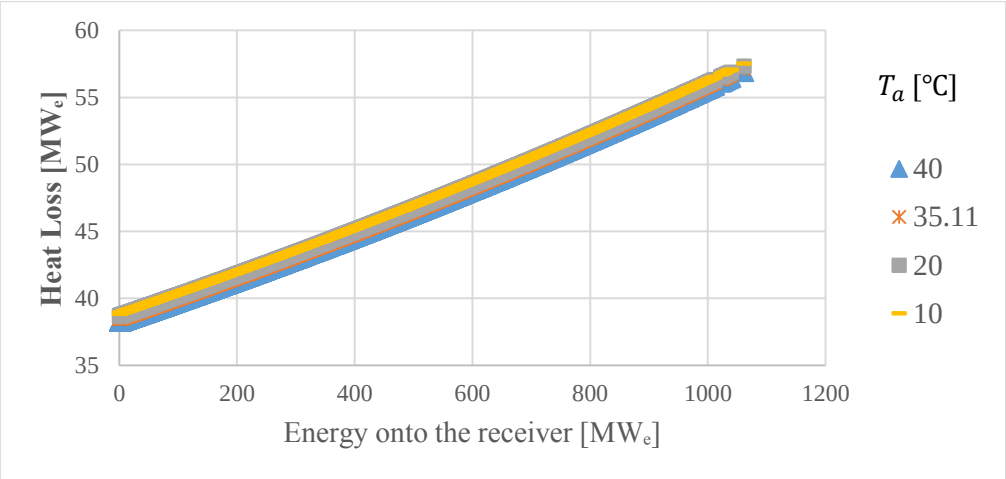

Figure 7-3: Effects of ambient temperature onto receiver

The major losses in the receiver due to radiation and convection were calculated at design point (see D.3) and these losses are represented in Figure 7-4.

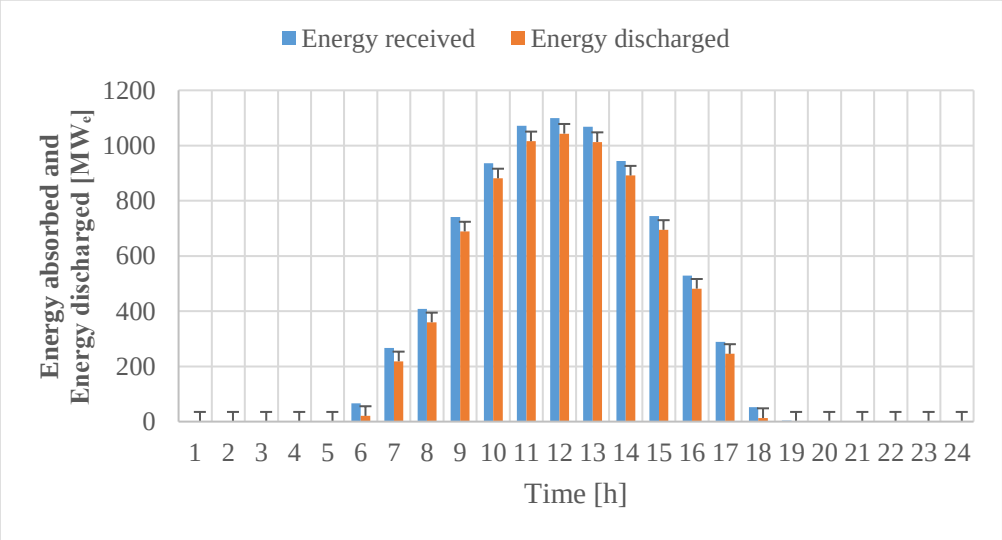

Figure 7-4: Energy received and discharged energy on December 22, 2017

Its shows that an hourly loss occurs on the receiver on the December 22, 2017 and by using the error bar, the difference between the energy absorbed and energy discharged to the salt from 06h00 to 18h00 is about 35 %.

7.3 Power block

The power block is modelled with fixed life steam parameters, corresponding to the design point. The model assumes that the plant operates in a turbine-follow-boiler mode. The thermal energy supplied to the steam generator coming from the hot tank affects the turbine output as shown in Figure 7-5.

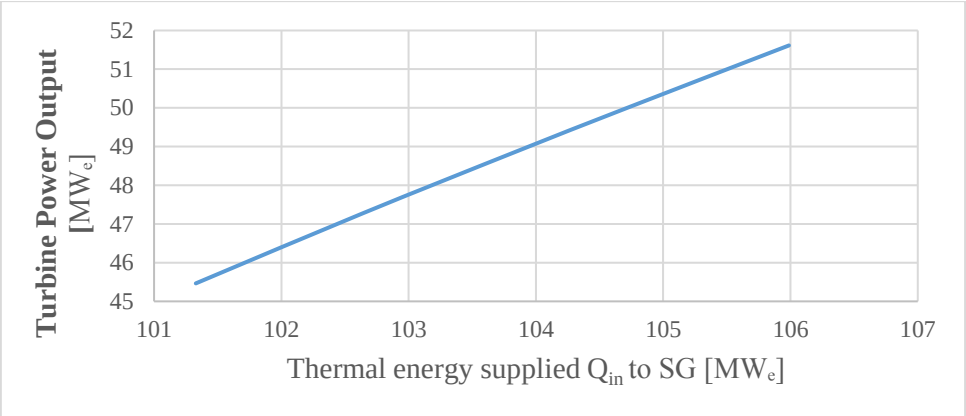

Figure 7-5: Effects of thermal energy supplied to steam generator on turbine output

When there is reduction of thermal energy from the steam generator, the turbine output is reduced at full load operation. The performance curve of the power block between the efficiency and the turbine output is shown in Figure 7-6.

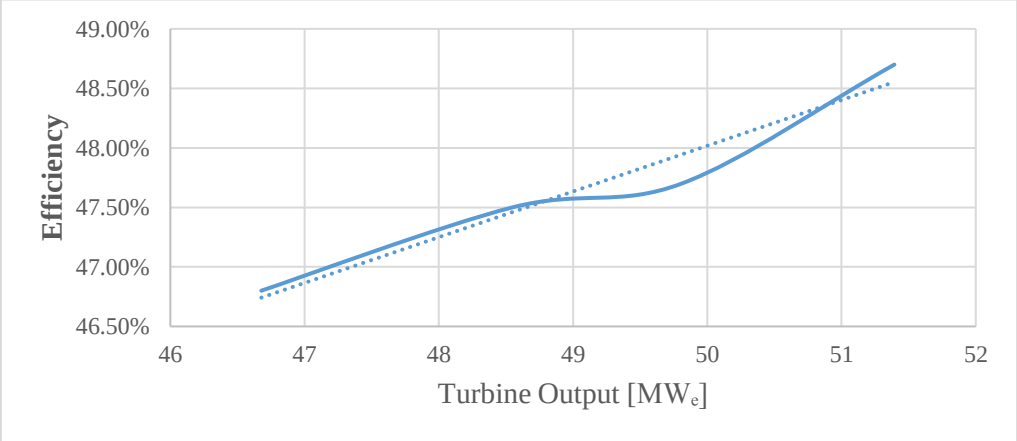

Figure 7-6: Performance curve of the power block based on turbine output

The power block performance curve between the efficiency and thermal energy supplied to the steam generator is represented in Figure 7-7.

Figures 7-5 to 7-7 explain how efficient the performance of the modelled power block at design inlet cooling water temperature is. The power block output is fixed at 50 MW_e by adjusting the salt and steam flow.

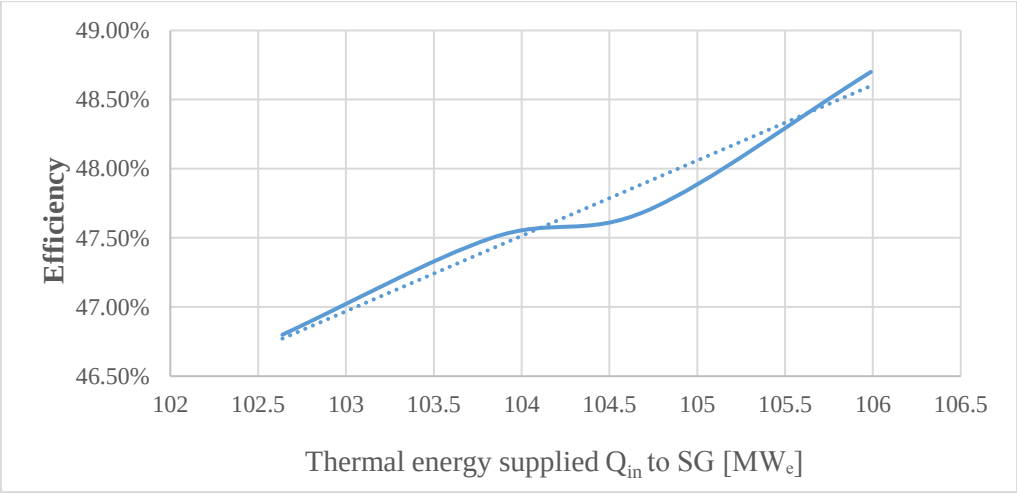

Figure 7-7: Performance of the power block based on thermal energy supplied

The effect of cooling water temperature on the power block performance is represented in Figure 7-8. By varying the inlet cooling water temperature entering the condenser, the turbine output increases as the power block efficiency increased. At design point, the terminal temperature difference is 5 ℃, the initial temperature difference is at 12 ℃ and the temperature difference between the inlet and outlet cooling water is calculated as 7 ℃ (see D.1). From these conditions, Table 7-2 is presented showing the result of the power block as design point.

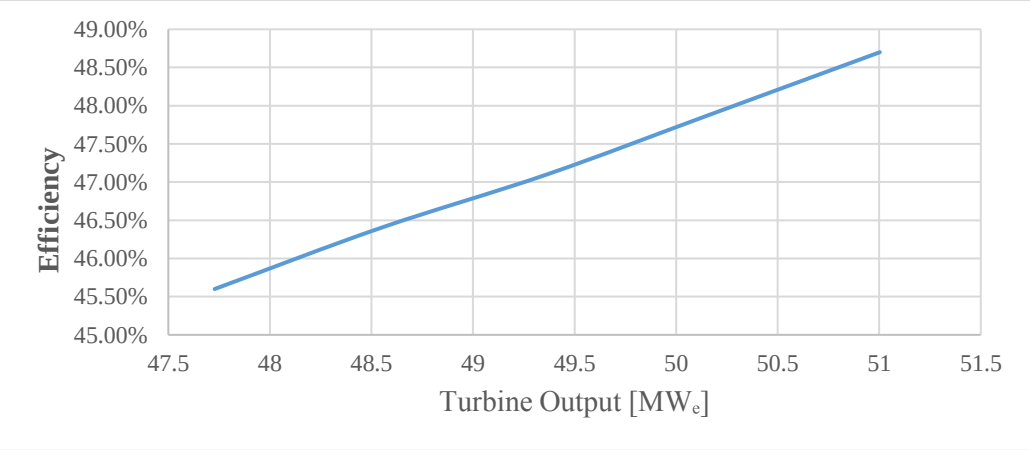

Figure 7-8: Effects of cooling water on power block

Bauder (s.a.) recorded up to 50 % crop losses if a lucerne (alfalfa) field is flooded for 2 days in water with a temperature of 32 °C. Although water will drain away within a few hours during flood irrigation, this value was adopted as a limiting temperature that should not be exceeded at the condenser outlet. To prevent thermal pollution, the cooling water is not allowed to experience a temperature rise above 10 ℃ (Girish *et al.*, 2017). This make the condenser model valid and appropriate for CSP plant. The cooling water inlet temperature at the design point is taken as 21.1 ℃.

Based on the outlet cooling water temperature and the fouling factor in Table 7-2 at reference inlet cooling water temperature, the outlet cooling water can return to irrigation system and used for agricultural irrigation purposes.

The analysis of hourly occurrence of the cooling water temperature experienced over the year from Orange River near Upington is represented in Figure 7-9. It shows that the reference inlet cooling water temperature (21.1 ℃) occurs more frequently than other cooling water temperature collected from South African Weather Service (SAWS). It might be necessary to curtail plant operation when the temperature of the river water exceeds 30 °C, something that occurs about 4 % of the time (figure 7-9). At mid-day (12 noon), the reference inlet cooling water temperature occur frequently over the year.

Table 7-2: STPP result at design point

	Units	Value
Energy supplied to steam generator	kJ/kg	104719.3
Efficiency	%	47.7
Outlet temperature	℃	28.1
Fouling factor	W/K	0.00131
Power output	MW_e	50

Comparing this temperature with the hourly occurrence of the air-ambient temperature (35 ℃) at mid-day experienced over the year, its shows that once through cooling has a great advantage of improving the thermal performance of the CSP plant than any other cooling systems.

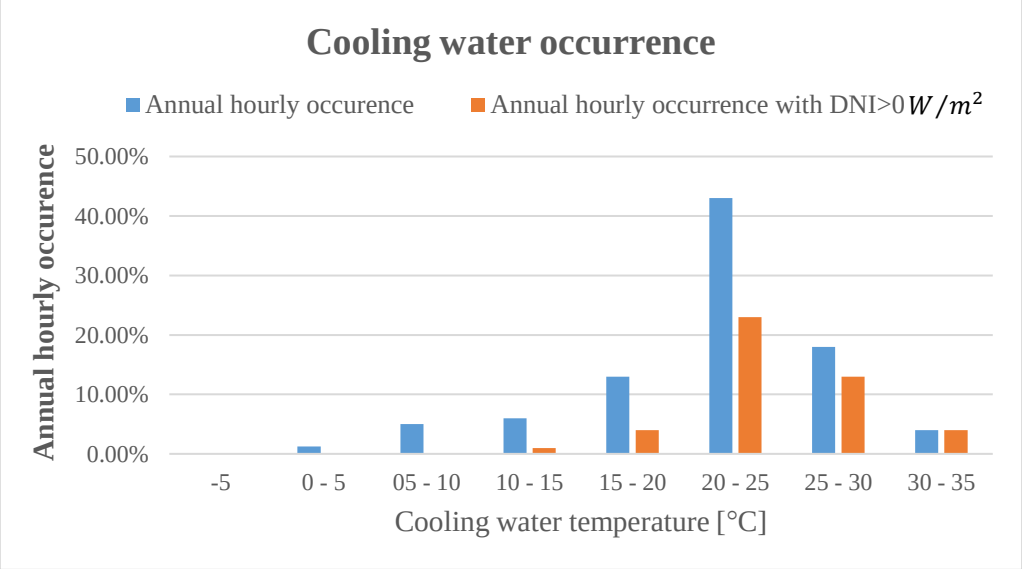

Figure 7-9: Annual hourly occurrence of inlet cooling water (Orange River) temperature

Because the temperature of deep river or sea changes seasonally and very slowly (Dallas, 2008) compared to the diurnal air temperature, a once-through cooling system is an attractive choice.

The blue colour in figure 7-9 implies the temperature of the cooling water over the year including the cooling water temperature when DNI is zero while the red colour is the annual hourly occurrence of the cooling water temperature when DNI is greater than zero. The latter instances mean that the receiver is actively collecting energy, and is more applicable to a CSP plant without thermal energy storage.

Figure 7-10 shows the fouling factor as a function of water temperature in the surface condenser. The increase occurs because of microbial activity increases with temperature, but kill-off will set in as temperature exceeds a certain limit (Zwietering et al., 1991).

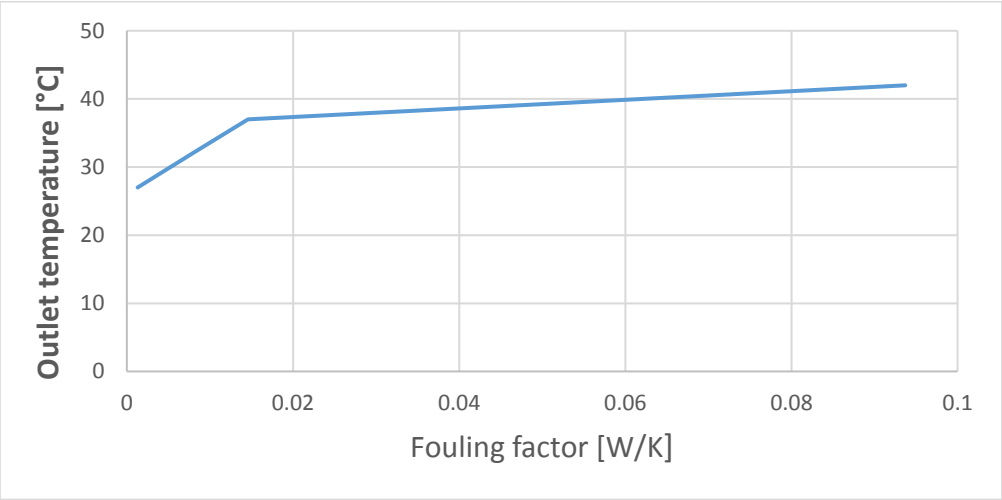

Figure 7-10: Function of growth with temperature

Figure 7-11 and Figure 7-12 shows the performance of the power block against the condenser fouling at variable inlet cooling water temperature. As the temperature of the cooling water is reduced, the resistance to condenser fouling reduces and there is an increase in the thermal efficiency of the CSP plant.

In SA, the major river runs through an arid region, with high solar irradiation. Flood irrigation is practiced on the riverbanks, using water that is extracted from the eco-system for agricultural use. One would expect the CSP plant to be constructed on low potential land above the canal. The water earmarked for agricultural use can be borrowed, run through the CSP plant and returned for agricultural use. This will increase the CSP plant thermal efficiency and reduce the pumping cost since the water is not taken from the river for CSP Plant but diverted from an existing irrigation-agricultural canal, closer to the plant.

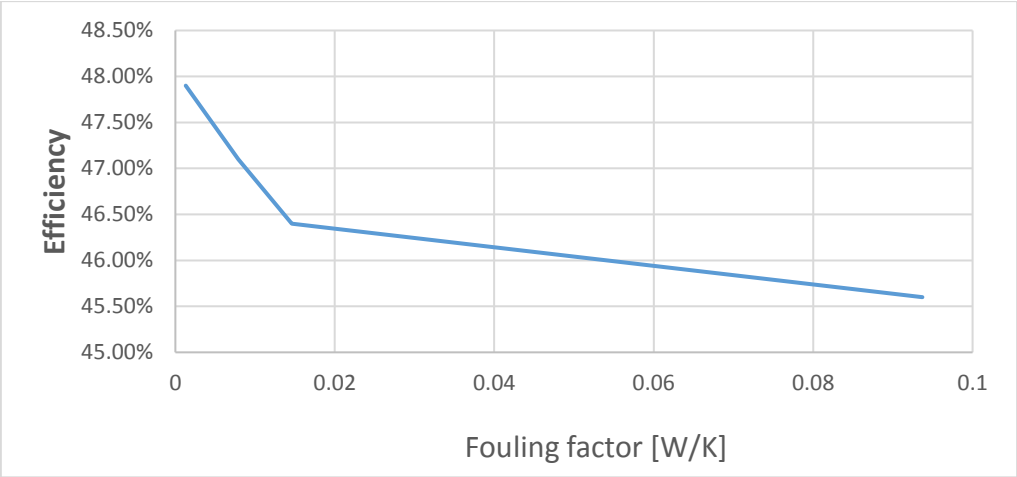

Figure 7-11: The performance of the drop in thermal efficiency against condenser fouling factor

The lower Orange River scheme uses 751 million cubic meters of water per year (a flow of about 24 m^3/s) (Water Affairs, 2013). Based on the cooling water flow rate at design point, which is 2.24 m^3/s , the design CSP plant will use about 70 million cubic meters of water per year. This means that the irrigated water can serve about 5 x 50 MW_e CSP plants using OTC.

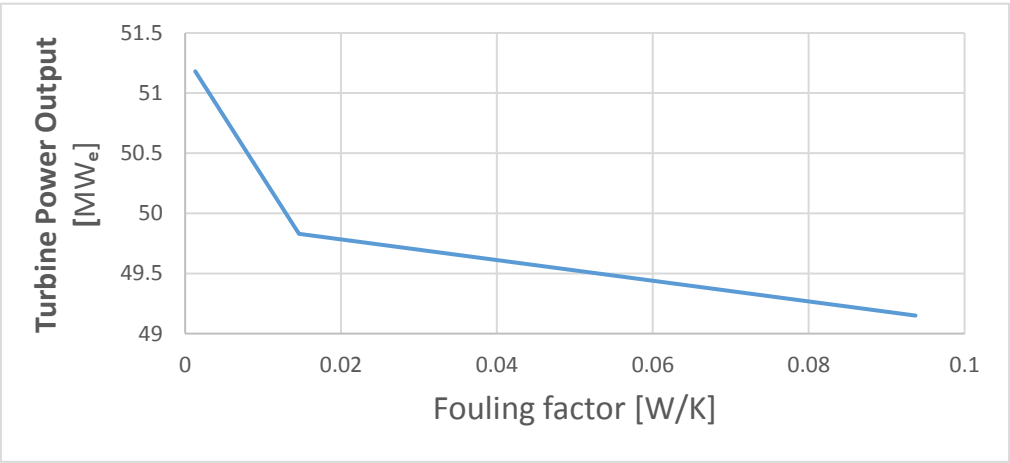

Figure 7-12: The performance of the turbine output against condenser fouling factor

This principle of using once through cooling for power plant can now solve the problem of power plant performance and at the same time provide water for irrigation or agricultural purposes. Since the outlet cooling water is not returning to the eco-system (i.e. not return to the river), there wouldn't be any impact on the environment (eco-system). It is assumed that the demand for irrigation will always exceed the demands of the CSP plant.

7.4 Agricultural and Environmental constraint

Environmental constraints has made once through cooling futile in power plants due to its inability to return the discharge water to the eco-system without the Government's approval. These constraints entail government policy on the discharge of effluent, which is approved by the SA's Government under the Department of Environmental Affairs (DEA, 2014). The constraints are meant to protect the living organism inside river and coastal environments. The Government policy under the Department of Environment Affairs (2014) set out rules related to the legislative framework and waste load on the discharge of effluent, which are listed below:

- The discharge of any effluent into the coastal environment from a land-based process in which it has been heated must be authorised by the Department of Environmental Affairs (DEA) in terms of section 69 of the Integrated Coastal Management Act (ICMA).
- The discharge of land-based effluent to any area declared a Marine Protected Area under the Marine Living Resources Act (Act No. 18 of 1998) is prohibited, unless the Minister of Environmental Affairs provides permission to do so.
- The discharge of any industrial effluent to the coastal environment without a licence is illegal under the Section 21 of the National Water Affairs (NWA). The industrial effluent include water used in an industrial process on land, contaminated(or polluted) water run-off originating from industrial areas that passes through man-made structures (such as canals, pipelines, etc.) directly into the coastal waters or seawater used as cooling water on land. E.g. Power Generation (Cooling water intake and discharge).

The above policy and regulations remains valid until appropriate guidelines are developed under the ICMA that will favour the discharge of cooling water from power generation. Currently, the policy does not allow new power plants to be constructed using water for cooling due to the fact that the returning cooling water can contain contaminants that are harmful to the eco-system. Fish and other smaller species get sucked into the inlet of cooling systems, and are killed due to impact on the screens. Furthermore, these animals find it difficult to adapt to wave movement of the water during pumping of intake cooling water and when discharging it (Water Affairs, 2013). It is necessary to properly design a flow pattern that does not create problem for the aquatic animal living inside the water.

We have identified a niche where an existing irrigation system can provide sufficient cooling water to small CSP plants. There are no policies or laws that constrain the use of irrigated water for CSP plant, or the discharge of cooling water back into the irrigation system. The water leaving the condenser should not have any adverse effect on crop growth, even for farms immediately downstream of the discharge point. It appears that the process is legal within the existing policy framework. To be safe, the water withdraw water from the canal would not be treated other than by filtering or screening. The downside is that untreated water is more susceptible to fouling, that has a detrimental effect on the CSP plant.

Chapter 8

Conclusion and recommendation

8.1 Conclusions

Once through cooling system has the potential to increase the performance of a CSP plant relative to that of a conventional dry-cooled plant. The temperature of the cooling water will determine how efficient the CSP plant will be. A design exploration, using once through cooling on a CSP plant has been done. This design will increase the production of electricity in South Africa and any other part of the world using CSP plant where similar conditions apply.

This thesis achieved its three main objectives listed in chapter one and its conclusions are discussed.

Objective one: To investigate the impact of condenser fouling factor on the improved thermal efficiency.

Details are provided for each component of CSP plant that was successfully modelled. These components entail heliostats, receiver, thermal storage and power block. Solar-PILOT was used to determine the heliostat optical efficiency, resulting in a 46.9 % at the design point. It was assumed that the plant is equipped with an external receiver to transfer energy from heliostat field to molten salt.

The power block, which contains of a steam generator, three-stage turbine, pump, feed-water heaters, and condenser, was analysed to determine the improved thermal efficiency of the CSP plant. The improved thermal efficiency of CSP plant was achieved by using once through cooling system for surface condenser. Life steam pressure and temperature was 13 MPa and 540 °C respectively.

A once through cooling system was successfully compared with an air-cooled system, which confirmed that there is an improvement in thermal efficiency of the CSP plant. It was observed that the hourly occurrence of surface cooling water temperature using Orange River as case study which near Upington is between 20 °C and 25 °C.

Because of relatively high inlet water temperature and deliberate avoidance of water treatment, condenser fouling was unavoidable and possible solutions to reduce it was discussed. A trade-off between improved thermal efficiency against condenser fouling was done. The results show that condenser fouling has an effect on overall performance of the CSP plant.

Objective two: To analyse the suitability of the condenser cooling water for irrigation-agricultural purposes.

Different inlet cooling water temperatures were used to achieve this objective. The cooling water temperature were varied from maximum cooling water temperature to the lowest cooling water temperature experienced from the Orange River's data. After the operation of the once-through condenser, the results show a great advantage of using the cooling water coming out from the condenser for irrigation and agricultural purposes.

Objective three: To Identify the environmental and agricultural constraints.

This objective was analysed based on the legislation and policies passed by the South African government. For agricultural constraints, no policy or laws constraint the use of discharge water for irrigation-agricultural purpose. For environmental constraints, the policy does not allow returning the discharge cooling water to the river without government approval. This is due to the harmful contaminant inside the discharge cooling water, which can affect the living organisms inside the water. This policy was discussed which identify different environmental limits on using once through cooling system for CSP plant. Based on the objective two of this thesis, a recommendation to use OTCS for CSP plant was made which will be a great benefit for the government and the entire people of SA.

8.2 Recommendations

The model for the once through cooling was based on Goodenough's surface condenser parameters, and tests done at the Kriel Power Station. The condenser is a double-pipe counter flow heat exchanger (a typical single shell, two-pass condenser) with admiralty brass tubes. It is recommended that field tests, using Goodenough's portable test facility should be performed to characterize fouling potential of water from the lower Orange River. A once through cooling model was developed for full load operation and it is recommended that the modelling should be repeated for part-load operations. The cooling water data should be updated for any further analysis on this research.

Proper site selection, system optimization, and a techno-economic study is required to bridge gaps in this study. The cost of CSP plant using once through cooling should be fully analysed.

References

Ávila-Marín, A. L. (2011) 'Volumetric receivers in Solar Thermal Power Plants with Central Receiver System technology: A review', *Solar Energy*, 85(5), pp. 891–910. doi: 10.1016/j.solener.2011.02.002.

Barlev, D., Vidu, R. and Stroeve, P. (2011) 'Innovation in concentrated solar power', *Solar Energy Materials and Solar Cells*. Elsevier, 95(10), pp. 2703–2725. doi: 10.1016/j.solmat.2011.05.020.

Bauder, W. J. (s.a) 'The Effective of Irrigation Water Quality, Temperature, and Length of Flooding on Alfalfa Production' *Montana State University*. Available at: http://waterquality.montana.edu/farm-ranch/irrigation/alfalfa/effects.html

Behbahani-Nia, A., Sayadi, S. and Soleymani, M. (2010) 'Thermoeconomic optimization of the pinch point and gas-side velocity in heat recovery steam generators', *Proceedings of the Institution of Mechanical Engineers, Part A: Journal of Power and Energy*, 224(6), pp. 761–771. doi: 10.1243/09576509JPE953.

Boyd, J. D. and Byron, J. D. (2010) 'IVANPAH SOLAR ELECTRIC GENERATING SYSTEM Commission Decision', (07).

Cabeza, L. F. *et al.* (2012) 'Review of solar thermal storage techniques and associated heat transfer technologies BT - SPECIAL ISSUE: The Intermittency Challenge: Massive Energy Storage in a Sustainable Future', 100(2), pp. 525–538. doi: 10.1109/JPROC.2011.2157883.

Cavallaro, F. (2009) 'Multi-criteria decision aid to assess concentrated solar thermal technologies', *Renewable Energy*. Elsevier Ltd, 34(7), pp. 1678–1685. doi: 10.1016/j.renene.2008.12.034.

Çengel, Y. A., Cimbala, J. M. and Turner, R. H. (2017) *Fundamentals of T H E R M a L-F L U I D Sciences*.

Çengel, Y. A. and Ghajar, A. J. (2015) *Heat and Mass Transfer-Fundamentals &Applications.* Fifth Edit.

Çengel, Y. and Boles, M. (2011) *Thermodynamics-An Engineering Approach*. Fifth Edit.

CMI (2016) 'Khi Solar One South Africa 50 MW CMI ' s first thermo solar receiver', *CMI Solar*. Available at: http://www.cmigroupe.com/sites/default/files/Documents/CMI Thermo Solar Study Case Khi Solar One.pdf.

Collado, F. J. and Guallar, J. (2013) 'A review of optimized design layouts for solar power tower plants with campo code', *Renewable and Sustainable Energy Reviews*, 20, pp. 142–154. doi: 10.1016/j.rser.2012.11.076.

Compton, S., and Maake, L. (2007) 'Source of the suspended load of the upper Orange River South Africa', *South African Journal of Geology*, 110(3), pp. 339-348. doi: 10.2113/gssajg.110.2/3.339

Curran, E. L. (2009) 'Solving Heat Exchanger Tube Problems with Thin Film Thermally Conductive Coating Applications and Novel Tube and Pipe Cleaning as a Precursor to Coating Application and NDT', 2009, pp. 414–419. Available at: http://heatexchanger-fouling.com/papers/papers2009/58_Curran_F.pdf.

Dallas, H. (2008) 'Water temperature and riverine ecosystems: An overview of knowledge and approaches for assessing biotic responses, with special reference to South Africa', *Water SA*, 34(3), pp. 393–404.

Department of Energy (2015) *State of Renewable Energy in South Africa*, *Livro*. doi: 9781920435080.

DEA (2014) 'National Guideline for the Discharge of Effluent from Land-Based Sources into the Coastal Environment', p. 201. Available at: http://www.environment.gov.za/

Dinter, F. and Möller, L. (2016) 'A review of Andasol 3 and perspective for parabolic trough CSP plants in South Africa', *AIP Conference Proceedings*, 1734, pp. 0–10. doi: 10.1063/1.4949193.

Dobersek, D. and Goricanec, D. (2007) 'Influence of water scale on thermal flow losses of domestic appliances', ... *Journal of Mathematical Models and Methods* ..., 1(2), pp. 55–61. Available at: http://www.naun.org/main/NAUN/ijmmas/mmmas-8.pdf.

DoE (2017) 'State of Renewable Energy in South Africa - 2017'. Available at: www.elsevier.com/locate/renene.

DoE (2018) 'State of Renewable Energy in South Africa - 2018'. Available at: www.elsevier.com/locate/renene.

Dunn, R. (2010) 'A global review of concentrated solar power storage', *Proceedings of Solar*, (December), pp. 1–10. Available at: http://citeseerx.ist.psu.edu/viewdoc/download;jsessionid=966DADC3BB86BF8A3B61260D23B895BB?doi=10.1.1.721.1106&rep=rep1&type=pdf.

Eck, M., Buck, R. and Wittmann, M. (2006) 'Dual Receiver Concept for Solar Towers up to 100 MW', *Journal of Solar Energy Engineering*. doi: 10.1115/1.2210501.

EPRI (2013) ‘research and development relating to the generation , delivery and use of electricity for the benefit of the public . An independent , nonprofit organization , EPRI brings together its scientists and engineers as well as experts from academia and industry’. Available at: http://eprijournal.com/wp-content/uploads/2015/07/Summer2013_Journal-low-3002001742.pdf.

ESTEA (2013) ‘SET-Plan - SOLAR THERMAL ELECTRICITY EUROPEAN INDUSTRIAL INITIATIVE (STE-EII)’, (December 2013), p. 41. Available at: http://www.solar-era.net/files/7613/9083/0789/Implementation_Plan_for_CSP_2013_2015.pdf.

Falchetta, M. and Rossi, A. G. (2013) ‘Dynamic simulation of the operation of a molten salt parabolic trough plant, comprising draining procedures’, *Energy Procedia*. Elsevier B.V., 49, pp. 1328–1339. doi: 10.1016/j.egypro.2014.03.142.

Fang, J. B. *et al.* (2011) ‘Thermal performance simulation of a solar cavity receiver under windy conditions’, *Solar Energy*. Elsevier Ltd, 85(1), pp. 126–138. doi: 10.1016/j.solener.2010.10.013.

Feeley, T. *et al.* (2008) 'Water: A critical resource in the thermoelectric power industry', *ScienceDirect*. Elsevier Ltd., 33(4), pp. 1-11. doi: 10.1016/j.energy.2007.08.007

Fernandes, D. *et al.* (2012) ‘Thermal energy storage: “How previous findings determine current research priorities”’, *Energy*. Elsevier Ltd, 39(1), pp. 246–257. doi: 10.1016/j.energy.2012.01.024.

Fleischli, S. and Hayat, B. (2014) ‘Power Plant Cooling and Associated Impacts’, *NRDC Issue Brief*, (April).

Fluri, T. P. (2009) ‘The potential of concentrating solar power in South Africa’, *Energy Policy*. Elsevier, 37(12), pp. 5075–5080. doi: 10.1016/j.enpol.2009.07.017.

García, E. and Calvo, R. (2012) ‘One Year Operation Experience of Gemasolar Plant’, *SolarPACES Conference 2012*, pp. 2–3. Available at: http://cms.solarpaces2012.org/proceedings/paper/85bc4b10b48.

Gauché, P., Backström, T. W.and Brent, A. C. (2012) ‘a Value Proposition of Csp for South Africa’, *Southern African Solar Energy Conference (SASEC)*, pp. 1–12. Available at: http://sterg.sun.ac.za/wp-content/uploads/2012/06/CSP-071.pdf.

Gil, A. *et al.* (2010) ‘State of the art on high temperature thermal energy storage for power generation. Part 1-Concepts, materials and modellization’, *Renewable and Sustainable Energy Reviews*, 14(1), pp. 31–55. doi: 10.1016/j.rser.2009.07.035.

Girish, S. *et al.* (2017) ‘Analysis of a condenser in a thermal power plant for possible augmentation in its heat transfer performance’, *International Journal of Civil Engineering and Technology*, 8(7), pp. 410–420. Available at: http://www.iaeme.com/IJCIET/issues.asp?JType=IJCIET&VType=8&IType=7.

Goodenough, J. (2013) 'Thermal performance evaluation of artificial protective coatings applied to steam surface condenser tubes by', (December).

Haldkar, V. *et al.* (2013) 'An Energy Analysis of Condenser', *International Journal of Thermal Technologies*, 3(4), pp. 120–125.

Hoffmann, J.E. and Madaly, K (2015) 'On Thermal Energy Storage Capacity for CSP Plant in South Africa', *R&D Journal of the South African Institution of Mechanical Engineering*, pp. 46-51

IRENA (2018) *IRENA: Renewable Power Generation Costs in 2017*, *International Renewable Energy Agency*.

Janikowski, D. S. (2003) 'Sel Tubing Mat for Pwr Gen _SW Chem_'. Available at: https://www.plymouth.com/wp-content/uploads/2017/03/Sel-Tubing-Mat-for-Pwr-Gen-_SW-Chem_-1.pdf.

Kenny, J. F. *et al.* (2005) *Estimated Use of Water in the United States in 2005 Circular 1344*, *Water*. Available at: http://hbg.psu.edu/etc/Newsletter/doc/October2009.pdf.

Lambert, A. (2010) 'Improved high temperature solar absorbers for use in concentrating solar power central receiver applications', (May 2014), pp. SAND2010-7080. doi: 10.2172/1008136.

Li, L. *et al.* (2016) 'Optics of solar central receiver systems: a review', *Optics Express*, 24(14), p. A985. doi: 10.1364/oe.24.00a985.

Madaly, K. (2015) 'Identifying the optimum storage capacity for a 100 MW concentrating solar power plant in South Afica', available at : http://scholar.sun.ac.za

Malaga, K. and Bengtsson, T. (2008) 'The Nordic method: performance tests for protective sacrificial coatings on mineral surfaces', *5th International Conference on Water Repellent Treatment of Building Materials*, 180, pp. 169–180.

Malayeri, M. R. (2007) 'an Overview of Fouling Mechanisms , Prediction and Mitigation Strategies for Thermal Desalination Plants', pp. 299–314.

Meybodi, M. A. and Beath, A. C. (2016) 'Impact of cost uncertainties and solar data variations on the economics of central receiver solar power plants: An Australian case study', *Renewable Energy*. Elsevier Ltd, 93, pp. 510–524. doi: 10.1016/j.renene.2016.03.016.

Micheletti, W. C. and Burns, J. M. (2002) 'Emerging Issues and Needs in Power Plant Cooling Systems by', pp. 1–14.

Montes, M. J., Abánades, A. and Martínez-Val, J. M. (2009) 'Performance of a direct steam generation solar thermal power plant for electricity production as a function of the solar multiple', *Solar Energy*, 83(5), pp. 679–689. doi: 10.1016/j.solener.2008.10.015.

Moon, H. and Zarrouk, S. J. (2012) 'Efficiency of geothermal power plants: A worldwide overview', *New Zealand Geothermal Workshop*, (November 2012).

Moore, R. C. *et al.* (2010) 'Design considerations for concentrating solar power tower systems employing molten salt.', (September). doi: 10.2172/1008140.

Nacional, B. and Brasile, D. (2012) 'Innovative technology solutions for sustainability', pp. 1–2. Available at: http://movil.abengoasolar.com/export/sites/abengoa_corp/resources/pdf/noticias_y_publicaciones/20161222-NP-RP_Khi-en.pdf.

Nag, P. K. (2007) *Power plant engineering.* 3rd editio. New Delhi. McGraw-Hill Education.

NREL (2018a) 'Concentrating Solar Power Projects Browse the Project Profiles About the Project Profiles', pp. 4–6. Available at: http://www.nrel.gov/csp/solarpaces/by_country_detail.cfm/country=ZA.

NREL (2018b) 'SolarPILOT'. Available at: https://www.nrel.gov/csp/solarpilot-download.html.

Pavlović, T. M. *et al.* (2012) 'A review of concentrating solar power plants in the world and their potential use in Serbia', *Renewable and Sustainable Energy Reviews*, 16(6), pp. 3891–3902. doi: 10.1016/j.rser.2012.03.042.

Plaza, N. (2008) 'Solar Power Plant Pre-feasibility Study', *Solar Energy*, (September).

Putman, R. E. (2001) 'Steam surface condensers: Basic principles, performance monitoring, and maintenance.', *ASME Press*.

Reuter, C., Owen, M., and Goodenough, J. (2017) 'Exprimental evaluation of the temporal effects of paint-based protective films in composite fouling inside admiralty brass and titanium steam surface condenser tubes' *Applied Themal Engineering*. pp. 848-857. http://dx.doi.org/10.1016/j.applthermaleng.2017.07.196

Rodríguez, I. *et al.* (2013) 'Modular object-oriented methodology for the resolution of molten salt storage tanks for CSP plants', *Applied Energy*. Elsevier Ltd, 109, pp. 402–414. doi: 10.1016/j.apenergy.2012.11.008.

Roux, S. *et al.* (2012) *a Comparison of the Cost Associated With Pollution Prevention Measures To That*.

Sánchez, M. and Romero, M. (2006) 'Methodology for generation of heliostat field layout in central receiver systems based on yearly normalized energy surfaces', *Solar Energy*, 80(7), pp. 861–874. doi: 10.1016/j.solener.2005.05.014.

Sargent and Lundy LLC Consulting Group (2003) 'Assessment of Parabolic Trough and Power Tower Solar Technology Cost and Performance Forecasts Assessment of Parabolic Trough and Power Tower Solar Technology Cost and Performance Forecasts - Report No. NREL/SR-550-34440 - National Renewable Energy Labora', (October). doi: NREL/SR-550-34440.

Scheffler, O. (2015) 'Optimization of an Optical Field for a Central Receiver Solar Thermal Power Plant', (May).

Sengupta, M. and Wagner, M. (2012) 'Estimating Atmospheric Attenuation in Central Receiver Systems', *ASME 2012 6th International Conference on Energy Sustainability, Parts A and B*, (1), p. 399. doi: 10.1115/ES2012-91229.

Siddiq, E. S. and Khushnood, P. S. (2013) 'Optimal performance analysis of a solar thermal energy storage plant based on submitted by optimal performance analysis of a solar thermal energy storage plant based on Approved by Internal Examiner (Research Supervisor) Department of Mechanical Enginee', (July).

Siemens (2011) 'Steam turbines for CSP plants', p. 16. Available at: http://www.energy.siemens.com/hq/pool/hq/power-generation/steam-turbines/downloads/steam-turbine-for-csp-plants-siemens.pdf.

Sioshansi, R. and Denholm, P. (2010) 'The value of concentrating solar power and thermal energy storage', *IEEE Transactions on Sustainable Energy*, 1(3), pp. 173–183. doi: 10.1109/TSTE.2010.2052078.

SoDa (2018) 'SoDa : a Web service on solar radiation', (February). Available at: http://www.soda-pro.com/.

Solar, A. (2013) 'Innovat ive t echnology solut ions f or sust ainabilit y A New Generat ion of Parabolic Trough Technology', *SunShot CSP Program Review Phoenix*, (April). Available at: https://energy.gov/sites/prod/files/2014/01/f7/csp_review_meeting_042513_price.pdf.

Solar Reserve (2017) 'Solar Reserve', (October). Available at: http://www.solarreserve.com/en/technology/molten-salt-energy-storage.

SolarGIS (2011) 'Site Assessment of Solar Resource', (58), pp. 1–33.

SolarReserve (2017) '5 th Annual STERG SolarPACES Symposium SolarReserve Overview', (July). Available at: http://sterg.sun.ac.za/wp-content/uploads/2017/03/20170714-SolarReserve-T-Govender-Presentation.pdf.

SolarReserve (2018) 'SolarReserve and ACWA Sign Power Purchase Agreement for 100 MW Solar Thermal Project with Energy Storage in South Africa'. Available at: http://www.solarreserve.com/.

Stine, W. and Geyer, M. (2001) *Power from the sun*. Available at: http://www.powerfromthesun.net/.

Talebizadeh, P., Mehrabian, M. A. and Rahimzadeh, H. (2013) 'Optimization of Heliostat Layout in Central Receiver Solar Power Plants', *Journal of Energy Engineering*, 140(4), p. 04014005. doi: 10.1061/(asce)ey.1943-7897.0000162.

Viebahn, P., Lechon, Y. and Trieb, F. (2011) 'The potential role of concentrated solar power (CSP) in Africa and Europe-A dynamic assessment of technology development, cost development and life cycle inventories until 2050', *Energy Policy*. Elsevier, 39(8), pp. 4420–4430. doi: 10.1016/j.enpol.2010.09.026.

Water Affairs (2013) 'Vision of the National Water Research Strategy 2 Sustainable, equitable and secure water for a better life and environment for all', p. 201. Available at: http://www.dwa.gov.za/documents/Other/Strategic Plan/NWRS2-Final-email-version.pdf.

Wikipedia (2018) 'Heliostat'. Available at: https://en.wikipedia.org/wiki/Heliostat.

Worthington, R. (2015) 'Challenging the State : Renewable Energy opportunities and electricity in South Africa in 2015', *Alternative Information & Development Centre*, (September).

Wu, S. , Xiano, L., Cao, Y., and Li, Y. (2010) 'A parabolic dish/AMTEC solar thermal power system and its performance evaluation', *Applied Energy*. Elsevier Lted, 87(10), pp. 452-462. doi:10.1016/j.apenergy.2009.08.041

Xu, C. *et al.* (2011) 'Energy and exergy analysis of solar power tower plants', *Applied Thermal Engineering*. Elsevier Ltd, 31(17–18), pp. 3904–3913. doi: 10.1016/j.applthermaleng.2011.07.038.

Yang, M. *et al.* (2010) 'Heat transfer enhancement and performance of the molten salt receiver of a solar power tower', *Applied Energy*. Elsevier Ltd, 87(9), pp. 2808–2811. doi: 10.1016/j.apenergy.2009.04.042.

Zoschak, R. J., Wu, S. F. and Gorman, D. N. (2009) 'Design and Testing of a Cavity-Type, Steam-Generating, Central Receiver for a Solar Thermal Power Plant', *Journal of Engineering for Power*. doi: 10.1115/1.323028

Zwietering, M. H., De Koos, J.T., Hasenack, B.E., De Wit, J.C., and Van 'T Riet, K. (1991) 'Modelling of Bacterial Growth as a Function of Temperature' *Applied and Environmental Microbology*. pp1094-1101. 0099-2240/91/041094-08$02.00/0

Appendix A

Thermo-physical properties

A.1 Thermo-physical properties of molten salt (Sandia National Laboratories, 2001)

- Density (kg/m^3)

$$\rho = 2090 - 0.636T_{salt} \tag{A.1}$$

- Specific heat (J/kg °C)

$$c_p = 1443 + 0.172T_{salt} \tag{A.2}$$

- Absolute Viscosity (mPa/s)

$$\mu = 22.714 - 0.120T_{salt} + 2.281 \times 10^{-4}T_{salt}^2 - 1.47 \times 10^{-7}T_{salt}^3 \tag{A.3}$$

- Thermal conductivity (W/m °C)

$$\kappa = 0.443 + 1.9 \times 10^{-7}T_{salt} \tag{A.4}$$

A.2 Thermo-physical properties of saturated water from 273.15 K to 380 K (Kröger, 1998)

- Density (kg/m^3)

$$\rho = (1.49343 \times 10^{-3} - 3.7164 \times 10^{-6} T_w + 7.09782 \times 10^{-9} T_w^2 - 1.90321 \times 10^{-20} T_w^6)^{-1} \quad \text{(A.5)}$$

- Specific heat (J/kg °C)

$$c_p = 8.15599 \times 10^3 - 2.80627 \times 10^1 T_w + 5.11283 \times 10^{-2} T_w^2 - 2.17582 \times 10^{-13} T_w^6 \quad \text{(A.6)}$$

- Absolute Viscosity (mPa/s)

$$\mu = 2.414 \times 10^{-5} \times 10^{\frac{247.8}{(T_w - 140)}} \quad \text{(A.7)}$$

- Thermal conductivity (W/m K)

$$k_f = -6.14255 \times 10^{-1} + 6.9962 \times 10^{-3} T_w - 1.01075 \times 10^{-5} T_w^2 + 4.74737 \times 10^{-12} T_w^4 \quad \text{(A.8)}$$

- Prandtl number

$$Pr = \frac{\mu c_p}{k_f} \quad \text{(A.9)}$$

Appendix B

Different types of CSP plant in South Africa

Different types of CSP plant in South Africa were listed in Table B-1 with their cooling system. Its shows that none of the CSP plants is using once through cooling, five of them is using air-cooled while the remaining one is using closed cooling system.

Table B-1: Various CSP in South Africa

BW no	Name	Technology	Location	Capacity	Owner	Storage capacity	Cooling System
1	KaXu	trough	Profadder	100 MWe	Abengoa	2.5	Air-cooled
	Khi	Central Receiver	Upington	50 MWe	Abengoa	2	Air-cooled
2	Bokpoort	trough	Groblershoop	50 MWe	ACWA	9.3	Closed cooling
3	Xina	trough	Pofadder	100 MWe	Abengoa	5	Air-cooled
	Ilanga 1	trough	Upington	100 MWe	Emvelo, Cobra	4.5	Air-cooled
3.5	Kathu solar park	trough	Kathu	100 MWe	Kathu Solar Park Consortium		Air-cooled
	Redstone	Central receiver	Postmasburg	100 MWe	ACWA, Solar reserve	12	Air-cooled
4				450 MWe	Bids established		

Appendix C

Heliostat field simulated result

Heliostat optical field efficiency was simulated in Solar-PILOT. The results contains the heliostat field boundary, heliostat field layout, and heliostat field efficiency

C.1 Heliostat field boundary

Figure C-1 shows a circular heliostat field boundary at which the heliostat occupied.

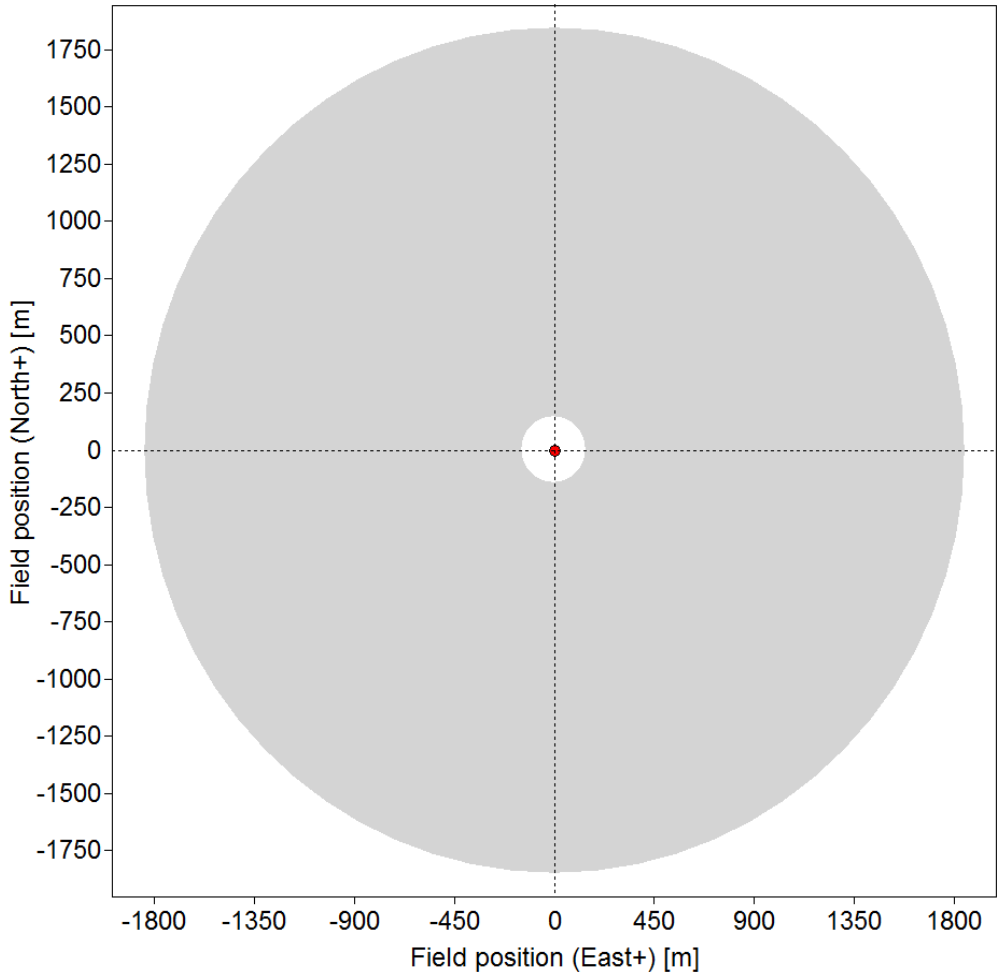

Figure C-1: Field boundary in Solar-PILOT

C.2 Heliostat field layout

Figure C-2 shows a circular heliostat field layout, which is occupied with heliostat. The red dot at the centre of the circle represents the receiver tower, which is at the middle of the circular heliostat field.

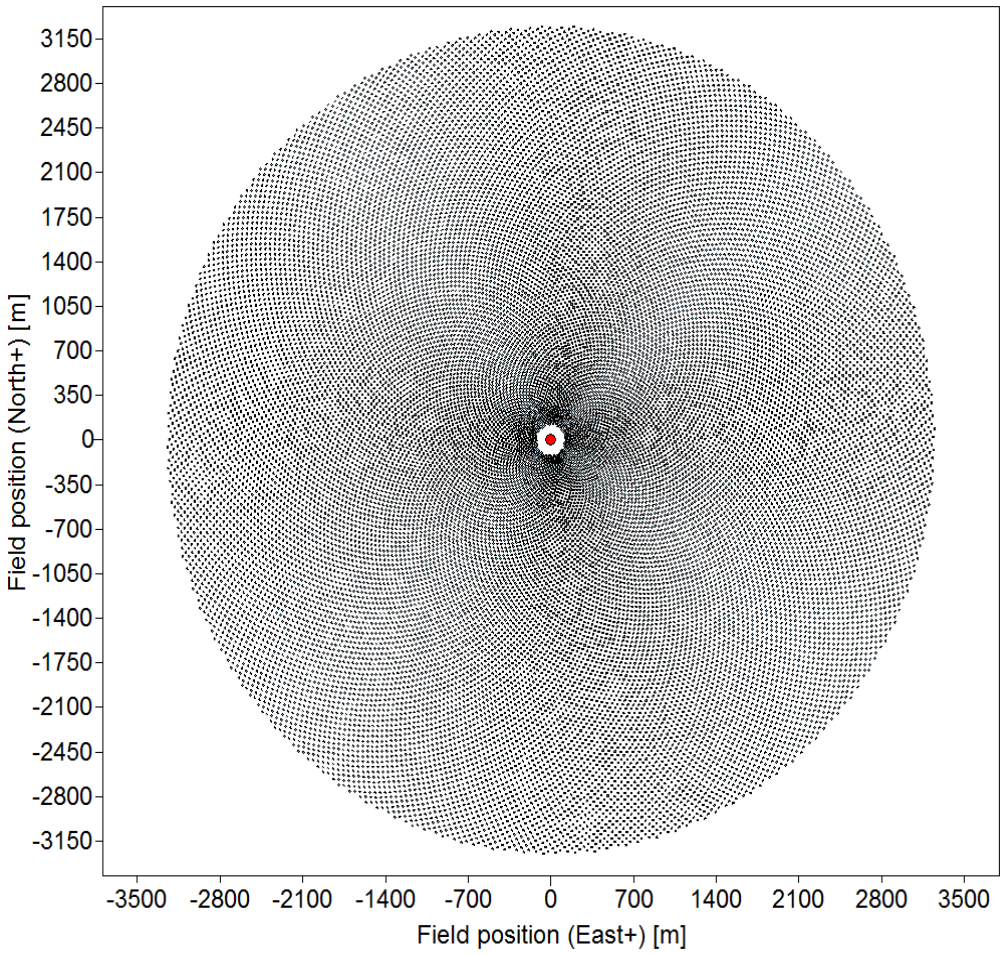

Figure C-2: Field layout in Solar-PILOT

C.3 Heliostat field efficiency

Figure C-3 shows a circular heliostat field efficiency, which is occupied with heliostat. The heliostat field efficiency occurs due to the position of sun at design point.

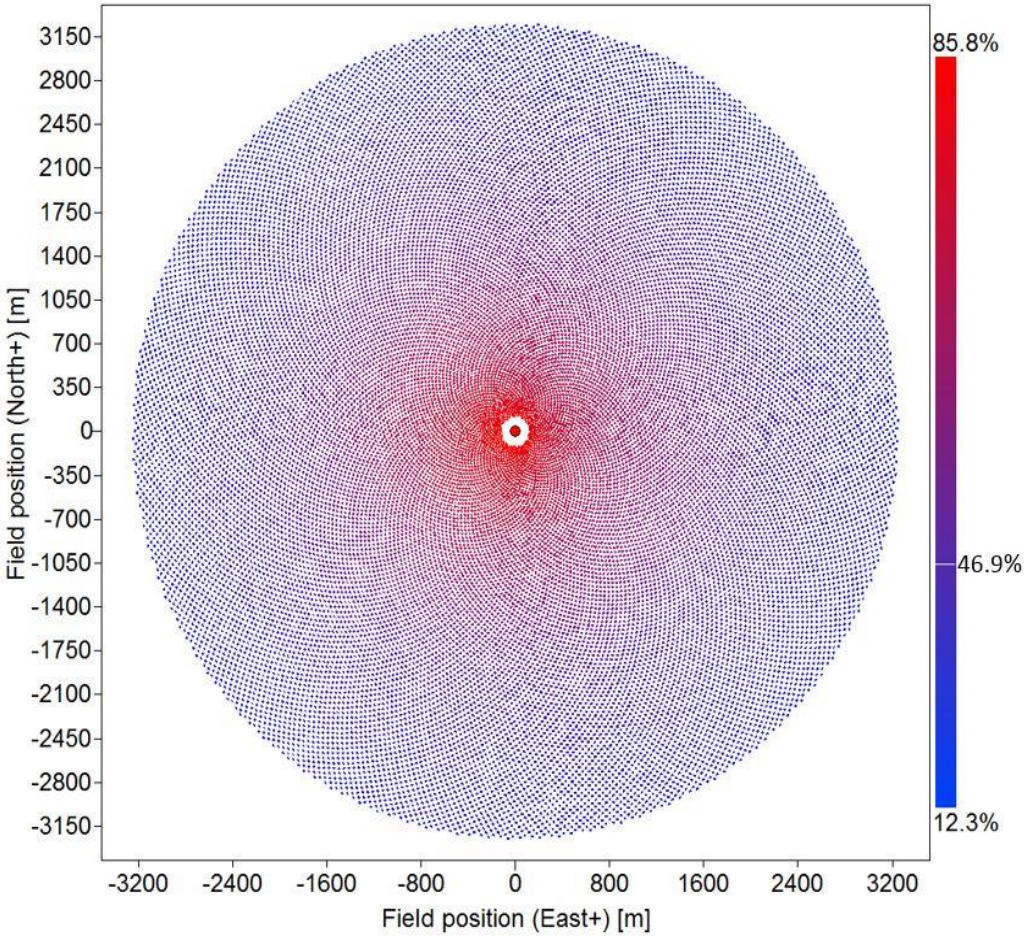

Figure C-3: Heliostat optical field efficiency

Appendix D

Analysis of modelled once-through cooling condenser

The modelling parameter for a double-pipe counter flow heat exchanger (typically single shell, two pass surface condenser) with admiralty brass tubes are represented in Table D-2

Table D-2: Modelling parameter for once-through cooling condenser

	Symbol	Unit	Value
Condenser heat duty	Q_{duty}	MW	200.2
Cleanliness factor	F_c		1
Cooling water flow	V_{cw}	[m^3/s]	6.85
Steam temperature	T_s	[°C]	33.1
Inlet Water temperature	T_{cwi}	[°C]	21.1
Annular diameter	d_3	[m]	301.644
Outer tube diameter	d_2	[m]	0.0277
Inner tube diameter	d_1	[m]	0.02291
Effective length	L	[m]	9
Number of tubes per pass	N_p		8400
Number of tubes rows	n		100
Pumping power (only along tube length)	$\Delta p.V$	[kW]	90
Specific heat capacity of water	$C_{p,cw}$	[J/m.K]	4180.8
Density of cooling water	ρ_{cw}	[kg/m^3]	997
Thermal conductivity of tube material	k_t	[J/m.K]	111

The mass flow rate of the cooling water is determined as

$$\begin{aligned} \dot{m}_{cw} &= \rho_{cw} V_{cw} \\ &= (997)(6.85) \\ &= 6829.45\ kg/s \end{aligned} \tag{D.1}$$

The surface areas based on the outer diameter of the tubes is evaluated as

$$A_h = \pi(0.0277)(9)(8400) = 6578.87\ m^2 \tag{D.2}$$

The cross sectional area of the cooling water inside each tube

$$A_{cw} = \frac{\pi(0.02291)^2}{4} = 0.0004122\ m^2 \tag{D.3}$$

The velocity of the cooling water inside each tube

$$v_{cw} = \frac{6.85}{(0.0004122)(8400)} = 1.980\ m/s \tag{D.4}$$

From the Table D.2, the inlet temperature, specific heat capacity of water, density of cooling water and thermal conductivity of tube material are 21.1°C, 4180.8 J/m.K, 997 kg/m^3, 111 J/m.K

From equation (5.47), the outlet cooling water temperature is calculated as

$$T_{cwo} = \frac{200200000}{(997)(0.0004122)(1.980)(4180.8)(8400)} + 21.1 = 28.1\ ℃ \tag{D.5}$$

From equation (5.48), the change in temperature is known as

$$\Delta T_{cw} = 28.1 - 21.1 = 7\ ℃ \tag{D.6}$$

And from equation (5.49), the terminal temperature difference is

$$TTD = 33.1 - 28.1 = 5\ ℃ \tag{D.7}$$

The initial temperature difference using equation 5.50 is

$$ITD = 33.1 - 21.1 = 12\ ℃ \tag{D.8}$$

The TTD, ITD and change in temperature ΔT_{cw} is constant in the power block model.

Appendix E

Sample calculations

The analysis of once-through cooling CSP plant at design point is calculated below. The analysis include heliostat field, central receiver, power block and fouling factor.

E.1 Analysis of heliostat field efficiency

E.1.1 Weather data

In determining the heliostat optical field efficiency, it is necessary to know the weather condition and location of the site using which is in Table E-3 and

Table E-4 respectively.

Table E-3: Upington weather data

YEAR	MONTH	DAY	HOUR	YEAR DAY	GHI [W/m^2]	DNI [W/m^2]	DHI [W/m^2]	T_a [°C]	WIND SPPED [m/s]
2017	09	22	12	356	1122	950	172	35.11	6.2

Table E-4: Upington site data

Parameter	Symbol	Units	Value
Altitude		[m]	879
Latitude	φ	[°]	-28.395
Local longitude	LL	[°]	21.2368
Time zone	TZ	[°]	30
Longitude correction	LC	[°]	-0.58421

The modelling parameter used in designing the heliostat field in Solar-PILOT can be seen from Table E-5 in order to know the heliostat field efficiency.

Table E-5: Modelling parameter used Solar-PILOT for heliostat field efficiency

Parameter	Unit	Value
Heliostat height	12.68	[m]
Heliostat width	10.58	[m]
Number of heliostats	24844	#
Heliostat area	248	
Reflective surface ratio	0.97	
Field aperture area (A_{fa})	3333104	[m^2]
Mirror reflectivity	0.95	

Mirror cleanliness	0.95	
Tower optical height	195	[m]

E.1.2 Sun's position

The Sun's position used in Solar-PILOT at design point is calculated below.

Firstly, convert the day of the year into an angular value using equation (5.2), table 5.2 and is evaluated as

$$\chi = \frac{(356 - 1)360}{365} = 350.14\,^{\circ} \tag{E.1}$$

From equation (5.1), the equation of time is

$$EOT = 0.25\cos(350.14) - 7.4168\sin(350.14) - 3.648\cos 2(350.14) - 9.2288\sin 2(350.14) \tag{E.2}$$

$$= 1.1959\ minutes$$

$$= 0.020\ seconds$$

The longitude correction is calculated from equation (5.4) as

$$LC = \frac{(21.2368) - (30)}{15} = -0.58421\,^{\circ} \tag{E.3}$$

The daylight saving is negligible. From equation (5.3), the solar time is known as

$$t_s = 12.00 + \frac{1.1959}{60} - (-0.58421) \tag{E.4}$$

$$= 12.60\ h$$

The hour angle ω, using equation (5.5)

$$\omega = 15(12.60 - 12) = 9.0\,^{\circ} \tag{E.5}$$

And the declination angle δ, using equation (5.6) is calculated as

$$\delta = \sin^{-1} 0.39795 \cos[0.98563(356 - 173)] = -23.45\,^\circ \tag{E.6}$$

From equation (5.7), the solar altitude angle is

$$\begin{aligned}\alpha = \sin^{-1}(&\sin(-23.45)\sin(-28.395) \\ &+ \cos(-23.45)\cos(9.0)\cos(-28.395))\end{aligned} \tag{E.7}$$

$$= 80.54\,^\circ$$

And the zenith angle using equation (5.8)

$$\theta_z = 90 - 80.54 = 9.46\,^\circ \tag{E.8}$$

From equation (5.9), the azimuth angle is calculated as

$$\gamma_s = \sin^{-1}\left(\frac{\cos(-23.45)\cos(9)}{\cos(80.54)}\right) = 60.8\,^\circ \tag{E.9}$$

Both the solar azimuth angle and solar altitude angle are inserted into Solar-PILOT before the simulation takes place. After the simulation, the heliostat field efficiency at design point is 46.9 % (see Table 7-1 in Chapter 7).

E.2 Analysis of Centre Receiver

The modelling parameter for receiver tower shown in Table E-6 and the analysis is given as follow:

Table E-6: Modelling parameter for receiver tower

Parameter	Value	Unit	Parameter	Value	Unit
Tower height	195	[m]	Receiver piping loss	0.5	[MW]
Receiver height	23.5	[m]	Number of panels	16	#
Receiver diameter	14.7	[m]	Tube thickness	1.5	#
Receiver absorber area	1085.3	[m^2]	Tube outer diameter	50	[mm]
Receiver surface ratio (H/W)	1.6		Tube inner diameter	47	[mm]
Receiver reflectivity	0.93		Inlet temperature	290	[°C]
Receiver emissivity	0.88		Outlet temperature	565	[°C]
Allowable peak flux	700	[kW/m^2]	Solar multiple	1	
	$5.67x10^{-8}$	W/m^2K^4	Ambient temperature	35.11	[°C]
Receiver absorption	0.94				

From equation (5.10), the total energy received from the heliostat field is calculated as

$$\mathbb{Q}_{of} = (950)(0.4690)(3333104.2)(1) = 1485064576\ W \qquad \text{(E.10)}$$

Losses due to convection and radiation at the receiver were calculated. Using thermos-physical properties of air, the thermal conductivity of the tube material at 600 ℃ = 21.1 W/m ℃ and the ambient temperature at design point is 35.11 ℃ . The maximum temperature received at the receiver using equation (5.19) is known as

$$\mathrm{T}_{max} = 565 + \frac{2)(700000)(0.05)\log(0.05/0.047)}{21.1} = 654.2\ ℃ \qquad \text{(E.11)}$$

And the minimum temperature received at the receiver using equation (5.20) is calculated as

$$\mathrm{T}_{max} = 290 + \frac{2)(700000)(0.05)\log(0.05/0.047)}{21.1} = 379.2\ ℃ \tag{E.12}$$

From equation (5.18), the mean radiation temperature at the receiver is calculated as

$$\overline{\mathrm{T}}_{mr}^{4} = \frac{(654.2)^4 + (654.2)^3(379.2) + (654.2)^2(379.2)^2 + (654.2)(379.2)^3 + (379.2)^4}{5} \tag{E.13}$$

$$\bar{T}_{mr} = 534.22\ ℃$$

From equation (5.15), the radiation losses is given as

$$\mathbb{Q}_{rad} = (5.67x10^{-8})(0.88)(\pi)(14.7)(23.5)\left(5432.22^4 - 35.11^4\right) \tag{E.14}$$

$$= 4410756.45\ W$$

Also, the mean receiver surface temperature using equation (5.23) is given as

$$\mathrm{T}_{mrs} = \frac{565 + 290}{2} + \frac{2)(700000)(0.05)\log(0.05/0.047)}{21.1} \tag{E.15}$$

$$= 516.65\ ℃$$

Using thermos-physical properties of air, the density, thermal conductivity, Prandtl number is calculated at the mean film temperature (35.11) at 1 bar as$\rho = 1.145\ kg/m^3$,$k_a = 0.02699\ W/m\ ℃$, $Pr = 0.71$, $\mu = 18.84x10^{-6}\ kg/\ m.s$

The wind speed (V_{10}) is given from the weather data at design point and the height of the receiver y is known from table D.4. Using equation (5.26), the wind speed profile at design point is given as

$$V(y) = (6.2)\left(\frac{23.5}{10}\right)^{1/7} = 7.0\ m/s \tag{E.16}$$

From equation (5.25), the Reynolds number is

$$Re = \frac{(1.145)(7.0)(14.7)}{0.0001884} = 6253742.038 \tag{E.17}$$

Since the external receiver is in a form of cylinder, the overall heat transfer coefficient using equation (5.24) calculated as

$$h_{fc} = \frac{0.027(6253742.038)^{0.805}(0.71)^{0.333}(0.02699)}{14.7} \tag{E.18}$$

$$= 13.08\ W/m^2℃$$

And the convectional losses using equation (5.27) is calculated as

$$\mathbb{Q}_{conv} = (\pi)(14.7)(23.5)(13.08)(516.65 - 35.11) \tag{E.19}$$

$$= 6836453.428\ \text{W}$$

The amount of heat transfer to the salt is calculated using equation (5.12) as

$$(0.94)(1485064576) = 4410756.447 + 6836453.428 + \mathbb{Q}_s \tag{E.20}$$

$$\mathbb{Q}_s = 1395960702 - 11247209.87$$

$$= 1384713492\ W$$

E.3 Analysis of power block

The analysis of the power block is based on the Rankine cycle with three feed-water heaters and once-through cooling condenser as shown in figure E-4. Table E-7 shows the modelling parameter obtained from add in X-steam in the Microsoft Excel at each points of the power block.

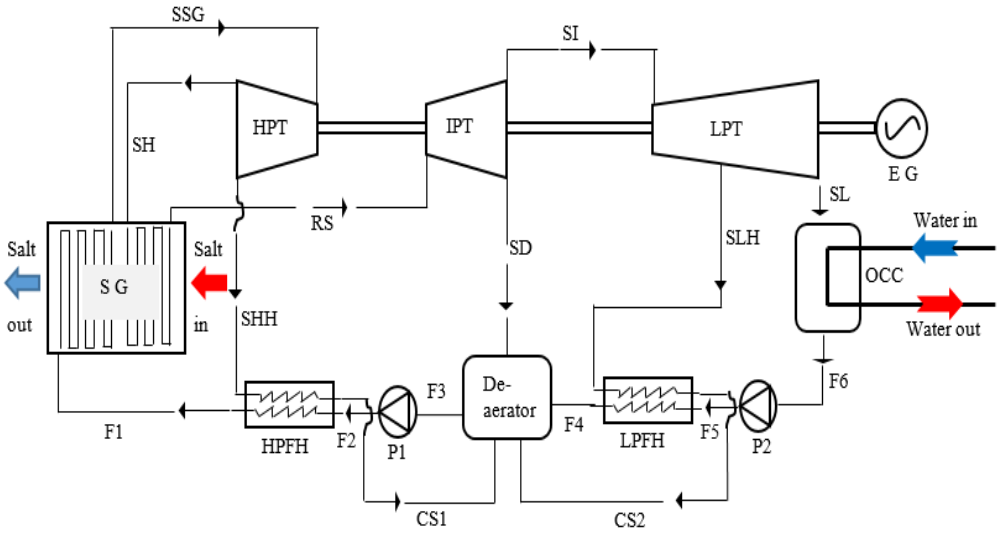

Figure E-4: Power block layout with three feed-water heaters

The modelling assumption for the modelled power block as follows:

- Steam pressure at outlet steam generator = 130 MPa
- Steam temperature at outlet steam generator = 540 ℃
- Reheat temperature = 540 ℃
- Feed-water heater at inlet steam generator = 130 MPa
- Feed-water heater temperature at inlet steam generator = 220 ℃
- Temperature rise across each feed-water heater are equal
- Total power output at the electric generator = 50 MW_e
- The efficiency of high pressure turbine = 0.90
- The efficiency of intermediate pressure turbine = 0.85
- The efficiency of low pressure turbine = 0.82
- Electric Generator efficiency = 0.98
- Change in cooling water temperature = 7 ℃
- Terminal temperature difference = 5 ℃
- Exit pressure pump (P2) is equal to the Deaerator pressure
- Exit pressure pump (P2) is equal to the SG inlet pressure

Table E-7: Modelling parameter for power block obtained from X-Steam

Steam point	Temperature [T] [°C]	Pressure [P] [kPa]	Enthalpy [h] [kJ/kg]	Entropy [S] [kJ/kgK]	Mass flow rate [m] [kg/s]	Initial mass flow rate [m] [kg/s]
SSG	540	13000	3445.053	6.5765	35.54	1
SH	344.09	32.5	3096.33	6.6783	35.54	1
RS	540	32.5	3544.625	7.3099	35.54	1
SHH	344.09	32.5	3096.33	6.6783	4.52	0.127
CS1	238.34	32.5	1029.607	2.6865	4.52	0.127
SD	354.33	8.13	3171.017	7.4177	1.68	0.0472
SI	354.33	8.13	317.017	7.4177	31.02	0.873
SLH	271.12	4.09	3007.633	7.4513	3.19	0.0897
CS2	144.4	4.09	608.099	1.7849	3.19	0.0897
SL	33.1	0.05	2354.315	7.714	29.34	0.826
F_6	33.1	0.05	138.704	0.4796	26.15	0.736
F_5	33.2	8.13	139.769	0.4804	29.34	0.826
F_4	95.47	8.13	400.535	1.255	29.34	0.826
F_3	157.73	8.13	665.863	1.92	35.54	1
F_2	157.73	130	683.802	1.9306	35.54	1
F_1	220	130	946.83	2.4987	35.54	1
Inlet water	21.1	2.50	189.8	0.70	2235.99	
Outlet water	28.1	3.80	267.24	0.91	2235.99	

E.3.1 Steam generator

The heat added at the steam generator is calculated using equation (5.31) is

$$\mathbb{Q}_{SG} = 35.54(3445.053 - 946.830) = 88786.84542\ kJ/s \qquad \text{(E.21)}$$

The heat required from the re-heater is determined using equation (5.32)

$$\mathbb{Q}_{RH} = 35.54(3544.625 - 3096.33) = 15932.4043\ kJ/s \qquad \text{(E.22)}$$

The total heat added in the steam generator is calculated using equation (5.33)

$$\mathbb{Q}_{T} = (88786.84542 + 15934.4043) = 104719.2497\ kJ/s \qquad \text{(E.23)}$$

E.3.2 Turbine

The work done by HPT is known using equation (5.35)

$$w_{HPT} = 35.54(3445.053 - 3096.33) + 4.52(3445.053 - 3096.33) \\ = 13969.84338\ kJ/s \tag{E.24}$$

The work done by the IPT using equation (5.36) is

$$w_{IPT} = 31.02(3544.625 - 3171.017) + 1.68(3544.625 - 3171.017) \\ = 12216.9816\,kJ/s \tag{E.25}$$

The work done by the LPT using equation (5.37) is

$$w_{LPT} = 29.34(3171.017 - 2354.315) + 3.19(3171.017 - 3007.633) \\ = 24483.23164\,kJ/s \tag{E.26}$$

The total work done is calculated using equation (5.38)

$$w_T = (13969.84338 + 12216.9816 + 24483.23164\ ) \\ = 50670.05662\ kJ/s \tag{E.27}$$

E.3.3 Feed-water heater

The temperature rise across feed-water heater is calculated using equation (5.39)

$$T_r = \frac{220-33.20}{3} = 63.3\ ℃ \tag{E.28}$$

At initial mass flow rate in table E-7, the total work done by the turbine is 1406.956 kJ/s and the actual mass flow rate is determined by

$$\dot{m}_{SHH} = \frac{50000}{1406.956} = 35.54\ kg/s \tag{E.28}$$

E.3.4 Feed-pump

The work required at the pump 1 is calculated using equation (5.43)

$$w_{P1} = 35.54(683.802 - 665.863) = 637.55206\ kJ/s \tag{E.29}$$

The work required at the pump 2 is calculated using equation (5.44)

$$w_{P2} = 26.15(139.769 - 138.704) = 27.84975\ kJ/s \tag{E.30}$$

Total work required by the pumps is known using equation (5.45) as

$$w_{TP} = (637.55206 + 27.84975) = 665.40181\ kJ/s \tag{E.31}$$

E.3.5 Condenser

The actual heat rejected from the condenser is calculated using equation (5.53)

$$\mathbb{Q}_{rej} = 29.34(2354.315) - 26.15(138.704) = 65448.4925\ kJ/s \tag{E.32}$$

And using equation (5.52), the log mean temperature difference for the cooling water is calculated as

$$\Delta T_{LMTD} = \left[\frac{28.1 - 21.1}{\ln\left(\frac{33.1 - 21.1}{33.1 - 28.1}\right)}\right] = 8\ ℃ \tag{E.33}$$

Using equation (5.55), the overall heat transfer coefficient is known as

$$U = \frac{65448492.5}{(6578.87)(8)} = 1243.54\ W/K \tag{E.34}$$

From equation (5.54), the mass flow rate of the cooling water inside the condenser is evaluated as

$$\dot{m}_{cwi} = \frac{65448492.5}{(4181.492)(7)} = 2235.99\, kg/s \tag{E.35}$$

E.3.6 Thermal efficiency

The thermal efficiency of the STPP is calculated using equation (5.66) as

$$\eta_t = \frac{50670.05662 - 665.40181}{104719.2497} = 0.4775 = 47.8\,\% \tag{E.36}$$

And the net work done of the STPP is determined by

$$W_{net} = 50670.05662 - 665.40181 = 50\, MW_e \tag{E.37}$$

E.4 Analysis of fouling factor

From the analysis in Appendix D, the following parameter below were used to calculate the fouling factor.

- The annulus diameter = 0.03591 m
- The annulus temperature = 33.1 ℃
- Inlet cooling water temperature = 21.1 ℃
- Outlet cooling water temperature = 28.1 ℃
- Inner tube diameter = 0.02291 m
- Outer tube diameter = 0.0277 m
- Effective length = 9 m
- Thermal conductivity of tubes = 111 $W/m.K$
- Number of tube per pass = 8400
- Number of tube row = 100

The total outer diameter of the tube per pass is calculated as

$$d_2 = (0.0277)(8400) = 232.68\, m \tag{E.38}$$

The total inner diameter of the tube per pass is known as

$$d_1 = (0.02291)(8400) = 192.444\, m \tag{E.39}$$

The total annular diameter per pass is known as

$$d_1 = (0.03591)(8400) = 301.644\, m \tag{E.40}$$

E.4.1 Calculating thermo-physical properties of water

The bulk mean temperature of the cooling water is

$$T_{mcw} = \frac{21.1 + 28.1}{2} + 273.15 = 297.75\, K \tag{E.41}$$

Using equation (A.5), the density of cooling water is

$$\rho_{cw} = (1.49343 \times 10^{-3} - 3.7164 \times 10^{-6}(297.75) + 7.09782 \times 10^{-9}(297.75)^2 - 1.90321 \times 10^{-20}(297.75)^6)^{-1} \quad \text{(E.42)}$$

$$= 997.14\ kg/m^2$$

Using equation (A.6), the specific heat capacity of the cooling water is

$$c_{p,cw} = 8.15599 \times 10^3 - 2.80627 \times 10^1(297.75) + 5.11283 \times 10^{-2}(297.75)^2 - 2.17582 \times 10^{-13}(297.75)^6 \quad \text{(E.43)}$$

$$= 4181.492\ J/kg.K$$

Using equation (A.7), the viscosity of cooling water is

$$\mu_{cw} = 2.414 \times 10^{-5} \times 10^{\frac{247.8}{(297.75-140)}} = 0.0009038\ kg/m.s \quad \text{(E.44)}$$

Using equation (A.8), the thermal conductivity of cooling water is

$$k_{f,cw} = -6.14255 \times 10^{-1} + 6.9962 \times 10^{-3}(297.75) - 1.01075 \times 10^{-5}(297.75)^2 + 4.74737 \times 10^{-12}(297.75)^4 \quad \text{(E.45)}$$

$$(297.75)^2 = 0.6101\ W/m.K$$

Using equation (A.9), the Prandtl number is

$$Pr_{cw} = \frac{(0.0009038)(4181.492)}{0.6101} = 6.20 \quad \text{(E.46)}$$

The same equations were used to calculate the thermos-physical properties of the condensed steam. Since the temperature of the steam, remain constant in the condenser. That is T_{si} = T_{so}= 33.1 ℃ = 306.25 K

$$\rho_s = 994.75\ kg/m^2 \quad \text{(E.47)}$$

$$c_{p,cw} = 4177.56\ J/kg.K$$

$$\mu_{cw} = 0.0007469\ kg/m.s$$

$$k_{f,cw} = 0.622\ W/m.K$$

$$Pr_{cw} = 5.02$$

E.4.2 Flow cross-sectional area

From Table E-7, the mass flow rate is $2235.99\ kg/s$ and the volumetric rate is calculated as

$$V_{cwi} = \frac{2235.99}{997.14} = 2.24\ m^3/s \tag{E.48}$$

The area of the tube per pass is calculated using equation (5.65) as

$$A = \frac{\pi(0.02291)^2(8400)}{4} = 3.463\ m^2 \tag{E.49}$$

The velocity in each tube is known by using equation (5.64)

$$v = \frac{2.24}{3.463} = 0.648\ m/s \tag{E.50}$$

E.4.3 Rate of heat transfer

The average rate of heat transfer in the condenser is calculated using equation (5.58) as

$$\mathbb{Q}_{C,m} = \frac{\big((2235.99)(4181.492)(7) + (29.34)(2354.315 - 138.7)\big)}{2} = 32756713.05\ MW_e \tag{E.51}$$

E.4.4 Reynolds number

Using equation (5.63), the Reynolds number per tube is

$$Re = \frac{(997.14)(0.648)(0.02291)}{0.0009038} = 16378.86851 \tag{E.52}$$

This is fully turbulent in each tube.

The total Reynolds number per N_p is

$$Re_T = (16378.86851)(8400) = 137582495.4 \tag{E.53}$$

E.4.5 Frictional factor

The frictional factor for each tube is calculated using equation (5.62) as

$$f_D = (1.8\log_{10}(16378.86851) - 1.5)^{-2} = 0.027 \tag{E.54}$$

Total frictional factor per N_p is

$$f_{D_T} = (0.027)(8400) = 226.8 \tag{E.55}$$

E.4.6 Nusselt number

The correction factor for inner Nusselt number presented by Goodenough (2013) is 1.016. Using equation (5.61), the inner Nusselt number for each tube is calculated as

$$Nu_i = \frac{\left(\frac{0.027}{8}(16378.86851)(6.20)\right)}{1 + 12.7\left(\frac{0.027}{8}\right)^{0.5}(6.20^{2/3} - 1)}(1.016) = 126.5 \tag{E.56}$$

The total Nusselt number per N_p is

$$Nu_{i,T} = (126.5)(8400) = 1062774.015 \tag{E.57}$$

The outer convection coefficient is determined using equation (5.60) as

$$Nu_s = \frac{301.644 - 232.68}{(0.622)(\pi)(232.68)(9)}\left[\frac{33.1 - 28.1}{32756713.05 \ln\left(\frac{33.1 - 28.1}{33.1 - 21.1}\right)} - \frac{1}{(\pi)(9)(0.6101)(10627774.015)} - \frac{\ln\left(\frac{232.68}{192.444}\right)}{2(\pi)(111)(9)}\right]^{-1} \tag{E.58}$$

$$= -561.56$$

E.4.7 Fouling factor

The fouling factor is calculated using equation (5.57) as

$$R''_{fc} = (\pi)(192.444)(9)\left[\frac{33.1 - 28.1}{32756713.05 \ln\left(\frac{33.1 - 28.1}{33.1 - 21.1}\right)} - \frac{\ln\left(\frac{232.68}{192.444}\right)}{2(\pi)(111)(9)} - \left((\pi)(9)(0.6101)(10627774.015)\right)^{-1} - \left(\frac{(0.622)(\pi)(232.68)(9)}{301.644 - 232.68}(-561.56)\right)^{-1}\right] \tag{E.59}$$

$$= 0.00131\ W/K$$